UNIVERSITAT DE BARCELONA

New Physics in the Electroweak Sector Under Scrutiny at LHC

Nuno Filipe Rosa Agostinho

New Physics in the Electroweak Sector Under Scrutiny at LHC

Nuno Filipe Rosa Agostinho

Departament d'Estructura i Constituents de la Matèria
Institut de Ciències del Cosmos
Universitat de Barcelona

PhD advisor:

Prof. Dr. María Concepción González García

Thesis submitted for the degree of *Philosophiae Doctor (PhD) in Physics*
Tesi presentada per obtar al grau de *Doctor en Física*
(Programa de Doctorat en Física)

Acknowledgements

This work would not have been possible without the people around me. Hopefully, I will try to mention everyone that either directly or indirectctly contributed to this work.

Without my mother, the possibility of doing this journey would be non-existent. She always fought to provide the best conditions to me and to my brother, and I will always be there for any help. This Thesis is also yours. Thank you Mária for all the support during this period. I would also like to dedicate this Thesis to someone really close to me, that at this moment is fighting the hardest battle of his life, against the cancer. I will try to keep the values that you pass me: honor in life and the will to help the others. To the rest of my family and my friends in Portugal, Cláudio, Paulo, Texugo, Vasco, Zé, Gamboa, Ricardo, Filipe, Dani, Silvério, Alex,..., obrigado a todos.

This journey in physics started in a special place called CFTP, in Lisbon. I am grateful to David, Gui, Gustavo, and Juca for our collaborations and for all the support while I was there. Especially to you Juca, even if we at some point stopped our collaborations, I will always be grateful for the opportunity that you gave me to work with you.

After leaving my country to embrace this opportunity, new people entered in my life. Some of them did not contribute directly to the result of the Thesis, but by making my life easier outside of the University, they somehow helped me in the work.

I would like to mention someone who I did not meet, but he was somehow present in my Thesis. Your past work was the seed of this Thesis, and by reading it I felt how good physicist you were. Thank you, Juan. I am also grateful to Tyler, for the many questions that he answered during his stays in Barcelona. I hope the best for your scientific career. I would like to thank to Eduardo, for our recent collaborations.

During the PhD training, I had the opportunity to travel and to visit some new

places. I will never forget my visit at Stony Brook, and one of the main reasons was my favourite chinese friend. We had a lot of fun eating spicy chinese food and playing table tennis every Friday afternoon in some dungeon at the institute. Also, you were a wonderful host there, helping me with the Multinest, with statistics and giving me a ride every time I needed. Thank you Ningqiang, I hope the best for you and your family.

I also had the opportunity to visit a small city in UK called Durham. I had some good moments there, sharing the office with Jakub and learning with him a lot about cosmology. His way of exploring physics with some crazy ideas and without being afraid of failing reminded me why at some point of my life I started to study physics. I am also grateful to other good friends from Durham like Matheus, Andres, Gurpreet, Miki, Silvia, Shankha, David, Maria and Nassim for being such good hosts!

My PhD training was part of an european network. The opportunity of making part of such a nice project was fantastic because of travelling and sharing knowledge with other physicists. I would like to mention Xabi, Josu, Sam, Julia Stadler, Arsenii, Bruno, Olcyr, Edoardo and Andrea. However, there are four that I would like to highlight: Elena, Rupert, Alvaro and Gonzalo. We shared fantastic experiences during the events of the network. It seemed like we were friends for so many years. I hope that we keep the contact after this incredible journey.

Besides travelling, most of my time was passed in Barcelona, an amazing place where I had the opportunity to meet human beings. I shared the apartment with incredible people: Jose and his wife Monica; my good friend Kostas; my friend Enrique, who taught me a lot about Spain history; my favourite Catalan, Ignasi, who always was available to help me with anything. Thank you all. Finally, some words to my actual flatmates, Dani and Fernando. Thank you for the good moments that you provided me after work. A mi maestro Miguel, thank you for training me at the club. Sometimes I need to disconnect from my daily life and kickboxing has always been the solution.

During these three years we both shared the same office and the same advisor. About the work experience, you helped me a lot with statistics and in my rediscovery of python, always in a good mood. I learned a lot about physics with you (in particular some optics related with ANITA) and I can proudly say that I shared the office with one of the best physicists of my generation. At personal level, we had very interesting discussions about politics, physics, and we had a lot of funny moments during the schools and workshops. Gracias, mi amigo Ivan!

Oscar, I was far from thinking that after leaving Portugal, one of the people that I would immediately meet in this journey was someone sharing the same native language. It was a pleasure to collaborate with you, after hundreds of emails, code changes, run cards... our fantastic Pheno conference. You showed me a good character, optimism and you always had nice words, even when I screwed some Madgraph runs. I will never forget how wonderful you were as a host while I was visiting São Paulo. Obrigado Oscar!

Finally, the most important person on this Thesis deserves the last words. Whithout her, this work would not be possible. I met in my life three "forces of nature" and you were clearly the third one. By far one of the best physicists with whom I worked. Any word is insufficient to express gratitude to you, for the opportunity of being in Barcelona. During these intense three years I have learned with you much more than you can think: ethics in work, which today is something more and more depreciated; your ability to make decisions; your incredible knowledge of physics that I have tried to absorb as much as I can (even if sometimes I seem too quiet); your optimism that collided with my natural pessimism and your incredible effort to always being present, even while traveling. You had a lot of patience with my non ending mistakes and every time I needed, you seated next to me and you solved the problem. You taught me a valuable lesson of hardworking, and the best that I can do is to apply not only that lesson, but also the other values that I have mentioned in the next steps of my life. I will never forget how you dealt with any bureaucratic problem that I had, since the first time that I stepped in Barcelona to ask for the NIE or the way that you handled every detail of my visit to Stony Brook. Clearly, during these three years living abroad, you were the closest thing that I had to a family. While finishing these acknowledgments, I have this feeling that at some moments I was not the student that you deserved, but you were the advisor that I needed. Muchas gracias por todo Concha!

This project has received funding/support from the European Union's Horizon 2020 research and innovation programme under the Marie Sklodowska-Curie grant agreement No 674896.

Resumen

Esta tesis se centra en la búsqueda de física mas allá del modelo estándar en el sector electrodébil, y en particular en el sector asociado con el mecanismo de la rotura expontánea de la simetría electrodébil y de la generación de masas, usando datos recogidos por los experimentos del Large Hadron Collider. Los resultados presentados en esta tesis se basan en trabajos publicados en revistas internacionales de física de altas energías (Refs. [1–4]).

El modelo estándar es una teoría de campos gauge con grupo de simetría $SU(3)_C \otimes SU(2)_L \otimes U(1)_Y$ para las interacciones fuertes y electrodébiles respectivamente, en la que las partículas observadas se identifican con excitaciones cuánticas de los campos correspondientes. En esta teoría, la simetría gauge implica que todas dichas partículas no pueden adquirir masas sin romper la simetría electrodébil. La rotura espontánea de dicha simetría – en la que es el estado fundamental de la teoría el que rompe la simetría – es una forma elegante de compatibilizar el principio de invariancia gauge del modelo estándar con la observación de partículas masivas. En su forma más simple se implementa via el mecanismo de Higgs que implica la existencia de un campo escalar fundamental que se transforma de forma no trivial bajo $SU(2)_L \otimes U(1)_Y$ y cuya única excitación física es una partícula escalar neutra que conocemos como el boson de Higgs.

Es por ello que podemos considerar que el zenit, tanto del modelo estándar como de la física experimental de colisionadores se alcanzó el 4 de Julio de 2012 en el CERN cuando en LHC anunció el descubrimiento de una nueva partícula que podría ser el boson de Higgs [5, 6], casi 50 años despues de que el mecanismo de Higgs para la rotura espóntanea de la simetría electrodébil fuera propuesto [7–12].

Hasta 2012 el boson de Higgs era la única pieza que faltaba en la construcción del modelo estándard y su descubrimiento abrió una nueva era en la física de partículas. Tras la observación de la nueva partícula la pregunta obvia era si el estado observado era de facto el boson de Higgs del modelo estándar en su versión más mínima o si era una variante del mismo, o si había otras partículas y/o

dinámicas asociadas al proceso de rotura y a la generación de masas. Una clara motivación para esperar dichas extensiones es que el mecanismo de Higgs, si bien funciona, no es la solución mas satisfactoria desde el punto de vista teórico por razones como el problema de las jerarquías que se origina porque la masa del boson de Higgs recibe correcciones de cualquier escala a la que aparezca nueva dinámica, como la escala de Plank característica de la interacción gravitatoria. Luego para mantener su masa a la escala electrodébil hace falta un nivel muy alto de ajuste fino entre los párametros del modelo.

Hay multitud de teorías, extensiones del modelo estándar, que intentan resolver los problemas del escenario mínimo y genericamente todas ellas predicen nuevos estados que deberían ser observados en colisiones de energías alcanzables en el LHC. Pero no fue así, y tras el análisis completo de los datos obtenidos durantel el Run 1 y con los resultados preliminares del Run 2, el posible boson de Higgs era la única nueva partícula observada y dentro de la precisión experimental sus propiedades coincidían con las del boson de Higgs del modelo estándar.

Esta situación es claramente "puzzling" para los físicos de párticulas porque además de argumentos teóricos, sabemos de forma feaciente que el modelo estándar no puede ser la teoría de la Naturaleza basandonos en hechos puramente observacionales tales como la existencia de materia oscura, de neutrinos masivos, y de la simetría materia-antimateria en el Universo.

Este era el escenario cuando el trabajo de esta tesis se inició. En particular, la falta de nuevos estados observados en el LHC nos sirvió como motivación para el uso de Lagrangianos efectivos como herramienta para testear en una forma independiente de modelo una amplia variedad de datos con el fin de buscar posibles desviaciones sobre las predicciones del modelo estándar.

En el contexto de teorías de campos efectivas, los efectos de nueva física, que se manifestarían de forma directa a una escala Λ superior a aquella alcanzable en los experimentos estudiados, pueden parametrizarse en una serie de operadores de dimensión mayor que cuatro y que aparecen en el Lagrangiano suprimidos por potencias de Λ. Los capítulos 2–5 se centran en este formalismo.

Para ello en el capítulo 2 tras una breve introdución sobre cómo se construye una teoría efectiva, presentamos en la secci]'on 2.1 el modelo estándar como una teoría de campos efectiva a bajas energías bajo la hipótesis de que la simetría gauge está realizada de forma linear, esto eso, que el campo de Higgs es un doblete fundamental de $SU(2)_L$. Dada nuestra ignorancia sobre sobre la teoría completa, aplicamos un metodo "bottom-up" y escogemos la base para los operadores que es

más conveniente para el estudio de los datos existentes sobre el sector electrodébil. En el mismo capítulo, tras describir en 2.2 como construir una prescripción consistente para la definición de todos los párametros, presentamos todos los tipos de interacciones que vamos a utilizar en los análisis descritos en los capítulos 3, 4. Las expresiones relevantes para la incorporación de los tests realizados a más bajas energías, en particular con datos del colisionador LEP (los llamados datos de precisión electrodébil, EWPD) estan contenidas en la sección 2.3. Las secciones 2.5 and 2.4 contienen todos los vértices relevantes para el estudio de los vértices de interacción de tres bosones de gauge electrodébil, asi como los relevantes para la producción y desintegración del boson de Higgs, respectivamente.

Los resultados presentados en los siguientes tres capítulos 3–5 representan la secuencia temporal que se ha seguido durante esta tesis en en la determinacón de la precisión con la que las diferentes interacciones del sector electrodébil del modelo estándar estaban siendo probadas con los nuevos datos que iban siendo disponibles. El objetivo último de estos análysis es buscar desviaciones de las predicciones del modelo estándar que pudieran darnos información sobre el modelo completo en el sector responsable para la generación de masas.

El contenido del capítulo 3 se basa en el trabajo publicado en la Ref. [1] y fue el primer trabajo del autor de esta tesis en el marco de teorías efectivas. Como mencionamos anteriormente, el Run 1 del LHC habia generado una cantidad importante de información sobre el nuevo estado "Higgs-like" detectado. Algunos de los test realizados con estos datos se habian llevado a cabo en el marco de Lagrangianos efectivos pero eran estudios en que el numero de operadores considerados se reducia asumiendo que sólo algunos podían ser quantitativamente relevantes en el LHC mientras que otros, en particular los que afectaban a los acoplamientos de los bosones de gauge con los fermiones, estaban ya tan limitados por experimentos anteriores (en particular por los experimentos de LEP) que no eran relevantes. Esta "jerarquía" en la precisión entre los experimentos de LEP y de bajas energías, y los de LHC se empezaba a cuestionar por un serie de estimativas que aprecieron en la literatura del momento. Esto nos motivó a realizar un estudio quantiativo que permitiera de facto determinar rigurosamente si era así. Para ello nos centramos en el estudio de las auto-interacciones de los bosones de gauge electrodébil, en particular en los vértices triples WWZ and $WW\gamma$. EL objetivo era determinar si los resultados obtenidos por los estudios sobre estos vértices, que usaban datos de producción de pares de bosones de gauge (WW or WZ) podrian verse afectados por la modificación del vértice fermionico involucrado en la producción del boson de

gauge intermediario en estos procesos. Para ello realizamos un analisis combinado de los datos relevantes de producción de pares de bosones de gauge en Run 1 del LHC junto con los datos de precisión de experimentos de bajas energías incluyendo en el análisis todos los operadores de dimensión–6 que puedieran contribuir a estos procesos, bien el en vértice WWV. bien en el vértice ffV. La conclusión a la que llegamos es que de facto, ya con los datos del Run 1, se estaban alcanzando precisiones comparables a lo que tradicionalmente se entendia como "datos de precisión electrodébil" para algunos operadores. Esto marca el final de los ánalisis parciales si uno quiere hacer un test estadísticamente consistente del sector electrodébil.

En el capítulo 4, que está basado en los resultados publicados en Ref. [2], nos movemos en la dirección obvia señalada por las conclusiones anteriores: si queremos testear consistentemente el sector electrodébil del modelo est andar necesitamos incluir todos los datos al alcance, de todos los sectores relvantes. así como los efectos de todos los operadores que pueden dar contribuciones a estos observables. Ello incluye EWPD de los tiempos pre-LHC junto con todo los datos disponibles del Run 1 de LHC asi como los dos primeros años del Run 2 sobre producción de pares de bosones de gauge, y sobre la producción y desintegración del boson de Higgs. Lo que constituye un total de 64 observables del Run 1 y 122 incluyendo Run 2. El Lagrangiano efectivo que usamos contiene 20 operadores cuyos coefficientes de Wilson son simultáneamente determinados en el fit global de todos estos observables. Además de quantificar la precisión en la determinacioń de los coeficientes, el análisis permite identificar las posibles quasi-degeneraciones que se presentan en el espacio de parámetros y en las que desde un punto de vista puramente observacional, nueva física podria esconderse sin contradecir ningun dato. EL capítulo se complementa con un estudio quantitativo del efecto de incluir términos de orden superior en la expansión effectiva a la hora de calcular los observables (sec 4.2.4).

En el capítulo 5 presentamos los resultados del último trabajo realizado en el contexto de Lagrangianos efectivos Ref. [3]. En él extendemos nuestro análisis para quantificar el posible efecto de operadores que inducen acoplamientos de tipo dipolar para los quarks ligeros y que no se habian considerado en los resultados presentados en el capítulo 4. Estos operadores generan acoplamientos de los quarks a los bosones de gauge con una estructura Lorentz diferente y por ello no se espera que afecten a los resultados obtenidos, un hecho que verificamos explicitamente en este capítulo. Alternativamente el estudio nos permite cuantificar la sensibilidad de LHC a este tipo de acoplamientos en un regimen en que los quarks ligeros se

pueden tratar como asintóticamente libres. También extendemos el tipo de observables considerados incluyendo los datos de Drell-Yan recogidos tanto en el Run 1 como el Run 2 de LHC. Concluimos que, de facto, para estos dipole-like couplings la precisión de LHC es mejor que la que se obtienía del analysis de EWPD.

Finalmente en el capítulo 6 presentamos los resultados de un estudio realizado en el contexto de un modelo de masa de neutrinos. En el modelo estándar la simetría gauge implica que los neutrinos no tiene masa. Y por lo tanto no hay mezcla de sabor en el sector leptónico. Pero sabemos por la observación de oscilaciones de neutrinos que los neutrinos tienen masa y que el sabor leptónico no se conserva y por lo tanto el modelo estándar debe extenderse para incorporar estas observaciones. Dado que el LHC es nuestra principal herramienta para testear las extensiones del modelo estándar, una cuestión obvia es si LHC puede darnos información acerca de las extensiones que permiten generar masas para los neutrinos. Para ello obviamente uno debe centrarse en modelos que implican una escala de nueva física que esta dentro del rango alcanzable en el LHC. En el capítulo 6, basado en Ref. [4], estudiamos un modelo de see-saw Type-III con "minimal lepton flavour violation" en el cual los estados pesados asociados a la generación de violación de sabor leptonico pueden tener masas del ordel del TeV. El modelo es muy predictivo ya que los modos de desintegracón de estos estados vienen determinados por la estructura de sabor determinada en los experimentos de oscilaciones de neutrinos. El objetivo es estudiar cómo algunos ánalisis de búsqueda de nueva física realizados en el Run 1 de LHC pueden aplicarse a este tipo de modelos altamente predictivos. En particular en el estudio presentado conseguimos extender el rango de masas testeadas usando los datos de ATLAS de eventos que contienen dos leptones cargados y dos jets procedentes del decay hadrónico del W y demostramos cómo es importante para la busqueda de este tipo de modelos que los experimentos estudien la dependencia de sus resultados con el sabor y la carga de los leptones producidos.

Contents

List of publications

The original contents of this thesis are based on the following publications:

1. N. R. Agostinho, O. J. P. Eboli and M. C. Gonzalez-Garcia, LHC Run I Bounds on Minimal Lepton Flavour Violation in Type-III See-saw: A Case Study, JHEP **1711**, 118 (2017) [arXiv:1708.08456 [hep-ph]].

2. A. Alves, N. Rosa-Agostinho, O. J. P. Eboli and M. C. Gonzalez–Garcia, Effect of Fermionic Operators on the Gauge Legacy of the LHC Run I, Phys. Rev. D **98**, no. 1, 013006 (2018) [arXiv:1805.11108 [hep-ph]].

3. E. da Silva Almeida, A. Alves, N. Rosa Agostinho, O. J. P. Eboli and M. C. Gonzalez-Garcia, Electroweak Sector Under Scrutiny: A Combined Analysis of LHC and Electroweak Precision Data, Phys. Rev. D **99**, no. 3, 033001 (2019) [arXiv:1812.01009 [hep-ph]].

4. E. da Silva Almeida, N. Rosa-Agostinho, O. J. P. Eboli and M. C. Gonzalez-Garcia, Light-Quark Dipole Operators at LHC, (Accepted to be published in Phys.Rev.D) arXiv:1905.05187 [hep-ph].

The following publications have been developed in parallel to the content of this thesis, although they have not been included in this dissertation:

1. D. Emmanuel-Costa, J. I. Silva-Marcos and N. R. Agostinho, Exploring the quark flavor puzzle within the three-Higgs doublet model, Phys. Rev. D **96**, no. 7, 073006 (2017) [arXiv:1705.09743 [hep-ph]].

2. N. R. Agostinho, G. C. Branco, P. M. F. Pereira, M. N. Rebelo and J. I. Silva-Marcos, Can one have significant deviations from leptonic 3×3 unitarity in the framework of type I seesaw mechanism?, Eur. Phys. J. C **78**, no. 11, 895 (2018) [arXiv:1711.06229 [hep-ph]].

List of abbreviations

BSM	Beyond the standard model
COM	Center–of–mass
EOM	Equations of motion
EW	Electroweak
EWDBD	Electroweak diboson data
EWPD	Electroweak precision data
EWPO	Electroweak precision observables
EWSB	Electroweak symmetry breaking
IO	Inverted ordering
LHC	Large Hadron Collider
LEP	Large Electron Positron
LFV	Lepton Flavour Violation
LNV	Lepton Number Violation
MLFV	Minimal lepton flavor violation
NLO	Next–to–leading order
NO	Normal ordering
NP	New physics
QCD	Quantum chromodynamics
SM	Standard model
TGC	Triple gauge coupling
TGV	Triple gauge boson vertex
UV	Ultraviolet
VBF	Vector boson fusion
vev	Vacuum expectation value
VH	Associated production

Chapter 1

Introduction

It is impossible to separate the success of particle physics from collider physics. The need of understanding the nature of the sub-atomic world was a driving force to develop these powerful machines. The simple act of accelerating a particle between two electrodes let Thomson discover the electron by studying the properties of the beam. By going one step further beyond the simple act of accelerating a particle and start to collide them, we are not simply probing some substructure or studying its interactions. We are entering in the creation domain, which is the only way that we know how to produce heavy or exceedingly rare particles.

For more than half a century, colliders have been in the forefront of studying the Standard Model (SM) predictions. Hadron colliders such as the Intersecting Storage Rings, which delivered the first pp collision or the Tevatron Collider, the Fermilab machine, and at the present the Large Hadron Collider (LHC) have held the high-energy frontier resulting in the discovery of particles, namely the W and Z bosons and the top quark. Since its start, the accelerator technology of the collider has progressed immensely, while the beam energy and luminosity have grown by several orders of magnitude. Currently, the LHC is operating at a center-of-mass (COM) energy of 13 TeV, which is roughly six times the operating energy of Tevatron.

In addition, collider experiments such as the Large Electron Positron (LEP) at CERN, the Positron Electron Project at SLAC and the Hadron Electron Ring Accelerator an ep collider at DESY, performed measurements that continuously tested the SM at the precision level. An example of how precision measurement can be important to physics Beyond the Standard Model (BSM) is the example of the top quark. The precision measurements of e^+e^- collisions allowed us to know about the existence of the top quark, and even to estimate the value of its mass

before it was directly discovered at the Tevatron. The synergy between precision and energy is something that we need to keep in mind for the next generation of colliders.

The pinnacle of both SM and colliders occurred when on July the 4th 2012, at CERN Large Hadron Collider, the Higgs discovery was announced [5, 6], almost 50 years after being postulated [7–12]. Why the discovery of the Higgs was so important? The answer relies on one of the key pillars of the Standard Model: its invariance under a particular gauge symmetry.

One may define the SM as a quantum relativistic Yang-Mills theory, described by the symmetry group $SU(3)_C \otimes SU(2)_L \otimes U(1)_Y$, where the subscripts are labels which correspond to colour, left-handedness and hypercharge, respectively. It describes the nature at the quantum level, in which fields are fundamental entities. Particles observed in the nature can be thought of as excitations of those fields. It is also compatible with special relativity, which implies that laws of physics prescribed by the Standard Model are invariant under the proper orthochronous Lorentz group of transformations. On the other hand, without the Higgs, we cannot construct a $SU(3)_C \otimes SU(2)_L \otimes U(1)_Y$ gauge invariant term with the known particle fields. In particular it is impossible to generate mass for the observed massive gauge bosons and for the fermions. Additionally, the Higgs mechanism allows for the careful cancellation of the center of mass energy s divergent amplitudes of longitudinal gauge boson scattering, which ensures perturbative unitarity for the SM at the TeV scale. Without Higgs, the theory would remain non–renormalizable.

Until 2012 the Higgs was the only missing piece of the SM, and its discovery was a milestone in the LHC. At that time the future was promising since just only after the first two years of recording LHC collisions and working at only half its designed center–of–mass (COM) energy, a new state was observed. After its observation, there was an obvious question. Was that the SM Higgs boson? Or is some other particle predicted by some BSM extension? There are other alternatives to explain the EWSB mechanism and solve some of the problems that the $SU(2)$ Higgs cannot solve. From the theoretical point of view it is not the most satisfactory solution for issues like the hierarchy problem. In brief, the Higgs mass can receive arbitrary high energy contributions up to the Planck scale, whose renormalization implies that the EW scale is really fine-tuned.

There is a plethora of BSM theories which can address the hierarchy problem of the minimal Higgs scenario. Some lead to an extended scalar sector such, as supersymmetry (SUSY) models. Other involve a new strongly interacting sector to

break the electroweak (EW) symmetry leading to composite Higgs-like particles. Notwithstanding, the complete analysis of Run 1 data and the preliminary ones from Run 2 data, indicate that this new particle is a scalar boson, with CP–even properties, as in the SM Higgs scenario. Furthermore, it seems that the observed state is directly connected to the electroweak symmetry breaking (EWSB), after analyzing interactions with gauge bosons.

The situation is even more puzzling: until the moment there is no evidence of any physics BSM at the LHC in the form of new states. Clearly this disfavours any extension of the SM that predicts new particles at the TeV scale. But, besides theoretical arguments as the hierarchy problem, we know the SM cannot be the theory of Nature because of observational facts: like the existence of dark matter, massive neutrinos and the baryon asymmetry in our Universe. Unfortunately with its minimal scalar sector of EWSB, the SM at short distances, is a complete weakly coupled theory in the sense that one cannot deduce an energy scale at which the SM would be forced to be extended, even with the observations of these BSM phenomena.

This was the scenario when this Thesis was initiated. The Run 1 of LHC had reached its final luminosity, and the Run 2 was starting its operation. The lack of NP states at LHC served us as motivation to look for an alternative approach, instead of constraining ourselves to an specific SM completion. Here enters the model-independent philosophy, where through the use of an effective Lagrangian we start to confront all the existing available data and search for any possible deviation of the SM predictions. Therefore, making use of the framework of Effective Field Theories (EFT), it is not only an ingenious and systematical method to scrutinize NP at the low energy scale but also it is a stringent test to the SM.

In the context of an EFT, we follow an atheist path: NP is expected to manifest directly at a scale Λ, which is higher than the scale at which the experiments are performed. Any effect of new physics (NP) at the low scale can be parametrized by a set of higher dimensional operators, that are suppressed by powers of the high energy scale. The bulk of the work presented in this dissertation focus on this approach.

With this aim, in Chapter 2 we introduce the SM as an EFT at low energy. Our ignorance about the ultraviolet (UV) theory, and with no guidance of where the scale of NP could be laying, lead us to a bottom-up approach, where the higher dimensional operators used are driven by the existing data on the EW sector. It is a pragmatic approach and a safe choice if one wants to minimize the theoretical bias.

In the same Chapter we start by introducing the relevant interaction vertex which contribute to the data sets which we use to scrutinize the EWSB, in a framework where the SM gauge symmetry is linearly realized, *i.e.*the Higgs is a fundamental $SU(2)_L$ doublet field. We use all the data available from Higgs interactions, from the triple gauge coupling (TGC) interactions at LHC in addition to the precision measurements from LEP, the so called electroweak precision data (EWPD). This Chapter is supposed to set the roots of the analysis done in Chapters 3, 4 and 5 . The results presented in these Chapters represent a step in the determination of the precision at which the different interactions in the EW sectors of the SM are being tested by the available data. The ultimate purpose of these analyses is to look for deviations that would be translated in the future on information regarding the UV completion of the SM. In particular testing the true nature of the particle responsible for the origin of the elementary particles' mass. The complementary between the different data can unveil interesting correlations to test the nature of the Higgs particle.

Chapter 3 is mainly based in the published work [1] and it is the first work of the author of this Thesis in this framework. As mentioned above the Run 1 of LHC had already provided important information about the properties of the discovered Higgs-like particle and its couplings. Some of the analysis of the Run 1 data were already performed in terms of effective Lagrangians. Still, they were performed somewhat "partially" under the assumption that only certain operators could be quantitatively relevant at LHC while others, in particular those affecting the couplings of the fermions to the EW gauge bosons, had been already too severely constrained by previous low energy colliders – in particular LEP– to be relevant at LHC. This "hierarchy" of precision was being challenged at the time by some estimates which appeared in the literature. This prompted us to quantify these estimates more rigorously. To do so we focus on the study of EW gauge-boson self-interactions. Our goal is to determine to what degree the extracted information about the TGC from diboson production processes, could be affected by the allowed modification of the gauge boson couplings to fermions. With this in mind we consider the available relevant data from both the Run 1 of LHC and EWPD from LEP, SLC and Tevatron to study the TGCs in the presence of NP in the coupling of the gauge bosons to light quarks. All in the framework of dimension–6 operators, which means that we extended the basis of operators included with the aim at studying the impact of the operators which affect the gauge couplings of fermions on the determination of the gauge boson self-couplings. The conclusions

were that, indeed, already at Run 1 LHC measurements were starting to reach the precision frontier. Good bye partial analysis.

In Chapter 4,which is based in the publication [2], we move in the obvious direction pointed out by the conclusions of Chapter 3: if we want to test the EWSB sector of the SM we need to perform a global analysis including all available data from all relevant sectors and the effects of all operators contributing to the data. Data included consist of EWPD from the pre-LHC times together with the available data from Run 1 and the first two years of Run 2 of LHC on diboson production, and the bulk of measurements of Higgs production and decays. The effective Lagrangian employed involved 20 operators whose Wilson coefficients are simultaneously determined by the global fit. Besides quantifying the precision on the determination of these coefficients, the analysis allows for study the possible quasi-degeneracies which are present in the large parameter space and where, at least from the pure data-driven point of view, NP could hide in plain sight. Furthermore with our analysis we could also quantify the effect of keeping higher order terms in the effective Lagrangian expansion in the observables within the present experimental precision. In brief, when making an analysis at given order in the dimension of the operators included, one faces the issue of the order in the Wilson coefficients at which the observables are to be evaluated. This is relevant when the data is not precise enough, so keeping the expansion at the canonical linear order may even lead to nonphysical results, such as negative cross sections. In Chapter 4 we present a comparative quantification of the dependence of the extracted information on the Wilson coefficients of the twenty operators on the order of the truncation of the effective Lagrangian series.

Chapter 5 contains the results presented in Ref. [3] where we extend our analysis to account for the possible effect of operators inducing dipole-like couplings for the light quarks. Because of the different Lorentz structure of the couplings they are not expected to modify the conclusions of Chapter 4, a fact that we explicitly verify in this Chapter. Conversely the analysis allows for tests of these dipole-like couplings in the asymptotic free regime for the light quarks applies. Also besides extending the basis of operators included in the analysis we also add another observable in our list of processes studied: the Drell-Yan production of light leptons. We find indeed that for these couplings LHC has well superseded the precision from EWPD.

As mentioned above, there are other open questions in the SM without a satisfactory answer. For example we ignore the origin of the Yukawa terms or how to

explain the flavor structure observed in Nature. The fact that the SM is being described by the $SU(3)_C \otimes SU(2)_L \otimes U(1)_Y$ gauge symmetry does not provide any argument for such structure. In addition, in the SM there are no right-handed neutrinos, so it is not possible to have Dirac mass terms for them. So after the EWSB, neutrinos remain strictly massless. Since, within the SM, neutrinos have definite zero mass in all bases, any rotation of the neutrino fields in flavour space has no consequence for the Yukawa Lagrangian. The charged-current Lagrangian remains unchanged when going to the mass eigenstates, meaning that lepton mixing is absent from the SM. However, neutrino oscillations have been detected, which is explained by the fact that neutrinos interact according to their flavour states and propagate according to their mass eigenstates [13]. This is a clear evidence that neutrinos have a small but nonzero mass. Consequently, the SM has to be modified in order to account for neutrinos' mass and the corresponding lepton flavour violation (LFV).

Up to this point our focus was on the scrutiny of the EWSB at LHC, and so the origin of the particles' mass from a model-independent point of view. But still there are other alternatives to study physics beyond the SM, like direct searches at the LHC for some particular signature in a model. Keeping ourselves in the domain of testing the mechanism of generation of masses the next step of this Thesis is to address the origin of neutrino masses. Indeed, a collider like LHC can also shed light on the neutrino mass generation and which models are already tested at the current COM energy.

Clearly this approach only applies to neutrino models which are testable at LHC. The main drawback in most of the simple models is the fact that the smallness of the neutrino masses is usually related to extremely massive partners, clearly out of the LHC reach. Nevertheless neutrino mass models with intermediate scales can be constructed. Thinking still in terms of the effective Lagrangian description, neutrino masses enter at dimension–five via the Weinberg operator which breaks total lepton number. So the smallness of the neutrino mass is associated to the scale of lepton number breaking. But LFV with lepton number conservation enters at dimension–six in form of four–fermion operators. Models where the scale of LNV and the scale of LVF are different can contain new states associated to LFV which can be reachable at the LHC. Generically, neutrino mass models which are being tested at LHC belong to this class of constructions. In the generic case, because what is being tested at LHC is the LFV sector of the model, there is no direct connection between the flavour structure being tested at LHC and that measured in

the neutrino oscillation experiments which is determined by the dimension–five operator. The connection exists, however, if the model is minimally flavour violating (MLFV). The possibility of constructing neutrino mass models which implement these two conditions, TeV scale states and direct connection to neutrino oscillation results, within the context of see-saw models has been explored in the literature. In Chapter 6 we will study one such model of Type-III see-saw where the heavy states can live in the TeV region and, not less important, the couplings of these states are determined by the light neutrino masses and mixings. The focus of the work is to stress how the condition of MLFV is very useful for direct searches at LHC as it leads to highly predictable signatures. As a test case we show how using the available data from LHC Run 1, we can establish exclusion regions for the model parameters which extend beyond those probed in generic Type-III see-saw models. The contents of this Chapter is based on the published work [4].

In brief, the purpose of this Thesis can be summarize as "to squeeze the juice" out of LHC available data in order to study the mechanism responsible for EWSB, or even trying to answer the question of how neutrinos acquired such a small mass.

Chapter 2

Search for the Footprints of New Physics Using Effective Field Theories

There are many different scales in nature, although we do not need to know the physics occurring at all scales to describe phenomena that occur at a given one. Here enters the perspective of an EFT. Let us suppose that we know the form of the high energy Lagrangian describing the observed light particles as well as the heavy states not observed by our experiments. For the purpose of describing the physics at energies below a certain threshold, one can integrate out the heavy degrees of freedom of the theory, and obtain an effective Lagrangian where the effects of heavy states are either absorbed in the renormalization of the existing operators in the Lagrangian of the observed light states, or encoded in the coefficients of an infinite set of new higher dimensional operators.

Following [14], we give a brief introduction on how one can integrate out the heavy states. Let us start by postulate a theory containing the light degrees of freedom Φ_l as well as the heavy ones, which we will denote by Φ_h. The most general Lagrangian describing the theory is :

$$\mathcal{L} = \mathcal{L}_{\Phi_l} + \mathcal{L}_{\Phi_h} + \mathcal{L}_{\Phi_h,\Phi_l} \ , \tag{2.1}$$

where $\mathcal{L}_{\Phi_l}$ contains only the interaction and kinetic terms involving the light degrees of freedom, whereas $\mathcal{L}_{\Phi_h}$ depends only on the heavy degrees of freedom. The interaction terms between light and heavy degrees of freedom are contained in $\mathcal{L}_{\Phi_h,\Phi_l}$.

For simplicity, we assume that the heavy states are only linearly coupled to the light states. Therefore, the Lagrangian containing both interacting and kinetic terms with the heavy state is:

$$\mathcal{L} = \frac{1}{2}\left(\partial^{\mu}\Phi_h \partial_{\mu}\Phi_h - M_{\Phi_h}\Phi_h^2\right) + \Phi_h L \tag{2.2}$$

such that L is some combination of the light fields, and represents the interaction between the different states.

We may write the effective action $W_{eff}\left[\Phi_{l,i}\right]$,

$$e^{iW_{eff}\left[\Phi_{l,i}\right]} \equiv \int \left[d\Phi_h\right] e^{i\int d^4x \mathcal{L}\left(\Phi_h,\Phi_{l,i}\right)} \tag{2.3}$$

and integrate out the heavy states. One way to do it is to complete the square. We begin by defining the following shorthand notations,

$$\begin{aligned}
&\mathcal{D} = \Box + m_{\Phi_h}^2 \ , \\
&\mathcal{D}^{-1}L = -\int d^4y \Delta_F\left(x-y\right) L\left(y\right) \ , \\
&\left(\Box_x + m_{\Phi_h}^2\right)\Delta_F\left(x-y\right) = -\delta^4\left(x-y\right) \ , \\
&H'\left(x\right) = H\left(x\right) + \int d^4y \Delta_F\left(x-y\right) L\left(y\right) \ .
\end{aligned} \tag{2.4}$$

The action can be rewritten as

$$\int d^4x \mathcal{L}\left(\Phi_h,\Phi_{l,i}\right) = \int d^4x \left[-\frac{1}{2}\Phi_h \mathcal{D}\Phi_h + L\Phi_h\right] \tag{2.5}$$

where we have integrated by parts. Then, using the relation $L\mathcal{D}^{-1}L - L\mathcal{D}^{-1}L = 0$ and followed by a succession of integration by parts:

$$\begin{aligned}
\int d^4x \mathcal{L}\left(\Phi_h,\Phi_{l,i}\right) &= -\frac{1}{2}\int d^4x \left[\Phi_h\mathcal{D}\Phi_h - L\Phi_h - L\Phi_h + L\mathcal{D}^{-1}L - L\mathcal{D}^{-1}L\right] \\
&= -\frac{1}{2}\int d^4x \left[\left(\Phi_h - \mathcal{D}^{-1}L\right)\mathcal{D}\left(\Phi_h - \mathcal{D}^{-1}L\right) - L\mathcal{D}^{-1}L\right] \\
&= -\frac{1}{2}\int d^4x \left[\Phi_h'\mathcal{D}\Phi_h' - L\mathcal{D}^{-1}L\right] \ .
\end{aligned} \tag{2.6}$$

In the previous expression, the heavy field was redefined as $\Phi_h' = \Phi_h - \mathcal{D}^{-1}L$ and we used the following relation

$$\int d^4x \left(\mathcal{D}\mathcal{D}^{-1}L\right)\Phi_h = \int d^4x \left(\mathcal{D}S\mathcal{D}^{-1}L\right) \ . \tag{2.7}$$

In addition, as we are integrating over all values of the field at each point of space time, we may change the variables $\mathcal{D}\Phi'_h = \mathcal{D}\Phi_h$, leaving us with an expression that does not depend on the heavy state,

$$\begin{aligned} e^{iW_{eff}[L]} &= \int [d\Phi_h]\, e^{i\int d^4x \mathcal{L}(\Phi_h, L)} \\ &= \int \left[d\Phi'_h\right] e^{i\int d^4x \left[-\frac{1}{2}\Phi'_h \mathcal{D}\Phi'_h + \frac{1}{2}L\mathcal{D}^{-1}L\right]} . \end{aligned} \tag{2.8}$$

where the term $\int [d\Phi'_h]\, e^{i\int d^4x\left[-\frac{1}{2}\Phi'_h\mathcal{D}\Phi'_h\right]}$ is an overall constant. From Eq. (2.8), one obtains the effective action,

$$W_{eff}[L] = -\frac{1}{2}\int d^4x d^4y L(x)\, \Delta_F(x-y)\, L(y) \ . \tag{2.9}$$

Since L is peaked at small distances, of order $-1/M^2_{\Phi_h}$, The local Lagrangian is obtained by Taylor expanding

$$L(y) = L(x) + (y-x)^\mu \left[\partial_\mu L(y)\right]_{y=x} + ... \ , \tag{2.10}$$

resulting in the approximate expression for the effective action,

$$W_{eff}[L] = \frac{1}{2}\int d^4x \frac{1}{m^2_{\Phi_h}} L(x)\, L(y) + ... \tag{2.11}$$

In the end, we integrated out the heavy states and, not less important, we see that the remaining effects from the full theory, represented by L appear in inverse powers of the heavy mass. Therefore, our theory at low energy will be described by $\mathcal{L}_{\Phi,l}$ plus the additional operators suppressed by the scale of the heavy states. An earlier example of the application of an EFT in particle physics was Fermi model of beta decay where the heavy degree of freedom has been identified with the fundamental particle now known as the W boson. The same fundamental principles can be applied to the SM. If that so, we would be able to compute the effective Lagrangian and see how the relevant observables change in the presence of effects coming from high scale new physics (NP). In the following sections we discuss the SM from the point of view of an EFT and the phenomenological implications of higher dimension operators formed with the light degrees of freedom in the low energy physics.

2.1 An Effective Lagrangian for the Electroweak Sector and its Linear Realization with a Light Higgs

We can think of the SM as an effective low energy theory that retains as main ingredients the gauge group $SU(2)_L \otimes U(1)_Y$ symmetry, the same particle spectrum

as the SM and the spontaneous symmetry breaking mechanism as the agent responsible for generating mass for each of the known elementary particle. The NP occur at some new energy scale Λ while the breaking of $SU(2)_L \otimes U(1)_Y$ takes place at the electroweak scale. If Λ is high enough, the new physics scale and with it all new particles are properly decoupled.

One of the first assumptions for the low energy theory is that, even if there is any NP effects on the EWSB sector, the observed Higgs particle is treated as a fundamental field transforming as a light doublet under the electroweak gauge symmetry, which is linearly realized in the effective theory [15–32]. For a sufficiently high NP scale relative to the energy scale being probed, the SM as complete description for the Nature differs from the SM as an effective theory by a well defined perturbative expansion. The NP effects modify the SM predictions, such that the small effects are encoded in non-renormalizable terms proportional to powers of $1/\Lambda$. This approach further assumes that there are no new light degrees of freedom. The most general Lagrangian that describes the theory in low energy limit is given by the following expansion:

$$\mathcal{L}_{eff} = \mathcal{L}_{SM} + \sum_{n>4,j} \frac{f_{n,j}}{\Lambda^{n-4}} \mathcal{O}_{n,j} \tag{2.12}$$

where $\mathcal{L}_{SM}$ is the SM Lagrangian. The coefficients from the new operators encode the NP effects and are suppressed by powers of the full theory scale. For sufficiently low momenta relative to the NP scale Λ and depending on the level of precision needed to describe the interactions and possible effects from NP, one can truncate the expansion series at some order. If we probe energies smaller than Λ, then the truncation is formally justified. The first local operator of increasing mass dimension $d > 4$ is the dimension–five the Weinberg operator [33], which generates Majorana mass for neutrinos and explicitly violates the Lepton number. Since we assume that NP does not violate both Lepton and Baryon numbers, the dimension five operator will be ignored in the effective Lagrangian. Also, given the strong constrains from neutrino sector, in particular the smallness of neutrino masses which makes cut-off scale much above the LHC energy, this operator does not play an important role at LHC physics. Notwithstanding, in Chapter 6 we will address the Weinberg operator, given its relevance to neutrino mass generation models.

The next group of higher dimension operators is the dimension–six operators. From the literature, we know that a minimal set of 59 dimension–six independent operators [34] (up to flavor and Hermitian conjugation) generates the most general

S-matrix elements while conserving the Lepton and Baryon numbers and respecting the SM gauge symmetry. We assume that dimension–eight operators' effects are negligible at the current level of precision available. Several analysis [35–37] shows that a fit of dimension–six operators to the LHC data is a valid approach to capture the relevant phenomenology, even if the LHC constraints do not induce a clear hierarchy of scales. In almost realistic weakly coupled scenarios, a basis constituted by dimension–six operators is adequate to probe with sufficient accuracy possible NP effects coming from specific UV-complete theories, with the exception of high-energy tails of distributions [38].

So the extension of the SM considered in this Thesis will contain dimension–six operators. Furthermore for the processes studied we will only need to focus on dimension–six operators $\mathcal{O}_n$ which conserve C and P. If we knew the full or UV theory, one may integrate out heavy degrees of freedom obtaining the operators whose form is tied to the higher scale physics. However, without "a priori" knowledge on the form of the new physics, a basis should contain a set of operators whose coefficients are more easily related to existing data from other well tested sectors of the theory, namely the EWPD. We shall work in what has been referred in the literature as the the Hagiwara, Ishihara, Szalapski, and Zeppenfeld (HISZ) basis [18, 21]. By choosing this basis, we maximize the use of bosonic operators in order to to take fully advantage of the available data on the EWSB.

The operators considered can be classified according to the fields involved. The relevant operators involving bosonic fields include:

$$\begin{aligned}
\mathcal{O}_B &= (D_\mu\Phi)^\dagger \hat{B}^{\mu\nu}(D_\nu\Phi)\,, & \mathcal{O}_{\Phi,1} &= (D_\mu\Phi)^\dagger\Phi\Phi^\dagger(D^\mu\Phi)\,,\\
\mathcal{O}_W &= (D_\mu\Phi)^\dagger \hat{W}^{\mu\nu}(D_\nu\Phi)\,, & \mathcal{O}_{\Phi,2} &= \tfrac{1}{2}\partial_\mu(\Phi^\dagger\Phi)\partial^\mu(\Phi^\dagger\Phi)\,,\\
\mathcal{O}_{BB} &= \Phi^\dagger \hat{B}_{\mu\nu}\hat{B}^{\mu\nu}\Phi\,, & \mathcal{O}_{\Phi,3} &= \tfrac{1}{3}(\Phi^\dagger\Phi)^3\,,\\
\mathcal{O}_{WW} &= \Phi^\dagger \hat{W}_{\mu\nu}\hat{W}^{\mu\nu}\Phi\,, & \mathcal{O}_{\Phi,4} &= (D_\mu\Phi)^\dagger(D^\mu\Phi)(\Phi^\dagger\Phi)\,,\\
\mathcal{O}_{BW} &= \Phi^\dagger \hat{B}_{\mu\nu}\hat{W}^{\mu\nu}\Phi\,, & & \\
\mathcal{O}_{GG} &= \Phi^\dagger\Phi G^a_{\mu\nu}G_a^{\mu\nu}\,, & \mathcal{O}_{WWW} &= \mathrm{Tr}[\hat{W}_\mu{}^\nu \hat{W}_\nu{}^\rho \hat{W}_\rho{}^\mu]\,,
\end{aligned} \tag{2.13}$$

Where the Higgs doublet is denoted by Φ. The covariant derivative is given by $D_\mu\Phi = (\partial_\mu + i\frac{1}{2}g'B_\mu + ig\frac{\tau_a}{2}W^a_\mu)\Phi$. The hatted field strength tensors are $\hat{B}^{\mu\nu} = i\frac{g'}{2}B_{\mu\nu}$ and $\hat{W}^{\mu\nu} = i\frac{g}{2}\tau_a W^a_{\mu\nu}$, while the fields strengths are given by:

$$\begin{aligned}
B_{\mu\nu} &= \partial_\mu B_\nu - \partial_\nu B_\mu\,,\\
W^a_{\mu\nu} &= \partial_\mu W^a_\nu - \partial_\nu W^a_\mu - g\epsilon^{abc}W^b_\mu W^c_\nu\,,\\
G^a_{\mu\nu} &= \partial_\mu G^a_\nu - \partial_\nu G^a_\mu - g_s f^{abc}G^b_\mu G^c_\nu\,.
\end{aligned} \tag{2.14}$$

The couplings, g, g', and g_s denote the $SU(2)_L$, $U(1)_Y$, and $SU(3)_C$ gauge cou-

plings, and τ_a are the Pauli matrices. G^a_μ are the gluon fields and the electroweak fields are defined as:

$$\begin{aligned} W^\pm_\mu &= \frac{1}{\sqrt{2}}\left(W^1_\mu \mp W^2_\mu\right) \ , \\ Z^{SM}_\mu &= \frac{1}{g^2+g'^2}\left(gW^3_\mu - g'B_\mu\right) \ , \\ A^{SM}_\mu &= \frac{1}{\sqrt{g^2+g'^2}}\left(g'W^3_\mu + gB_\mu\right) \ . \end{aligned} \tag{2.15}$$

For completeness we also list an additional set of four operators made up of only EW and strong gauge fields. They do not contribute to the Higgs interactions nor to triple electroweak gauge boson vertices and therefore do not generate effects in the observables discussed in this Thesis:

$$\begin{aligned} &\mathcal{O}_{GGG} = i f_{abc} G^{a\,\nu}_\mu G^{b\,\rho}_\nu G^{c\,\mu}_\rho \ , \\ &\mathcal{O}_{DW} = \left(D^\mu \hat{W}_{\mu\nu}\right)^i \left(D_\rho \hat{W}^{\rho\nu}\right)^i , \quad \mathcal{O}_{DB} = \left(\partial^\mu \hat{B}_{\mu\nu}\right)\left(\partial_\rho \hat{B}^{\rho\nu}\right) \ , \\ &\mathcal{O}_{DG} = \left(D^\mu G_{\mu\nu}\right)^a \left(D_\rho G^{\rho\nu}\right)^a \ , \end{aligned} \tag{2.16}$$

where $\left(D^\mu W_{\mu\nu}\right)^i = \partial^\mu W^i_{\mu\nu} - g\epsilon^{ijk} W^{\mu j} W^k_{\mu\nu}$ and where, in $\mathcal{O}_{DG}$, D^μ denotes the covariant derivative acting on a field transforming in the adjoint of $SU(3)_C$, $\left(D^\mu G_{\mu\nu}\right)^a = \partial^\mu G^a_{\mu\nu} - g_s f^{abc} G^{\mu b} G^c_{\mu\nu}$. It is worth noting this set is not minimal as the operators $\mathcal{O}_{DW}$, $\mathcal{O}_{DB}$ and $\mathcal{O}_{DG}$ are usually traded using the Equations of Motion (EOM) for $\mathcal{O}_{WWW}$ and $\mathcal{O}_{GGG}$ and some fermionic operators.

Next we also list the dimension–six operators which couple fermions to the Higgs boson [34] which can be classified according to the number of Higgs fields involved. Those with three Higgs fields are:

$$\begin{aligned} \mathcal{O}_{e\Phi,ij} &= (\Phi^\dagger\Phi)(\bar{L}_i \Phi e_{R,j}) \ , \\ \mathcal{O}_{u\Phi,ij} &= (\Phi^\dagger\Phi)(\bar{Q}_i \tilde{\Phi} u_{R,j}) \ , \\ \mathcal{O}_{d\Phi,ij} &= (\Phi^\dagger\Phi)(\bar{Q}_i \Phi d_{R,j}) \ , \end{aligned} \tag{2.17}$$

and those involving two Higgs fields read:

$$\begin{aligned} \mathcal{O}^{(1)}_{\Phi L,ij} &= \Phi^\dagger (i \overleftrightarrow{D}_\mu \Phi)(\bar{L}_i \gamma^\mu L_j), & \mathcal{O}^{(3)}_{\Phi L,ij} &= \Phi^\dagger (i \overleftrightarrow{D}^a_\mu \Phi)(\bar{L}_i \gamma^\mu T_a L_j), \\ \mathcal{O}^{(1)}_{\Phi Q,ij} &= \Phi^\dagger (i \overleftrightarrow{D}_\mu \Phi)(\bar{Q}_i \gamma^\mu Q_j), & \mathcal{O}^{(3)}_{\Phi Q,ij} &= \Phi^\dagger (i \overleftrightarrow{D}^a_\mu \Phi)(\bar{Q}_i \gamma^\mu T_a Q_j), \\ \mathcal{O}^{(1)}_{\Phi u,ij} &= \Phi^\dagger (i \overleftrightarrow{D}_\mu \Phi)(\bar{u}_{R_i} \gamma^\mu u_{R_j}), & \mathcal{O}^{(1)}_{\Phi d,ij} &= \Phi^\dagger (i \overleftrightarrow{D}_\mu \Phi)(\bar{d}_{R_i} \gamma^\mu d_{R_j}), \\ \mathcal{O}^{(1)}_{\Phi ud,ij} &= \tilde{\Phi}^\dagger (i \overleftrightarrow{D}_\mu \Phi)(\bar{u}_{R_i} \gamma^\mu d_{R_j} & \mathcal{O}^{(1)}_{\Phi e,ij} &= \Phi^\dagger (i \overleftrightarrow{D}_\mu \Phi)(\bar{e}_{R_i} \gamma^\mu e_{R_j}) \ , \\ & \quad + \text{h.c.}), \end{aligned} \tag{2.18}$$

where we define $\tilde{\Phi} = \sigma_2 \Phi^*$, $\Phi^\dagger \overleftrightarrow{D}_\mu \Phi = \Phi^\dagger D_\mu \Phi - (D_\mu \Phi)^\dagger \Phi$ and $\Phi^\dagger \overleftrightarrow{D}^a_\mu \Phi = \Phi^\dagger \sigma^a D_\mu \Phi - (D^\mu \Phi)^\dagger \sigma^a \Phi$. We use the notation of L for the lepton doublet, Q for the quark doublet and f_R for the $SU(2)$ singlet fermions, where i, j are flavor indices.

The complete basis of dimension–six operators also contains a group of dipole fermionic operators (*i.e.* with tensor Lorentz structure). They are:

$$\begin{aligned}
\mathcal{O}_{eW,ij} &= i\bar{L}_i \sigma^{\mu\nu} \ell_{R,j} \widehat{W}_{\mu\nu} \Phi \quad , & \mathcal{O}_{eB,ij} &= i\bar{L}_i \sigma^{\mu\nu} \ell_{R,j} \widehat{B}_{\mu\nu} \Phi \quad , \\
\mathcal{O}_{uW,ij} &= i\bar{Q}_i \sigma^{\mu\nu} u_{R,j} \widehat{W}_{\mu\nu} \tilde{\Phi} \quad , & \mathcal{O}_{uB,ij} &= i\bar{Q}_i \sigma^{\mu\nu} u_{R,j} \widehat{B}_{\mu\nu} \tilde{\Phi} \quad , \\
\mathcal{O}_{dW,ij} &= i\bar{Q}_i \sigma^{\mu\nu} d_{R,j} \widehat{W}_{\mu\nu} \Phi \quad , & \mathcal{O}_{dB,ij} &= i\bar{Q}_i \sigma^{\mu\nu} u_{R,j} \widehat{B}_{\mu\nu} \Phi \quad ,
\end{aligned} \tag{2.19}$$

where i,j are family indices.

Finally at dimension–six there is a plethora of four-fermion operators. For the purpose of the work presented in this dissertation we only need the effects associated to the dimension–six four-fermion operator which (ignoring flavour indexes) we write as

$$\mathcal{O}_{LLLL} = (\bar{L}\gamma^\mu L)(\bar{L}\gamma^\mu L) \, , \tag{2.20}$$

and which contributes a finite renormalization to the Fermi constant (see Eq. (2.29)).

We notice that the listed basis of operators is not the minimal set, this is, not all operators are independent as they can be related by the use of the classical EOM thus leading to the same S-matrix elements [39–42]. This means that we have the freedom to choose a basis containing the operators better constrained by low energy physics.

In the next sections, we derive the relevant vertices generated from extending the SM Lagrangian with these new operators after accounting for finite renormalization effects. Also we will use the freedom of choice provided by the EOM to chose a basis for which each of the observables considered provides an independent constraint.

2.2 Finite Renormalization: Definitions

Many of the operators induce finite field renormalization which requires us to expand the operators to account for their effects on the different canonical normalized field definition, coupling constants and mass renormalizations.

Working in the unitary gauge the Higgs doublet is given by:

$$\Phi = \frac{1}{\sqrt{2}} \begin{pmatrix} 0 \\ v + h(x) \end{pmatrix} . \tag{2.21}$$

where v is the Higgs vacuum expectation value (vev). First we note that there is an induced shift to the Higgs potential from $\mathcal{O}_{\Phi,3}$:

$$V(\Phi) = \mu_0^2(\Phi^\dagger\Phi) + \lambda_0(\Phi^\dagger\Phi)^2 - \frac{f_{\Phi,3}}{3\Lambda^2}(\Phi^\dagger\Phi)^3. \tag{2.22}$$

Leading to a shift in the minimum of the potential with respect to the SM,

$$v^2 = -\frac{\mu_0^2}{\lambda_0}\left(1 + \frac{v^2}{4\Lambda^2}\frac{f_{\Phi,3}}{\lambda_0}\right) \equiv v_0\left(1 + \frac{v^2}{4\Lambda^2}\frac{f_{\Phi,3}}{\lambda_0}\right), \tag{2.23}$$

where the index "0" denotes the SM value. As $\mathcal{O}_{\Phi,1}$, $\mathcal{O}_{\Phi,2}$, and $\mathcal{O}_{\Phi,4}$ contain derivatives of the Higgs field they therefore induce a finite wavefunction renormalization for the Higgs field, so that the field with a canonical kinetic term is H:

$$H = h\left[1 + \frac{v^2}{2\Lambda^2}(f_{\phi,1} + 2f_{\phi,2} + f_{\phi,4})\right]^{1/2}. \tag{2.24}$$

To linear order this leads to a shift of the Higgs mass:

$$M_H^2 = 2\lambda_0 v^2\left[1 - \frac{v^2}{2\Lambda^2}\left(f_{\phi,1} + 2f_{\phi,2} + f_{\phi,4} + \frac{f_{\phi,3}}{\lambda_0}\right)\right]. \tag{2.25}$$

Next we consider similar effects on the gauge fields. We note that $\mathcal{O}_{BW}$ affects $Z\gamma$ mixing shifting the mass eigenstates from those in the SM:

$$\begin{aligned} Z_\mu &= \left[1 - \tfrac{g^2g'^2}{2(g^2+g'^2)}\tfrac{v^2}{\Lambda^2}f_{BW}\right]^{-1/2} Z_\mu^{\rm SM}, \\ A_\mu &= \left[1 + \tfrac{g^2g'^2}{2(g^2+g'^2)}\tfrac{v^2}{\Lambda^2}f_{BW}\right]^{-1/2} A_\mu^{\rm SM} - \left[\tfrac{gg'(g^2-g'^2)}{4(g^2+g'^2)}\tfrac{v^2}{\Lambda^2}f_{BW}\right] Z_\mu^{\rm SM}, \end{aligned} \tag{2.26}$$

and, additionally, that there are effects on the gauge boson masses:

$$\begin{aligned} M_Z^2 &= \tfrac{g^2+g'^2}{4}v^2\left[1 + \tfrac{v^2}{2\Lambda^2}\left(f_{\Phi,1} + f_{\Phi,4} - \tfrac{g^2g'^2}{(g^2+g'^2)}f_{BW}\right)\right], \\ M_W^2 &= \tfrac{g^2}{4}v^2\left[1 + \tfrac{v^2}{2\Lambda^2}f_{\Phi,4}\right]. \end{aligned} \tag{2.27}$$

where we have defined $g = \frac{e^0}{s_W^0}$, $g' = \frac{e^0}{c_W^0}$ and again we have used the index "0" to denote the SM Lagrangian parameters. Notice that $\mathcal{O}_{BW}$ and $\mathcal{O}_{\Phi,1}$ contribute to the Z mass, but not the W mass, therefore violating the custodial $SU(2)$ symmetry and contributing to the T parameter as will be discussed in more detail in Sec. 2.3.

In the next Chapters we will work in what is commonly referred as Z-scheme. Besides having the most precise measured value of the strong constant α_S, the measured mass of the Higgs and the fermion masses as inputs, we also use the most precise measured values of the Fermi constant G_F, M_Z and the electromagnetic

fine-structure constant α, extracted from the muon decay rate, the Z line-shape at LEP I and the Thompson scattering.

In this scheme Eq. (2.26) implies that the measured electric charge receives a correction from the operator $\mathcal{O}_{BW}$,

$$e \equiv \sqrt{4\pi\alpha} = e^0 \left(1 + \frac{1}{4} e^2 f_{BW} \frac{v^2}{\Lambda^2}\right). \tag{2.28}$$

The measured Fermi constant as the coupling measured in the muon decay receives the following corrections

$$G_F = G_F^0 \left[1 + \frac{v^2}{\Lambda^2}\left(-2 f_{LLLL} + f^{(3)}_{\Phi L,11} + f^{(3)}_{\Phi L,22} - \frac{1}{2} f_{\Phi,4}\right)\right], \tag{2.29}$$

with $4G_F^0/\sqrt{2} = 1/v^2$ where here v is defined in Eq. (2.23), ie it already contains the shift in the potential minimum due to $\mathcal{O}_{\Phi,3}$.

In this scheme the Weinberg angle is defined in terms of the input quantities by

$$s_W^2 \equiv \frac{1}{2}\left(1 - \sqrt{1 - \frac{4\pi\alpha}{\sqrt{2} G_F M_Z^2}}\right) \tag{2.30}$$

so it is related to the $''0''$ quantities by

$$\begin{aligned} s_W^2 = \; & (s_W^0)^2 \left\{1 + \tfrac{v^2}{\Lambda^2}\left[\tfrac{e^2 c_W^2}{c_W^2 - s_W^2} f_{BW} \right.\right. \\ & \left.\left. - \tfrac{c_W^2}{c_W^2 - s_W^2}\left(\tfrac{1}{2} f_{\phi,1} - 2 f_{LLLL} + f^{(3)}_{\Phi L,11} + f^{(3)}_{\Phi L,22}\right)\right]\right\} \end{aligned} \tag{2.31}$$

$$\begin{aligned} c_W^2 = \; & (c_W^0)^2 \left\{1 - \tfrac{v^2}{\Lambda^2}\left[\tfrac{e^2 s_W^2}{c_W^2 - s_W^2} f_{BW} \right.\right. \\ & \left.\left. - \tfrac{s_W^2}{c_W^2 - s_W^2}\left(\tfrac{1}{2} f_{\phi,1} - 2 f_{LLLL} + f^{(3)}_{\Phi L,11} + f^{(3)}_{\Phi L,22}\right)\right]\right\} \end{aligned} \tag{2.32}$$

Correspondingly the W boson mass is defined from the relation $M_W^0 = M_Z^0 c_W^0$ where $M_W^0 = \frac{gv}{2}$ and $M_Z^0 = \frac{\sqrt{g^2+g'^2}v}{2}$, so

$$\begin{aligned} M_W^2 \equiv M_Z^2 c_W^2 \quad & \left\{1 + \tfrac{v^2}{\Lambda^2}\tfrac{c_W^2}{c_W^2 - s_W^2}\left[\tfrac{1}{2} f_{\Phi,1} - \tfrac{e^2}{2c_W^2} f_{BW} \right.\right. \\ & \left.\left. + \tfrac{s_W^2}{c_W^2}\left(-2 f_{LLLL} + f^{(3)}_{\Phi L,11} + f^{(3)}_{\Phi L,22}\right)\right]\right\}. \end{aligned} \tag{2.33}$$

Finally we also notice that naively because of the bosonic operators $\mathcal{O}_{GG}$, $\mathcal{O}_{BB}$ and $\mathcal{O}_{WW}$ one would expect some contribution to the two-point functions of gauge bosons as well as to WWV three-point-functions. Nevertheless, if we redefine the

field strengths and coupling constants as [21]

$$W_{\mu\nu} = \left[1 + \frac{2M_W^2}{\Lambda^2} f_{WW}\right]^{1/2} W_{\mu\nu}^{SM} \ , \quad g = \left[1 + \frac{2M_W^2}{\Lambda^2} f_{WW}\right]^{-1/2} g^{SM} \ , \tag{2.34}$$

$$B_{\mu\nu} = \left[1 + \frac{2M_Z^2 s_W^2}{\Lambda^2} f_{BB}\right]^{1/2} W_{\mu\nu}^{SM} \ , \quad g' = \left[1 + \frac{2M_Z^2 s_W^2}{\Lambda^2} f_{BB}\right]^{-1/2} g'^{SM} \ , \tag{2.35}$$

their contributions are completely absorbed.

2.3 Corrections to the Electroweak Precision Observables

The electroweak observables provide information on the couplings of the Z and W bosons to fermions which receive contribution both from corrections to the gauge boson self-energies as well as to the vertices. The strongest constraints come from LEP, where the processes $e^+ + e^- \to V^* \to f\bar{f}$ are in a good agreement with the SM [48].

When we adopt an effective description of the nature at low energies, these observables are modified by the new operators. For the sake of completeness and closely following [49], we briefly summarize here the deviations from the SM,

$$X = X_{SM} + \Delta X \ , \tag{2.36}$$

where X_{SM} is the SM part of the quantity X and ΔX is the anomalous part of the same quantity. Let us start by considering the correction $\Pi^{\mu\nu}_{V_1V_2}$ to the gauge-boson two-point-functions,

$$-i\Pi^{\mu\nu}_{V_1V_2}\left(q^2\right) = -i\Pi_T^{V_1V_2}\left(q^2\right)\left(g^{\mu\nu} - \frac{q^\mu q^\nu}{q^2}\right) - i\Pi_L^{V_1V_2}\left(q^2\right)\left(\frac{q^\mu q^\nu}{q^2}\right) \tag{2.37}$$

where we make a decomposition into the longitudinal contribution, $\Pi_L^{V_1V_2}$ and the transversal one, $\Pi_T^{V_1V_2}$. The super-scripts V_1 and V_2 indicate the vectors under consideration. As for the Vf_1f_2 vertex corrections, and neglecting the fermion masses, we have:

$$-i\Delta\Gamma_\mu^{\gamma f_1 f_2}(q) = -i\gamma_\mu \frac{1}{2}(1-\gamma_5)\, g I_3^f \Delta\Gamma_L^\gamma\left(q^2\right) \ , \tag{2.38}$$

$$-i\Delta\Gamma_\mu^{Z f_1 f_2}(q) = -i\gamma_\mu \frac{1}{2}(1-\gamma_5)\, g I_3^f \Delta\Gamma_L^Z\left(q^2\right) \ , \tag{2.39}$$

$$-i\Delta\Gamma_\mu^{W f_1 f_2}(q) = -i\gamma_\mu \frac{1}{2}(1-\gamma_5)\, \frac{g}{\sqrt{2}} \Delta\Gamma_L^W\left(q^2\right) \ , \tag{2.40}$$

with I_3^f as the third component of weak isospin for the external fermion f.

Finally, we form the gauge-invariant combinations,

$$\begin{aligned}
\Delta\bar{\Pi}_T^{\gamma\gamma}\left(q^2\right) &= \Delta\bar{\Pi}_T^{\gamma\gamma}\left(q^2\right) - 2s_W q^2 \Delta\Gamma_L^{\gamma}\left(q^2\right) \ , \\
\Delta\bar{\Pi}_T^{\gamma Z}\left(q^2\right) &= \Delta\bar{\Pi}_T^{\gamma Z}\left(q^2\right) - s_W q^2 \Delta\Gamma_L^{Z}\left(q^2\right) - c_W\left(q^2 - M_Z^2\right)\Delta\Gamma_L^{\gamma}\left(q^2\right) \ , \\
\Delta\bar{\Pi}_T^{ZZ}\left(q^2\right) &= \Delta\bar{\Pi}_T^{ZZ}\left(q^2\right) - 2c_W\left(q^2 - M_Z^2\right)\Delta\Gamma_L^{Z}\left(q^2\right) \ , \\
\Delta\bar{\Pi}_T^{WW}\left(q^2\right) &= \Delta\bar{\Pi}_T^{\gamma\gamma}\left(q^2\right) - 2\left(q^2 - M_W^2\right)\Delta\Gamma_L^{W}\left(q^2\right) \ ,
\end{aligned} \tag{2.41}$$

which allow us to define the contributions of these two-point-functions to four-fermion amplitudes. The contributions are summarized by so-called oblique parameters S, T and U [47]

$$\begin{aligned}
\alpha\Delta S &= 4s_W^2 c_W^2 \left(-\Delta\bar{\Pi}_{T,Z}^{ZZ}(0) + \frac{c_W^2 - s_W^2}{s_W c_W}\Delta\bar{\Pi}_{T,\gamma}^{\gamma Z}\left(M_Z^2\right) \right. \\
&\quad \left. + \Delta\bar{\Pi}_{T,\gamma}^{\gamma\gamma}\left(M_Z^2\right)\right) \ , \qquad (2.42) \\
\alpha\Delta T &= \left(\frac{\Delta\bar{\Pi}_T^{ZZ}(0)}{M_Z^2} - \frac{\Delta\bar{\Pi}_T^{WW}(0)}{M_W^2} \right) \ , \qquad (2.43) \\
\alpha\Delta U &= 4s_W \left(c_W^2 \Delta\bar{\Pi}_{T,Z}^{ZZ}(0) - \Delta\bar{\Pi}_{T,W}^{WW}(0) + s_W^2 \Delta\bar{\Pi}_{T,\gamma}^{\gamma\gamma}\left(M_Z^2\right) \right. \\
&\quad \left. + 2s_W c_W \Delta\bar{\Pi}_{T,\gamma}^{\gamma\gamma}\left(M_Z^2\right)\right) \ . \qquad (2.44)
\end{aligned}$$

where

$$\Delta\bar{\Pi}_{T,V3}^{V_1V_2}\left(q^2\right) = \frac{\Delta\bar{\Pi}_T^{V_1V_2}\left(q^2\right) - \Delta\bar{\Pi}_T^{V_1V_2}\left(m_{V_3}^2\right)}{q^2 - m_{V_3}^2} \ . \tag{2.45}$$

From the operators studied in the previous sections we see that $\mathcal{O}_{\Phi,1}$ contributes to the T parameter at tree level,

$$\alpha\Delta T = \frac{1}{2}\frac{v^2}{\Lambda^2} f_{\Phi,1} \ . \tag{2.46}$$

The reason is the following: we can see that T is the difference between corrections to W and Z propagator, thus if any operator which induce different behavior for the Z from that of the W, this parameter will be corrected. Since $\mathcal{O}_{\Phi,1}$ induces a shift to the Z propagator but not to W, the T parameter will receive a contribution at tree-level. We would like to emphasize that, despite the contribution of $\mathcal{O}_{BW}$ to the Z mass and not that of the W, it does not contribute directly to the T parameter since it does not modify the Z propagator.

Instead, $\mathcal{O}_{BW}$ gives a tree-level contribution to the $Z\gamma$ two-point function and consequently a correction to S:

$$\alpha\Delta S = \frac{1}{2}\frac{v^2}{\Lambda^2} f_{BW} \ . \tag{2.47}$$

As for the U parameter, it does not receive any contribution at tree-level from the previous operators, but only at the one loop level [49] by $\mathcal{O}_{BB}$, $\mathcal{O}_{WW}$, $\mathcal{O}_B$, $\mathcal{O}_W$ and $\mathcal{O}_{\Phi,2}$.

The electroweak precision observables also receive linear contributions from operators involving fermions, gauge bosons and the Higgs field listed in Eq.(2.18). In what follows in order to prevent the generation of too large flavor violation, we assume no generation mixing in the above operators and for simplicity we consider the operators to be generation independent.

Altogether the interactions between the gauge bosons and the fermions are given by:

$$\begin{aligned}\mathcal{L}_{Vff} = &-\frac{e}{c_W s_W} Z_\mu \sum_f \bar{\psi}^f \gamma^\mu \left(g_L^f + g_R^f\right) \psi^f \\ &-\frac{e}{\sqrt{2} s_W} W_\mu^+ \left(g_{WL}^{ud} \bar{\psi}^u \gamma^\mu P_L \psi^d + g_{WL}^{e\nu} \bar{\psi}^e \gamma^\mu P_L \psi^\nu\right) + h.c.\end{aligned} \tag{2.48}$$

At linear order, we can write the corrections to the SM couplings of the Z boson $g_{L(R)}^f$ and the W boson $g_{WL(R)}^{ff'}$ as [51]:

$$\Delta g_{L,R}^f = g_{L,R}^f \Delta g_1 + Q^f \Delta g_2 + \Delta \tilde{g}_{L,R}^f \,, \tag{2.49}$$

$$\Delta g_{WL}^{ff'} = \Delta g_W + \Delta \tilde{g}_{WL}^{ff'} \,,\ \Delta g_{WR}^{ff'} = \Delta \tilde{g}_{WR}^{ff'} \,. \tag{2.50}$$

The first contributions to the anomalous couplings of Z are given in terms of the oblique parameters,

$$\Delta g_1 = \frac{1}{2}\left(\alpha \Delta T - \frac{\delta G_F}{G_F}\right) \,, \tag{2.51}$$

$$\Delta g_2 = \frac{s_W^2}{c_{2W}}\left(c_W^2 \left(\alpha \Delta T - \frac{\delta G_F}{G_F}\right) - \frac{1}{4 s_W^2} \alpha \Delta S\right) \,, \tag{2.52}$$

and the same exercise can be done for the universal shifts in the couplings of the W boson with left-handed fermions,

$$\Delta g_W = \frac{\Delta M_W}{M_W} - \frac{1}{2}\frac{\delta G_F}{G_F} \,. \tag{2.53}$$

where, for convenience we have introduced the notation

$$\frac{\delta G_F}{G_F} \equiv \frac{v^2}{\Lambda^2}\left(-2 f_{LLLL} + f_{\Phi L,11}^{(3)} + f_{\Phi L,22}^{(3)}\right) . \tag{2.54}$$

The coupling modifications that depend on the fermion flavor are given by

$$\begin{aligned}
\Delta \tilde{g}_L^u &= -\tfrac{v^2}{8\Lambda^2}(4 f_{\Phi Q}^{(1)} - f_{\Phi Q}^{(3)}) \,, & \Delta \tilde{g}_R^u &= -\tfrac{v^2}{2\Lambda^2} f_{\Phi u}^{(1)} \,, \\
\Delta \tilde{g}_L^d &= -\tfrac{v^2}{8\Lambda^2}(4 f_{\Phi Q}^{(1)} + f_{\Phi Q}^{(3)}) \,, & \Delta \tilde{g}_R^d &= -\tfrac{v^2}{2\Lambda^2} f_{\Phi d}^{(1)} \,, \\
\Delta \tilde{g}_L^\nu &= -\tfrac{v^2}{8\Lambda^2}(4 f_{\Phi L}^{(1)} - f_{\Phi L}^{(3)}) \,, & \Delta \tilde{g}_R^\nu &= 0 \,, \\
\Delta \tilde{g}_L^e &= -\tfrac{v^2}{8\Lambda^2}(4 f_{\Phi L}^{(1)} + f_{\Phi L}^{(3)}) \,, & \Delta \tilde{g}_R^e &= -\tfrac{v^2}{2\Lambda^2} f_{\Phi e}^{(1)} \,.
\end{aligned} \tag{2.55}$$

As for the couplings of the W to fermions, in the SM we normalize the left (right)–handed couplings as 1 (0) and the corresponding shifts on these couplings due dimension–six operators are

$$\Delta g_{WL}^{ff'} = \Delta g_W + \Delta \tilde{g}_{WL}^{ff'}\,, \qquad \Delta g_{WR}^{ff'} = \Delta \tilde{g}_{WR}^{ff'}\,. \tag{2.56}$$

Finally the correction to the W mass in Eq. (2.33) can also be written in terms of the oblique parameters and the correction to the Fermi constant as

$$\frac{\Delta M_W}{M_W} = \frac{c_W^2}{2c_{2W}}\alpha\Delta T - \frac{1}{4c_{2W}}\alpha\Delta S + \frac{1}{8s_W^2}\alpha\Delta U - \frac{s_W^2}{2c_{2W}}\frac{\delta G_F}{G_F}\,. \tag{2.57}$$

The relevant subset of observables constrained by the EWPD are:

- Z observables: Γ_Z, σ_h^0, $A_l\left(\tau^{pol}\right)$, R_f^0, A_f, $A_{FB}^{0,l}$.
- W observables: M_W, Γ_W and $Br_W^{l\nu}(W \to l\nu)$,that are, respectively, its average mass, its width and the leptonic W branching ratio.

It is useful to write the departures of these observables, $\Delta OBS \equiv \frac{OBS-OBS_{SM}}{OBS}$, in terms of the corrections to the SM fermions couplings of the gauge bosons:

$$\Delta\Gamma_Z = 2\Gamma_{Z,SM}\left(\frac{\sum_f \left(g_L^f \Delta g_L^f + g_R^f \Delta g_R^f\right) N_C^f}{\sum_f \left(\left|g_L^f\right|^2 + \left|g_R^f\right|^2\right) N_C^f}\right) , \tag{2.58}$$

$$\Delta\sigma_h^0 = 2\sigma_{h,SM}^0\left(\frac{(g_L^e \Delta g_L^e + g_R^e \Delta g_R^e)}{\left|g_L^e\right|^2 + \left|g_R^e\right|^2} + \frac{\sum_q \left(g_L^q \Delta_L^q + g_R^q \Delta g_R^q\right)}{\sum_q \left(\left|g_L^q\right|^2 + \left|g_R^q\right|^2\right)} - \frac{\Delta\Gamma_Z}{\Gamma_{Z,SM}}\right) , \tag{2.59}$$

$$\Delta R_l^0 \equiv \Delta\left(\frac{\Gamma_Z^{had}}{\Gamma_Z^l}\right) = 2R_{l,SM}^0\left(\frac{\sum_q \left(g_L^q \Delta_L^q + g_R^q \Delta g_R^q\right)}{\sum_q \left(\left|g_L^q\right|^2 + \left|g_R^q\right|^2\right)} - \frac{\left(g_L^l \Delta g_L^l + g_R^l \Delta g_R^l\right)}{\left|g_L^l\right|^2 + \left|g_R^l\right|^2}\right) , \tag{2.60}$$

$$\Delta R_q^0 \equiv \Delta\left(\frac{\Gamma_Z^q}{\Gamma_Z^{had}}\right) = 2R_{q,SM}^0\left(\frac{\left(g_L^l \Delta g_L^l + g_R^l \Delta g_R^l\right)}{\left|g_L^l\right|^2 + \left|g_R^l\right|^2} - \frac{\sum_{q'} \left(g_L^{q'} \Delta_L^q + g_R^{q'} \Delta g_R^{q'}\right)}{\sum_{q'} \left(\left|g_L^{q'}\right|^2 + \left|g_R^{q'}\right|^2\right)}\right) , \tag{2.61}$$

$$\Delta A_f = 4A_{f,SM}\frac{g_L^f g_R^f}{\left|g_L^f\right|^4 - \left|g_R^f\right|^4}\left(g_R^f \Delta g_L^f - g_L^f \Delta g_R^f\right) , \tag{2.62}$$

$$\Delta P_\tau^{pol} = \Delta A_l , \tag{2.63}$$

$$\Delta A_{FB}^{0,f} = A_{FB,SM}^{0,f}\left(\frac{\Delta A_l}{A_l} + \frac{\Delta A_f}{A_f}\right) , \tag{2.64}$$

$$\Delta\Gamma_W = \Gamma_{W,SM}\left(\frac{4}{3}\Delta g_{WL}^{ud} + \frac{4}{3}\Delta g_{WL}^{e\nu}\right) , \tag{2.65}$$

$$\Delta Br_W^{e\nu} = Br_{W,SM}^{e\nu}\left(-\frac{4}{3}\Delta g_{WL}^{ud} + \frac{4}{3}\Delta g_{WL}^{e\nu}\right) . \tag{2.66}$$

Notice that $\mathcal{O}_{\Phi ud,ij}^{(1)}$ contributes only to the right-handed coupling of the W, therefore it does not interfere with the SM amplitudes and consequently is not constrained by the EWPD at the linear order employed in the analysis. Notwithstanding $pp \to W^+W^-$ and $pp \to ZW^\pm$ at LHC can be used to study $\mathcal{O}_{\Phi ud,ij}^{(1)}$ at quadratic order as we will see in Chapter 4.

As mentioned above the set of operators introduced in Sec. 2.1 is not independent but they are related by the EOM. Since we truncate our expansion in effective operators at dimension–six it is only necessary to consider the SM EOM. In particular, the EOM for the Higgs field and the EW gauge bosons lead to three relations

between the operators:

$$2\mathcal{O}_{\Phi,2} + 2\mathcal{O}_{\Phi,4} = \sum_{ij} \left(y^e_{ij} \mathcal{O}^\dagger_{e\Phi\, ij} + y^u_{ij} \mathcal{O}_{u\Phi\, ij} + y^d_{ij} \mathcal{O}^\dagger_{d\Phi\, ij} + h.c. \right)$$
$$+2\mu_0 \left(\Phi^\dagger \Phi \right) + 12\lambda_0 \mathcal{O}_{\Phi,3} \ , \tag{2.67}$$

$$2\mathcal{O}_B + \mathcal{O}_{BW} + \mathcal{O}_{BB} + g'^2 \left(\mathcal{O}_{\Phi,1} - \frac{1}{2} + \mathcal{O}_{\Phi,2} \right) =$$
$$-\frac{g'^2}{12} \sum_i \left(-3\mathcal{O}^{(1)}_{\Phi L,ii} + \mathcal{O}^{(1)}_{\Phi Q,ii} - 6\mathcal{O}^{(1)}_{\Phi e,ii} + 4\mathcal{O}^{(1)}_{\Phi u,ii} - 2\mathcal{O}^{(1)}_{\Phi d,ii} \right) , \tag{2.68}$$

$$2\mathcal{O}_W + \mathcal{O}_{BW} + \mathcal{O}_{WW} + g^2 \left(\mathcal{O}_{\Phi,4} - \frac{1}{2}\mathcal{O}_{\Phi,2} \right)$$
$$= -\frac{g^2}{4} \sum_i \left(\mathcal{O}^{(3)}_{\Phi L,ii} + \mathcal{O}^{(3)}_{\Phi Q,ii} \right) \ . \tag{2.69}$$

These constraints allow for the elimination of three operators of those listed in Sec. 2.1.

At this point we are faced with the decision of which operators to leave in the basis to be used in the analysis. First we need to be sure that there is no combination of the anomalous operators whose contribution at the tree level to the electroweak precision observables (EWPO) cancels out, *i.e.*, we need to avoid what has been referred in the literature as blind directions [17, 52]. In general even when considering all LEP observables, there are always two blind directions [30]:

$$\begin{aligned} \mathcal{O}_{blind\,1} &= g'^2 \left(\mathcal{O}_{\Phi,1} - \frac{1}{4} \sum_i \mathcal{O}^{(1)}_{\Phi L,ii} - \frac{1}{2} \mathcal{O}^{(3)}_{\Phi L,ii} \right) + \mathcal{O}_{BW} \ , \\ \mathcal{O}_{blind\,2} &= \mathcal{O}_{BW} + \sum_i \mathcal{O}^{(3)}_{\Phi L,ii} \frac{g^2}{4} \ . \end{aligned} \tag{2.70}$$

This means that any two linear combinations of Eq. (2.70) do not contribute to the EWPO.

There is a deep relation between operators that do not lead to any tree level contribution to the EWPO and blind directions. In fact, if the elimination of one of these operators using the EOM leads to a combination of operators, each of which contributes at tree level to the EWPO, then that combination defines a blind direction because it has the same S matrix element than the original operator and therefore it should have no impact on the EWPO [17].

As an example of it, we have the operator $\mathcal{O}_{\Phi,2}$. This operator does not contribute to the EWPO, which means that we cannot constrain its Wilson coefficient,

therefore it is a blind operator. If we use the EOMs (2.67)–(2.68) we can write

$$\begin{aligned} 3g^2\mathcal{O}_{\Phi,2} = \Bigg[& 2\mathcal{O}_{BW} + 4\mathcal{O}_W + 2\mathcal{O}_{WW} + \frac{g^2}{2}\sum_i \left(\mathcal{O}^{(3)}_{\Phi L,ii} + \mathcal{O}^{(3)}_{\Phi Q,ii}\right) \\ & + g^2 \left(\sum_{ij} \left(y^e_{ij}(\mathcal{O}_{e\Phi,ij})^\dagger + y^u_{ij}\mathcal{O}_{u\Phi,ij} + y^d_{ij}(\mathcal{O}_{d\Phi,ij})^\dagger + \text{h.c.} \right) \right. \\ & \left. + 2\mu_0 \left(\Phi^\dagger\Phi\right) + 12\lambda_0\mathcal{O}_{\Phi,3} \right) \Bigg]. \end{aligned} \tag{2.71}$$

Only the operators $\mathcal{O}_{BW}$ and $\sum_i \mathcal{O}^{(3)}_{\Phi L,ii}$ contribute to the leptonic observables, therefore the effect of $\mathcal{O}_{\Phi,2}$ is equivalent to

$$\frac{2}{3g^2}\left(\mathcal{O}_{BW} + \frac{g^2}{4}\sum_i \mathcal{O}^{(3)}_{\Phi L,ii}\right) \tag{2.72}$$

which defines the blind direction in Eq. (2.70).

Altogether Eqs. (2.67)–(2.69) allow for the elimination of three of the operators. We need to take into account which data is going to be used to constrain the Wilson coefficients from the operators. We want a basis that allow us to take full advantage of the TGC, the Higgs data and the EWPD, by keeping all the operators contributing to TGC and at least one operator per each new Lorentz structure in Eq. (2.78). Therefore, we will remove $\mathcal{O}_{\Phi,4}$ and both $\mathcal{O}^{(3)}_{\Phi L,ii}$ and $\mathcal{O}^{(1)}_{\Phi L,ii}$ to avoid blind directions (see Eq. (2.70)).

2.4 Triple Gauge Vertices

Within the framework of the SM, the trilinear vector-boson couplings are completely determined by the $SU(2)_L \otimes U(1)_Y$ symmetry. In the SM there are subtle cancellations between contributions from s-channel γ and Z exchange and t-channel fermion exchange that maintain perturbative unitarity. If there exists NP at a higher scale, the form of these interactions can be changed, and consequently spoils the cancellations that impose unitarity conservation, which makes the diboson production a stringent test of the Standard Model.

The most general parametrization that describes the WWZ and $WW\gamma$, under our assumptions of C and P conservation as well as assuming at least one W boson

on-shell, can be cast in the following Lorentz invariant form [43]:

$$\begin{aligned}\mathcal{L}_{WWV} &= -ig_{WWV}\left\{g_1^V\left(W^+_{\mu\nu}W^{-\mu}-W^{+\mu}W^-_{\mu\nu}\right)V^\nu + k_V W^+_\mu W^-_\nu V^{\mu\nu}\right. \\ &\left. + \frac{\lambda_V}{M_W^2}W^+_{\lambda\mu}W^{-\mu}_\nu V^{\nu\lambda}\right\}\ , \end{aligned} \tag{2.73}$$

where $V_{\mu\nu}=\partial_\mu V_\nu-\partial_\nu V_\mu$, $W_{\mu\nu}=\partial_\mu W_\nu-\partial_\nu W_\mu$, $\tilde{V}_{\mu\nu}=\epsilon^{\mu\nu\rho\sigma}V_{\mu\nu}$ and $V=Z,\gamma$. By definition, $g_{WW\gamma}\equiv e=gs_W$ and $g_{WWZ}=gc_W$ and electromagnetic invariance requires $g_1^\gamma=1$, such that $s_W\equiv g'/\sqrt{g^2+g'^2}=\sin\theta_W$ stands for the tree level sine of the SM weak mixing angle.

These effective couplings were constrained by results from LEP2 and Tevatron with a good precision [44].

Any departure from the SM, while studying the diboson production, can be parametrized as a shift of the dimensionless couplings in Eq. (2.73),

$$g_i^V \to g_i^{V(SM)} + \Delta g_i^V\ , \tag{2.74}$$

such that the SM values of the couplings are $g_1^{Z(SM)}=k_\gamma^{(SM)}=k_Z^{(SM)}=1$.

This parametrization is traditionally used by the experimental collaborations at LEP, Tevatron and LHC to measure the triple gauge vertices. Notwithstanding, we can relate the dimensionless couplings with the new dimension–six operators that parametrize our ignorance of what happens at a higher scale. First, we need to know which operators are relevant for the diboson HISZ basis, the relevant pure bosonic operators that conserve C and P are:

$$\begin{aligned}&\mathcal{O}_W=(D_\mu\Phi)^\dagger\widehat{W}^{\mu\nu}(D_\nu\Phi)\ ,\quad \mathcal{O}_B=(D_\mu\Phi)^\dagger\widehat{B}^{\mu\nu}(D_\nu\Phi)\ ,\\ &\mathcal{O}_{BW}=\Phi^\dagger\widehat{B}_{\mu\nu}\widehat{W}^{\mu\nu}\Phi\ ,\qquad \mathcal{O}_{\Phi,1}=(D_\mu\Phi)^\dagger\Phi\Phi^\dagger(D^\mu\Phi)\\ &\mathcal{O}_{WWW}=\mathrm{Tr}[\widehat{W}^\nu_\mu\widehat{W}^\rho_\nu\widehat{W}^\mu_\rho]\ .\end{aligned} \tag{2.75}$$

After renormalization and redefinition of the EW fields, coupling constants and masses as described in Sec.2.2, any deviation of the dimensionless couplings can be expressed in terms of the linear dimension–six operators Wilson coefficients:

$$\begin{aligned}\Delta g_1^Z &= \frac{g^2v^2}{8c_W^2\Lambda^2}\left(f_W+2\frac{s_W^2}{c_{2W}}f_{BW}\right)-\frac{1}{4c_{2W}}f_{\Phi,1}\frac{v^2}{\Lambda^2}\ ,\\ \Delta k_\gamma &= \frac{g^2v^2}{8\Lambda^2}\left(f_W-f_B-2f_{BW}\right)\ ,\\ \Delta k_Z &= \frac{g^2v^2}{8c_W^2\Lambda^2}\left(c_W^2f_W-s_W^2f_B+\frac{4s_W^2c_W^2}{c_{2W}}f_{BW}\right)-\frac{1}{4c_{2W}}f_{\Phi,1}\frac{v^2}{\Lambda^2}\ ,\\ \lambda_\gamma=\lambda_Z &= \frac{3g^2M_W^2}{2\Lambda^2}f_{WWW}\ .\end{aligned} \tag{2.76}$$

It is interesting to notice that the number of independent parameters is not five but three, since the following relation holds,

$$\lambda_Z = \lambda_\gamma \ , \quad \Delta k_z = \Delta g_1^Z - \frac{s_W^2}{c_W^2}\Delta k_\gamma \ . \tag{2.77}$$

2.5 Higgs Vertices

As the only new state discovered by the LHC, the Higgs boson and its interactions may unveil some hints about the origin of the EWSB. Analogous to the TGC, the most general parametrization that describes the Higgs interactions with the gauge bosons, under our assumptions of C and P conservation as well as assuming the Higgs boson on-shell, is given by the following Lorentz invariant form in the unitary gauge:

$$\begin{aligned}\mathcal{L}_{HVV} \ = \ & g_{Hgg}G^a_{\mu\nu}G^{a\mu\nu} + g_{H\gamma\gamma}A_{\mu\nu}A^{\mu\nu}H \\ & + g^{(1)}_{HZ\gamma}A_{\mu\nu}Z^\mu\partial^\nu H + g^{(2)}_{HZ\gamma}A_{\mu\nu}Z^{\mu\nu}H \\ & + g^{(1)}_{HZZ}Z_{\mu\nu}Z^\mu\partial^\nu H + g^{(2)}_{HZZ}Z_{\mu\nu}Z^{\mu\nu}H + g^{(3)}_{HZZ}Z_\mu Z^\mu H \\ & + g^{(1)}_{HWW}\left(W^+_{\mu\nu}W^{-\mu}\partial^\nu H + \text{h.c.}\right) + g^{(2)}_{HWW}W^+_{\mu\nu}W^{-\mu\nu}H \\ & + g^{(3)}_{HWW}W^+_\mu W^{-\mu}H\end{aligned} \tag{2.78}$$

with $V = A, W, Z, G$. It turns out that, following the same procedure as in Eq. (2.74), where the dimensionless couplings are separated in terms of its SM value and a shift introduced by the NP contribution, the tree-level SM value vanishes for every dimensionless coupling, with the exception of two cases:

$$g^{(3)SM}_{HZZ} = \frac{M_Z^2}{v} \ , \quad g^{(3)SM}_{HWW} = \frac{2M_Z^2c_W^2}{v} \ . \tag{2.79}$$

In the same way as TGC interactions, we can write the shifts of the dimensionless couplings in Eq. (2.78) as functions of contributions from linear dimension–six operators. Besides the operators presented in Eq. (2.13), we also have the following CP even operators contributing to the Higgs interactions with the gauge bosons:

$$\begin{aligned}&\mathcal{O}_{GG} = \Phi^\dagger\Phi\ G^a_{\mu\nu}G^{a\mu\nu} && , \quad \mathcal{O}_{WW} = \Phi^\dagger\hat{W}_{\mu\nu}\hat{W}^{\mu\nu}\Phi \ , \\ &\mathcal{O}_{BB} = \Phi^\dagger\hat{B}_{\mu\nu}\hat{B}^{\mu\nu}\Phi && , \quad \mathcal{O}_{\Phi,2} = \tfrac{1}{2}\partial^\mu\left(\Phi^\dagger\Phi\right)\partial_\mu\left(\Phi^\dagger\Phi\right) \ , \\ &\mathcal{O}_{\Phi,4} = (D_\mu\Phi)^\dagger(D^\mu\Phi)\left(\Phi\Phi^\dagger\right) \ .\end{aligned} \tag{2.80}$$

In deriving the form of the couplings in Eq. (2.78) we account for renormalization and redefinition of the EW fields, coupling constants and masses as described

in Sec.2.2. Altogether the dimension–six effective operators in Eq. (2.13) and Eq. (2.80) give rise to the following anomalous couplings:

$$\Delta g_{Hgg} = -\frac{\alpha_s}{8\pi} f_{GG} \frac{v}{\Lambda^2} \,, \tag{2.81}$$

$$\Delta g_{H\gamma\gamma} = -\frac{e^2}{4} \left(f_{BB} + f_{WW} - f_{BW}\right) \frac{v}{\Lambda^2} \,, \tag{2.82}$$

$$\Delta g^{(1)}_{HZ\gamma} = \frac{e^2}{2 s_{2W}} \left(f_W - f_B\right) \frac{v}{\Lambda^2} \,, \tag{2.83}$$

$$\Delta g^{(2)}_{HZ\gamma} = \frac{e^2 c_W}{4 s_W} \left(2 \frac{s_W^2}{c_W^2} f_{BB} - 2 f_{WW} + \frac{c_{2W}}{c_W^2} f_{BW}\right) \frac{v}{\Lambda^2} \,, \tag{2.84}$$

$$\Delta g^{(1)}_{HZZ} = \frac{e^2}{4 c_W^2} \left(\frac{c_W^2}{s_W^2} f_W + f_B\right) \frac{v}{\Lambda^2} \,, \tag{2.85}$$

$$\Delta g^{(2)}_{HZZ} = \frac{e^2 c_W^2}{4 s_W^2} \left(\frac{s_W^4}{c_W^4} f_{BB} + f_{WW} + \frac{s_W^2}{c_W^2} f_{BW}\right) \frac{v}{\Lambda^2} \,, \tag{2.86}$$

$$\Delta g^{(3)}_{HZZ} = \frac{M_Z^2}{4} \left(f_{\Phi,1} - 2 f_{\Phi,2} + 2 f_{\Phi,4}\right) \frac{v}{\Lambda^2} \,, \tag{2.87}$$

$$\Delta g^{(1)}_{HWW} = \frac{e^2}{4 s_W^2} f_W \frac{v}{\Lambda^2} \,, \tag{2.88}$$

$$\Delta g^{(2)}_{HWW} = -\frac{e^2}{2 s_W^2} f_{WW} \frac{v}{\Lambda^2} \,, \tag{2.89}$$

$$\Delta g^{(3)}_{HWW} = \frac{M_Z^2 c_W^2}{4} \left[\frac{-2\left(3 c_W^2 - s_W^2\right)}{c_{2W}} f_{\Phi,1} - 4 f_{\Phi,2} + 4 f_{\Phi,4} + \frac{4 e^2}{c_{2W}} f_{BW}\right] \frac{v}{\Lambda^2} \,, \tag{2.90}$$

where $c_{2W} = \sin 2\theta_W$. For convenience, the Wilson coefficient f_{GG} of the gluon-gluon operator was rescaled with $\alpha_s/(8\pi)$ to include a loop suppression factor such that its limits are of the same order of the Wilson coefficients of other operators. Also in the expressions above, for completeness we have included the contribution from $f_{\Phi,4}$ although as explained in Sec. 2.3 we will remove this operator from our final basis by making use of EOM.

Notice that the canonical coefficients f_W and f_B from TGC also contribute to Higgs interactions. Such correlation is due to the fact that the Higgs is a doublet charged under $SU(2)_L$, and would be absent in a chiral EFT, where one considers a non-linear realization of the SM gauge symmetry breaking with a composite Higgs [45]. Here comes the importance of the complementarity between different sources of data to constrain the dimension–six operators. In [46] it was shown that Higgs boson production data at the LHC and Tevatron give rise to strong bounds

on TGC, which are complementary to the bounds from the direct study of these couplings in gauge boson production.

Concerning the Higgs interactions with fermions and recalling that in the SM the Yukawa interactions take the form

$$\mathcal{L}_{Yuk} = -y^e_{ij}\bar{L}_i\Phi e_{Rj} - y^d_{ij}\bar{Q}_i\Phi d_{Rj} - y^u_{ij}\bar{Q}_i\tilde{\Phi}u_{Rj} + \text{h.c.}\,, \tag{2.91}$$

where y^f is a 3×3 matrix, we find that the operators in Eq. (2.17) modify the Yukawa interactions. So after spontaneous symmetry breaking and renormalization of fermion masses, mixing and Higgs wave function, the $H\bar{f}f$ couplings can be written as

$$\mathcal{L}_{Hff} = g^f_{Hij}\bar{f}_{L_i}f_{R_j}H + \text{h.c.}\,, \tag{2.92}$$

which in terms of the dimension–six Wilson coefficients has the following couplings

$$g^f_{Hij} = -\frac{m^f_i}{v}\delta_{ij}\left[1 - \frac{v^2}{4\Lambda^2}\left(f_{\Phi,1} + 2f_{\Phi,2}\right)\right] + \frac{v^2}{\sqrt{2}\Lambda^2}f_{f\Phi,ij}\,. \tag{2.93}$$

We have denoted m^f_i as the physics masses of the fermions and $f_{(L)R_i}$ as the respective mass eigenstate, with $f = u, d, e$. The Wilson coefficients $f_{f\Phi,ij}$ in Eq. (2.93) are 3×3 matrices in the generation space and correspond to the operators in the mass basis.

We can easily identify the terms in Eq. (2.93) proportional to the fermion masses as the SM-like interactions, whereas the terms proportional to $f_{f\Phi,ij}$ correspond to the new interactions and are not necessarily flavor diagonal in the mass basis (unless $f_{f\Phi} \propto y^f$).

In the Chapter 4, we consider only the diagonal couplings of Higgs to the third family and also to muon pairs, which are the only ones being currently tested at LHC.

2.6 Dipole-like Couplings

Finally, we present the last set of dimension–six operators, relevant for the analysis on the following chapters, which are the operators containing electroweak dipole couplings to light quarks and which for simplicity we refer to as dipole operators in what follows. More specifically, these operators are

$$\begin{aligned} \mathcal{O}_{uW,ij} &= i\overline{Q}_i\sigma^{\mu\nu}u_{R,j}\widehat{W}_{\mu\nu}\tilde{\Phi} \quad , & \mathcal{O}_{uB,ij} &= i\overline{Q}_i\sigma^{\mu\nu}u_{R,j}\widehat{B}_{\mu\nu}\tilde{\Phi} \quad , \\ \mathcal{O}_{dW,ij} &= i\overline{Q}_i\sigma^{\mu\nu}d_{R,j}\widehat{W}_{\mu\nu}\Phi \quad , & \mathcal{O}_{dB,ij} &= i\overline{Q}_i\sigma^{\mu\nu}u_{R,j}\widehat{B}_{\mu\nu}\Phi \quad . \end{aligned} \tag{2.94}$$

For simplicity, we will assume that the Wilson coefficient of the dipole operators are flavour diagonal and family independent so they induce dipole-like couplings to photons, Z's and $W^{\pm}$'s of the form

$$\begin{aligned}\mathcal{L} = &-\frac{e\,v}{\sqrt{2}}\left[\frac{F_{f\gamma}}{\Lambda^2}\bar{f}\,\sigma^{\mu\nu}\,f\,\partial_\mu A_\nu \;+\; \frac{F_{fZ}}{\Lambda^2}\,\bar{f}\,\sigma^{\mu\nu}\,f\,\partial_\mu Z_\nu\right] \\ &- ev\left[\bar{f}\,\sigma^{\mu\nu}\left(\frac{F^L_{ff'W}}{\Lambda^2}\,P_L \,+\, \frac{F^R_{ff'W}}{\Lambda^2}\,P_R\right) f'\,\partial_\mu W^+_\nu \;+\; \text{h.c.}\right]\end{aligned} \tag{2.95}$$

where $P_{L(R)}$ is the left- (right-)handed chiral projector and

$$\begin{aligned}\frac{F_{u\gamma}}{\Lambda^2} &= \frac{f_{uW}}{\Lambda^2} + \frac{f_{uB}}{\Lambda^2}\;, \qquad \frac{F_{uZ}}{\Lambda^2} = \frac{c_W}{s_W}\frac{f_{uW}}{\Lambda^2} - \frac{s_W}{c_W}\frac{f_{uB}}{\Lambda^2}\;, \\ \frac{F_{d\gamma}}{\Lambda^2} &= \frac{f_{dW}}{\Lambda^2} - \frac{f_{dB}}{\Lambda^2}\;, \qquad \frac{F_{dZ}}{\Lambda^2} = \frac{c_W}{s_W}\frac{f_{dW}}{\Lambda^2} + \frac{s_W}{c_W}\frac{f_{dB}}{\Lambda^2}\;, \\ \frac{F^R_{udW}}{\Lambda^2} &= \frac{1}{s_W}\frac{f_{uW}}{\Lambda^2}\;, \qquad \frac{F^L_{udW}}{\Lambda^2} = \frac{1}{s_W}\frac{f_{dW}}{\Lambda^2}\;.\end{aligned} \tag{2.96}$$

The contributions of the dipole operators to the decay widths of the weak gauge bosons are:

$$\frac{\Delta\Gamma^Z_{ff}}{\Gamma^Z_{ff}} = \frac{1}{g_L^{f\,2} + g_R^{f\,2}}\frac{e^2v^4}{8\Lambda^4}|F_{fZ}|^2\;,\; \frac{\Delta\Gamma^W_{ud}}{\Gamma^W_{ud}} = \frac{e^2v^4}{4\Lambda^4}(|F^L_{udW}|^2+|F^R_{udW}|^2)\;. \tag{2.97}$$

The electroweak dipole operators are relevant since they contribute to any process at the LHC initiated by the quark and antiquark components of the colliding protons, which means that they take part in the diboson production. We will test their possible effect on the extracted information on the gauge boson self-couplings and also quantify the constrains that the analysis can impose in the Wilson coefficients of these operators.

2.7 Summary

In this Chapter, we lay the foundations of our analysis framework. It was discussed how the SM can be described as an effective field theory at low energies, due to the lack of experimental evidence of any new light state.

The machinery of the EFT applied to the SM consists in the addition of a new set of operators, which we chose to write in the so called HISZ basis. The new operators change the couplings, wave function, and mass renormalization for the SM fields. We have shown how to account those effects and then, we found the Lorentz structures generated for the TGC and Higgs interactions with gauge bosons and

fermions. By also including the EWPO, we have the complete analysis framework that shall be used in the next chapters to constrain the Wilson coefficients of the dimension–six operators.

At this point there are several phenomenological aspects about the new operators that we need to emphasize. One of the first things that stands out is the fact that dimension–six operators do not give rise to anomalous TGC among neutral gauge bosons. It is also interesting to notice that the dimension–six operators containing gauge field strengths $\mathcal{O}_B$, $\mathcal{O}_W$, $\mathcal{O}_{WW}$, $\mathcal{O}_{BB}$ provide a rich phenomenology, in the sense that they contribute to the interactions between gauge bosons and the Higgs state with new Lorentz structures. Furthermore, $\mathcal{O}_B$, $\mathcal{O}_W$ contribute to both Higgs interactions and TGC, which shows the importance of complementary searches to constrain the Wilson coefficients being studied. In Chapter 4 we will use different sources of data to constrain the Wilson coefficients in our basis. On the other hand, the operator $\mathcal{O}_{WWW}$ only contributes to the diboson production, therefore its Wilson coefficient can only be constrained by measuring the TGC.

In addition, $\mathcal{O}_{BW}$, $\mathcal{O}_{WW}$, $\mathcal{O}_{BB}$ operators also contribute at the tree level to the diphoton decay of the Higgs boson. This channel, which is a loop decay in the SM, is currently the decay mode measured with the highest precision. Taking into account that $\mathcal{O}_{BW}$ contributes to the S parameter and so its Wilson coefficient is really constrained, we expect a strong correlation between the Wilson coefficients of $\mathcal{O}_{WW}$, $\mathcal{O}_{BB}$.

Meanwhile, $\mathcal{O}_{BW}$, $\mathcal{O}_{\Phi,1}$, $\mathcal{O}_{\Phi,2}$ contributions are ubiquitous and stem from their effect on the finite renormalization of the SM fields and couplings once the Lagrangian is canonically normalized.

The Wilson coefficient of the operator $\mathcal{O}_{GG}$ contains not only contributions of new possible colored states appearing in the loop connecting gluon pairs to the Higgs, but also the effects of the anomalous operators that modify the SM Yukawa coupling to bottom and top quarks running in the loop. This operator is especially important, since it contributes at tree-level to one of the main production channels of the Higgs, the gluon fusion.

We summarize the anomalous couplings of gauge and Higgs bosons induced the bosonic dimension–six operators in Table 2.1.

The fermionc operators in Eq. (2.18) mainly contribute to the fermion interactions with the gauge bosons and to the EWPO. Therefore, we would expect that they are really constrained and can hardly have any impact on the LHC processes. Notwithstanding, in Chapter 3 we discuss how the analysis of the diboson pro-

	ZWW	γWW	$H\gamma\gamma$	HZZ	$HZ\gamma$	HWW
$\mathcal{O}_{WWW}$	X	X				
$\mathcal{O}_{W}$	X	X		X	X	X
$\mathcal{O}_{B}$	X	X		X	X	
$\mathcal{O}_{BW}$	X	X	X	X	X	X
$\mathcal{O}_{WW}$			X	X	X	X
$\mathcal{O}_{BB}$			X	X	X	
$\mathcal{O}_{\Phi,1}$	X			X		X
$\mathcal{O}_{\Phi,2}$				X		X

Table 2.1: Anomalous couplings of gauge and Higgs bosons induced the dimension–six operators the we consider.

duction is changed when including these fermionic operators. In Table 2.2 we summarize the anomalous couplings to fermions generated by the dimension–six fermionic operators (and the omnipresent $\mathcal{O}_{BW}$, $\mathcal{O}_{\Phi,1}$, $\mathcal{O}_{\Phi,2}$). The same discussion is applied to the light-quark dipole operators. We will see in Chapter 5 how the LHC is already better than the LEP to constrain the Wilson coefficients of these operators.

	$H\bar{f}f$	$Z\bar{q}q$	$Z\bar{l}l$	$W\bar{u}d$	$W\bar{l}\nu$
$\mathcal{O}_{BW}$		X	X	X	X
$\mathcal{O}_{\Phi,1}$	X	X	X	X	X
$\mathcal{O}_{\Phi,2}$	X				
$\mathcal{O}^{(1)}_{\Phi Q}$, $\mathcal{O}^{(1)}_{\Phi u}$, $\mathcal{O}^{(1)}_{\Phi d}$		X			
$\mathcal{O}^{(3)}_{\Phi Q}$,		X		X	
$\mathcal{O}^{(1)}_{\Phi e}$,			X		
$\mathcal{O}^{(1)}_{\Phi ud}$				X	
$\mathcal{O}_{u\Phi,33}$	X (if $f=t$)				
$\mathcal{O}_{d\Phi,33}$	X (if $f=b$)				
$\mathcal{O}_{e\Phi,33}$	X (if $f=\tau$)				
$\mathcal{O}_{u\Phi,22}$	X (if $f=\mu$)				

Table 2.2: Anomalous couplings to fermions generated by the dimension–six operators considered in the analysis.

In summary and after eliminating some of the redundant operators using EOM, we can write the different parts of the total effective Lagrangian in the following

way:

$$\mathcal{L}_{\rm eff} = \mathcal{L}_{\rm SM} + \mathcal{L}_{\rm eff}^{\rm EWPD} + \mathcal{L}_{\rm eff}^{\rm TGC} + \mathcal{L}_{\rm eff}^{\rm Yuk} + \mathcal{L}_{\rm eff}^{\rm HVV} + \mathcal{L}_{\rm eff}^{\rm DIP} \ , \tag{2.98}$$

where

$$\begin{aligned}\mathcal{L}_{\rm eff}^{\rm EWPD} &= \frac{f_{\Phi Q}^{(1)}}{\Lambda^2}\mathcal{O}_{\Phi Q}^{(1)} + \frac{f_{\Phi Q}^{(3)}}{\Lambda^2}\mathcal{O}_{\Phi Q}^{(3)} + \frac{f_{\Phi u}^{(1)}}{\Lambda^2}\mathcal{O}_{\Phi u}^{(1)} + \frac{f_{\Phi d}^{(1)}}{\Lambda^2}\mathcal{O}_{\Phi d}^{(1)} + \frac{f_{\Phi e}^{(1)}}{\Lambda^2}\mathcal{O}_{\Phi e}^{(1)} \\ &+ \frac{f_{BW}}{\Lambda^2}\mathcal{O}_{BW} + \frac{f_{\Phi,1}}{\Lambda^2}\mathcal{O}_{\Phi,1} + \frac{f_{LLLL}}{\Lambda^2}\mathcal{O}_{LLLL} \ . \end{aligned} \tag{2.99}$$

$$\mathcal{L}_{eff}^{TGC} = \frac{f_W}{\Lambda^2}\mathcal{O}_W + \frac{f_B}{\Lambda^2}\mathcal{O}_B + \frac{f_{WWW}}{\Lambda^2}\mathcal{O}_{WWW} + \frac{f_{\Phi,ud}}{\Lambda^2}\mathcal{O}_{\Phi ud,ij}^{(1)} \ , \tag{2.100}$$

$$\mathcal{L}_{eff}^{HVV} = \frac{f_{GG}}{\Lambda^2}\mathcal{O}_{GG} + \frac{f_{WW}}{\Lambda^2}\mathcal{O}_{WW} + \frac{f_{BB}}{\Lambda^2}\mathcal{O}_{BB} + \frac{f_{\Phi,2}}{\Lambda^2}\mathcal{O}_{\Phi,2} \ , \tag{2.101}$$

$$\mathcal{L}_{\rm eff}^{\rm Yuk} = \frac{f_\mu m_\mu}{\Lambda^2 v}\mathcal{O}_{e\Phi,22} + \frac{f_\tau m_\tau}{\Lambda^2 v}\mathcal{O}_{e\Phi,33} + \frac{f_b m_b}{\Lambda^2 v}\mathcal{O}_{d\Phi,33} + \frac{f_t m_t}{\Lambda^2 v}\mathcal{O}_{u\Phi,33} + \text{ h.c.} \tag{2.102}$$

$$\begin{aligned}\mathcal{L}_{\rm eff}^{\rm DIP} &= \frac{f_{uB}}{\Lambda^2}\sum_{i=1,2}\mathcal{O}_{uB,ii} + \frac{f_{uW}}{\Lambda^2}\sum_{i=1,2}\mathcal{O}_{uW,ii} + \frac{f_{dB}}{\Lambda^2}\sum_{i=1,2}\mathcal{O}_{uB,ii} \\ &+ \frac{f_{dW}}{\Lambda^2}\sum_{i=1,2}\mathcal{O}_{uW,ii} + \text{h.c.}\end{aligned} \tag{2.103}$$

We decided to include the $\mathcal{O}_{\Phi,ud}^{(1)}$ in the TGC effective Lagrangian because it does not interfere with the SM contributions to the EWPD observables at the order considered in the analyses of the next chapters, which is linear. As for the operators $\mathcal{O}_{BW}$ and $\mathcal{O}_{\Phi,1}$, they are included in the EWPD effective Lagrangian due to the fact that S and T parameters are responsible for the stringent constrains on their Wilson coefficients but their contribution due to the finite renormalization effects. We notice that we make this labeling of the sectors of the full effective Lagrangian for convenience but all operators contributing to given set of observables are always consistently considered in the analyses presented in the next Chapters.

Chapter 3

Approaching the Precision Frontier with LHC: Effect of Fermionic Operators on the Gauge Legacy of the LHC Run 1

Within the framework of the SM, the trilinear and quartic vector-boson couplings are completely determined by the $SU(2)L \otimes U(1)_Y$ gauge symmetry. Therefore, the scrutiny of these interactions can either lead to an additional confirmation of the SM or give some hint on the existence of new phenomena at a higher scale.

The TGCs have been measured using data from e^+e^- and pp colliders in the hope of finding any deviation from the SM. The TGCs were for the first time directly probed at LEP2 [53] and also in LHC, where the ATLAS and CMS collaborations studies of the W^+W^- [54, 55] and $W^\pm Z$ [56, 57] productions were used to constrain the TGCs. The combined analysis of the LHC Run 1 production of electroweak gauge boson pairs performed in Ref. [32] showed that the TGC measurement is already dominated by the LHC data with better precision than the previous results from LEP2 [53].

Because of the strong constrains from the EWPD, it was always assumed TGCs dominance, *i.e.*, the assumption that NP effects other than anomalous TGC are negligible in diboson production and therefore the analysis could be cast in terms of an effective triple gauge vertex (TGV) parametrized as Eq. (2.73). This hypothesis is not obviously satisfied for arbitrary NP scenarios. Furthermore in a set of publications [58, 59] it was estimated that changes in the couplings of gauge bosons to

fermions, even within the constraints from EWPD, could lead to modifications of the kinematical distributions in gauge boson pair production at LHC of comparable size to the ones stemming from the purely anomalous TGV.

This motivate us to extend the analyses of diboson production performed in Ref. [32], where only the effects of NP stemming from pure dimension–six bosonic operators was considered, with the inclusion of the effects associated to the full set of operators potentially contributing to these processes, which involves also the fermionic operators (2.18) as well as including $\mathcal{O}_{BW}$ and $\mathcal{O}_{\phi 1}$ (these operators were also ignored due to the strong constrains on the S and T parameters). So in this Chapter we revisit the analyses of the LHC Run 1 data on the W^+W^- and $W^\pm Z$ production to quantify the impact of anomalous couplings of gauge bosons to fermion pairs on the TGC bounds when consistently including in the statistical analysis also the EWPD.

3.1 Theoretical Framework

The effective Lagrangian relevant for study the TGCs from the LHC Run 1 data on diboson production reads

$$\begin{aligned}\mathcal{L}_{eff} = \mathcal{L}_{SM} &+ \frac{f_{WWW}}{\Lambda^2}\mathcal{O}_{WWW} + \frac{f_W}{\Lambda^2}\mathcal{O}_W + \frac{f_B}{\Lambda^2}\mathcal{O}_B + \frac{f_{BW}}{\Lambda^2}\mathcal{O}_{BW} \\ &+ \frac{f_{\Phi,1}}{\Lambda^2}\mathcal{O}_{\Phi,1} + \frac{f_{\Phi Q}^{(1)}}{\Lambda^2}\mathcal{O}_{\Phi Q}^{(1)} + \frac{f_{\Phi Q}^{(3)}}{\Lambda^2}\mathcal{O}_{\Phi Q}^{(3)} + \frac{f_{\Phi u}^{(1)}}{\Lambda^2}\mathcal{O}_{\Phi u}^{(1)} + \frac{f_{\Phi d}^{(1)}}{\Lambda^2}\mathcal{O}_{\Phi d}^{(1)} \\ &+ \frac{f_{\Phi e}^{(1)}}{\Lambda^2}\mathcal{O}_{\Phi e}^{(1)} + \frac{f_{LLLL}}{\Lambda^2}\mathcal{O}_{LLLL}\,, \end{aligned} \tag{3.1}$$

where we have included the fermionic operators as well as the ubiquitous operators $\mathcal{O}_{BW}$ and $\mathcal{O}_{\phi 1}$. The inclusion of the Higgs interactions is done in Chapter 4. Here the main purpose is to quantify how the couplings of gauge bosons to fermions, even within the constraints EWPD, could lead to modifications of the kinematical distributions in gauge boson pair production.

First we notice that the anomalous TGC as well as the anomalous gauge bosons interactions to quarks modify the high energy behavior of the scattering of quark pairs into two electroweak gauge bosons since the anomalous interactions can spoil the cancellations built in the SM. For the W^+W^- and $W^\pm Z$ channels the leading

scattering amplitudes in the helicity basis are

$$A(d_-\bar{d}_+ \to W_0^+W_0^-) = i\frac{s}{\Lambda^2}\sin\theta\left\{-\frac{g^2}{24c_W^2}(3c_W^2 f_W - s_W^2 f_B) + \frac{1}{4}(f_{\Phi Q}^{(3)} - 4f_{\Phi Q}^{(1)})\right\}, \tag{3.2}$$

$$A(d_-\bar{d}_+ \to W_\pm^+W_\pm^-) = -i\frac{s}{\Lambda^2}\sin\theta\frac{3g^4}{8}f_{WWW}, \tag{3.3}$$

$$A(d_+\bar{d}_- \to W_0^+W_0^-) = -i\frac{s}{\Lambda^2}\sin\theta\left\{\frac{g^2 s_W^2}{12c_W^2}f_B + f_{\Phi d}^{(1)}\right\}, \tag{3.4}$$

$$A(u_-\bar{u}_+ \to W_0^+W_0^-) = i\frac{s}{\Lambda^2}\sin\theta\left\{\frac{g^2}{24c_W^2}(3c_W^2 f_W + s_W^2 f_B) - \frac{1}{4}(f_{\Phi Q}^{(3)} + 4f_{\Phi Q}^{(1)})\right\}, \tag{3.5}$$

$$A(u_+\bar{u}_- \to W_0^+W_0^-) = i\frac{s}{\Lambda^2}\sin\theta\left\{\frac{g^2 s_W^2}{6c_W^2}f_B - f_{\Phi u}^{(1)}\right\}, \tag{3.6}$$

$$A(d_-\bar{u}_+ \to W_0^-Z_0) = i\frac{s}{\Lambda^2}\sin\theta\left\{\frac{g^2}{4\sqrt{2}}f_W - \frac{1}{2\sqrt{2}}f_{\Phi Q}^{(3)}\right\}, \tag{3.7}$$

$$A(d_-\bar{u}_+ \to W_0^-Z_0) = i\frac{s}{\Lambda^2}\sin\theta\left\{\frac{g^2}{4\sqrt{2}}f_W - \frac{1}{2\sqrt{2}}f_{\Phi Q}^{(3)}\right\}, \tag{3.8}$$

where s stands for the center-of-mass energy and θ is the polar angle in the center-of-mass frame.

We notice that the leptonic operator $\mathcal{O}_{\Phi e}^{(1)}$ does not contribute to the gauge boson production amplitudes at LHC. It only contributes to the decay rate of the Z boson in the ZW channels and in the narrow width approximation its effect is subdominant as it cancels in the corresponding Branching Ratios. For this reason in this chapter we will not consider it in the TGC analysis but it is kept in the EWPD analysis.

3.2 Analysis Framework

In order to constrain the parameters in the effective Lagrangian in Eq. (3.1) we study W^+W^- and $W^\pm Z$ productions in the leptonic channel since these are the measurements with the highest sensitivity for charged triple gauge boson vertices. In doing so we consider the same kinematic distributions employed by the experiments for their anomalous gauge boson coupling analyses what allows us to

validate our results against the bounds obtained by the experiments in each of the final states. More specifically, the channels that we analyze and their kinematical distributions are

Channel (a)	Distribution	# bins (N_b)	Data set	$\sigma_{\rm sig}$	$\sigma_{\rm bck}$	$\sigma_{i,\rm unc}$
$WW \to \ell^+\ell'^- + \not{E}_T\ (0j)$	$p_T^{\rm leading,lepton}$	3	ATLAS 8 TeV, 20.3 fb^{-1} [54]	0.049	0.02	0.08 – 0.14
$WW \to \ell^+\ell^{(\prime)-} + \not{E}_T\ (0j)$	$m_{\ell\ell^{(\prime)}}$	8	CMS 8 TeV, 19.4 fb^{-1} [55]	0.069	0.02	0.01 – 0.08
$WZ \to \ell^+\ell^-\ell^{(\prime)\pm}$	m_T^{WZ}	6	ATLAS 8 TeV, 20.3 fb^{-1} [56]	0.1	0.02	0.12 – 0.18
$WZ \to \ell^+\ell^-\ell^{(\prime)\pm} + \not{E}_T$	Z candidate $p_T^{\ell\ell}$	10	CMS 8 TeV, 19.6 fb^{-1} [57]	0.15	0.02	0.15 – 0.25

For each experiment and channel, we extract from the experimental publications the observed event rates in each bin, $N^a_{i,\rm d}$, as well as the background expectations $N^a_{i,\rm bck}$, and the SM W^+W^- ($W^\pm Z$) predictions, $N^a_{i,\rm sm}$.

The procedure to obtain the relevant kinematical distributions predicted by Eq. (3.1) is as follows. First we simulate the W^+W^- and $W^\pm Z$ productions using MADGRAPH5 [63] with the UFO files for our effective Lagrangian generated with FEYNRULES [64,65]. We employ PYTHIA6.4 [66] to perform the parton shower, while the fast detector simulation is carried out with DELPHES [67]. In order to account for higher order corrections and additional detector effects we simulate SM W^+W^- and $W^\pm Z$ productions in the fiducial region requiring the same cuts and isolation criteria adopted by the corresponding ATLAS and CMS studies, and normalize our results bin by bin to the experimental collaboration predictions for the kinematical distributions under consideration. Then we apply these correction factors to our simulated WV distributions in the presence of the anomalous couplings. This procedure yields our predicted number of signal events in each bin i for the "a" channel, $N^{a,\rm nosys}_{i,\rm sig}$.

The statistical confrontation of these predictions with the LHC Run 1 data is made by means of a binned log-likelihood function based on the contents of the different bins in the relevant kinematical distribution of each channel. Depending on the number of data events in the bin we use a Poissonian or a Gaussian probability distribution for its statistical error. In constructing the log-likelihood function we simulate the effect of the systematic and theoretical uncertainties by introducing two sets of pulls: two globally affecting the predictions of the event rates in all bins in fully correlated form – which parametrize, among others, the luminosity uncertainty, and theoretical errors on the total cross-section for the process and its backgrounds– and N^a_b independent pulls, one per-bin, to account for the bin-uncorrelated errors arising from the theoretical errors affecting the distributions, experimental energy resolutions and, in general, any energy and/or momentum dependence of the uncertainties. With this, the number of predicted events in bin i

for channel a is $N_i^a = \left[(1+\xi_{\rm sig}^a)(1+\xi_{i,\rm unc}^a)N_{i,\rm sig}^{a,\rm nosys} + (1+\xi_{\rm bck}^a)N_{i,\rm bck}^a\right]$. The errors of these pulls are introduced as Gaussian bias in the log-likelihood functions and are extracted from the information given by the experiments. For completness they are reported in the table above.

In order to validate our simulation we obtain first the 95% CL allowed regions for the TGC for each channel and experiment under the same assumptions the collaboration used. For example, we present in Figure 3.1 our two-dimensional allowed regions using the ATLAS W^+W^- data and assuming that the only non-vanishing Wilson coefficients are f_{WWW}, f_W and f_B, two different from zero at a time, as in the ATLAS analysis. As seen in the figure, our results for the 95% CL allowed region (blue region) agrees well with the one obtained by ATLAS, whose border is represented by the black curve.

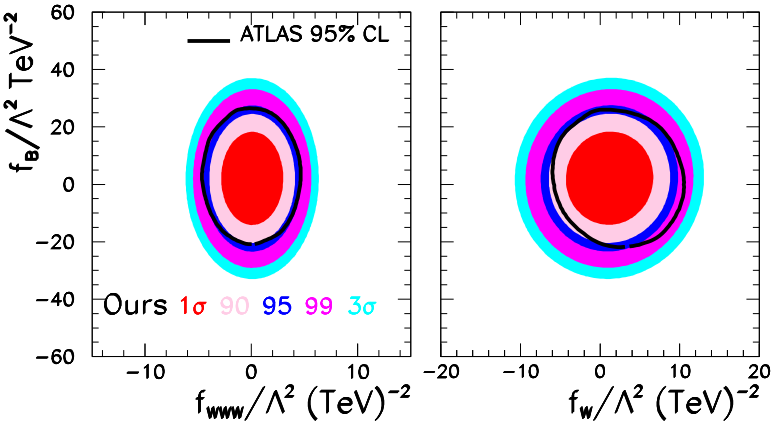

Figure 3.1: Allowed regions in the planes $f_B/\Lambda^2 \otimes f_{WWW}/\Lambda^2$ (left panel) and $f_B/\Lambda^2 \otimes f_W/\Lambda^2$ (right panel) at 1σ, 95%, 99%, and 3σ CL. The black line stands for the border of the 95% CL allowed region obtained by ATLAS [54].

When including the effect of the additional operators we must also account for their contribution to the EWPD. All the relevant expressions of the modificationof the observables can be found in Sec. 2.3. With that and the data collected we construct the χ^2 function for the EWPD following the analysis in Ref. [51]. In brief

in our EWPD analysis we fit 15 observables of which 12 are Z observables [68]:

$$\Gamma_Z\ ,\ \sigma_h^0\ ,\ \mathcal{A}_\ell(\tau^{\rm pol})\ ,\ R_\ell^0\ ,\ \mathcal{A}_\ell({\rm SLD})\ ,\ A_{\rm FB}^{0,l}\ ,\ R_c^0\ ,\ R_b^0\ ,\ \mathcal{A}_c\ ,\ \mathcal{A}_b\ ,\ A_{\rm FB}^{0,c}\ ,$$
$$\text{and } A_{\rm FB}^{0,b}\ (\text{SLD/LEP-I})\ ,$$

complemented by three W observables

$$M_W\ ,\ \Gamma_W\ \text{ and Br}(W\to\ell\nu)$$

that are, respectively, its average mass taken from [69], its width from LEP2/Tevatron [48], and the leptonic W branching ratio for which the average in Ref. [69] is considered. The correlations among these inputs are presented in Ref. [68] and we take them into consideration in the analyses. The SM predictions and their uncertainties due to variations of the SM parameters were extracted from [70].

Altogether we construct a combined χ^2 function

$$\begin{aligned}\chi^2_{\rm LHC-R1+EWPD} \equiv \chi^2_{\rm LHC-RI}(f_W, f_B, f_{WWW}, f_{BW}, f_{\Phi,1}, f^{(1)}_{\phi,Q}, f^{(3)}_{\phi,Q}, f^{(1)}_{\phi,u}, f^{(1)}_{\phi,d}) \\ + \chi^2_{\rm EWPD}(f_{BW}, f_{\Phi,1}, f^{(1)}_{\phi,Q}, f^{(3)}_{\phi,Q}, f^{(1)}_{\phi,u}, f^{(1)}_{\phi,d}, f^{(1)}_{\phi,e}, f_{LLLL})\ ,\end{aligned} \tag{3.9}$$

from which we derive the allowed ranges for each coefficient or pair of coefficients after marginalization over all the others.

Finally, for comparison, we also consider the constraints from LEP2 global analysis of TGC [53]. In order to do so we follow the procedure in Ref. [32] and construct a simplified gaussian $\chi^2_{\rm LEP2}$ using the central values, σ and correlation matrix for the couplings Δg_Z^1, $\Delta\kappa_\gamma$ and λ and their correlation coefficients from the final combined LEP2 analysis in Ref. [53] (reproduced in Table 3.1 for completness) which was performed in terms of these effective TGC coefficients under the relations implied by dimension-six effective operator formalism for TGC. We notice, however, that in extracting those bounds on the effective TGC couplings, the LEP collaborations did not include the effect of fermion operators. For that reason the combination of those LEP2 bounds with our LHC Run 1 and EWPD is only shown for the purpose of illustration.

3.3 Bounds on Triple Gauge Interactions

Having the analysis framework defined, we can show the results in terms of the allowed ranges for the Wilson coefficients of the three traditional TGC operators f_{WWW}/Λ^2, f_W/Λ^2 and f_B/Λ^2. We depict first in Fig. 3.2 the 95% CL (2

	LEP			
	68 % CL	Correlations		
Δg_1^Z	$0.051^{+0.031}_{-0.032}$	1.00	0.23	−0.30
$\Delta\kappa_\gamma$	$-0.067^{+0.061}_{-0.057}$	0.23	1.00	−0.27
λ	$-0.067^{+0.036}_{-0.038}$	−0.30	0.27	1.00

Table 3.1: Δg_1^Z, $\Delta\kappa_\gamma$ and λ central values, standard deviations and correlation coefficients from LEP2 [53].

dof) allowed regions in the planes $f_B/\Lambda^2 \otimes f_W/\Lambda^2$, $f_{WWW}/\Lambda^2 \otimes f_B/\Lambda^2$ and $f_{WWW}/\Lambda^2 \otimes f_W/\Lambda^2$ for the W^+W^- and $W^\pm Z$ channels and for ATLAS and CMS, as well as the combination of these results.

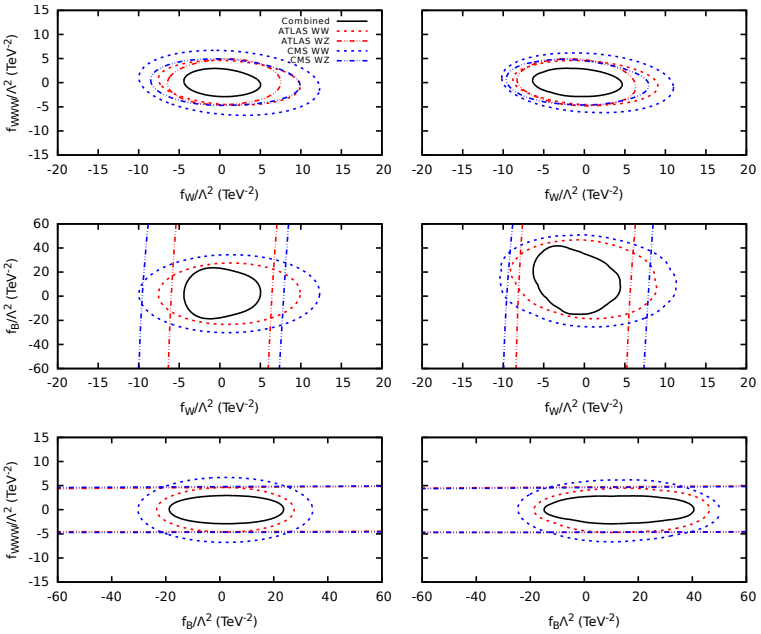

Figure 3.2: Allowed 95% CL regions in the planes $f_{WWW}/\Lambda^2 \otimes f_B/\Lambda^2$ (top row), $f_B/\Lambda^2 \otimes f_W/\Lambda^2$ (middle row) and $f_{WWW}/\Lambda^2 \otimes f_W/\Lambda^2$ (lower row) for the different channels as labeled in the figure. In the left panels only f_{WWW}, f_W and f_B were considered non-zero in the fit, while the right panels display the result from the 11 parameter fit. In each case we marginalize over the undisplayed non-zero variables.

We can check the impact the impact of additional operators in the TGC extrac-

tion at LHC by performing first an analysis where we fit just these three coefficients and setting the coefficient of all other operators to zero. The corresponding allowed regions are shown in the left panels after marginalizing over the third coefficient which is not displayed. Conversely the results of the global analysis of the LHC Run 1 data together with EWPD performed in terms of 11 non-zero Wilson coefficients (see Eq. (3.1)) are shown on the right panels. These regions are obtained after marginalization over the 9 undisplayed coefficients.

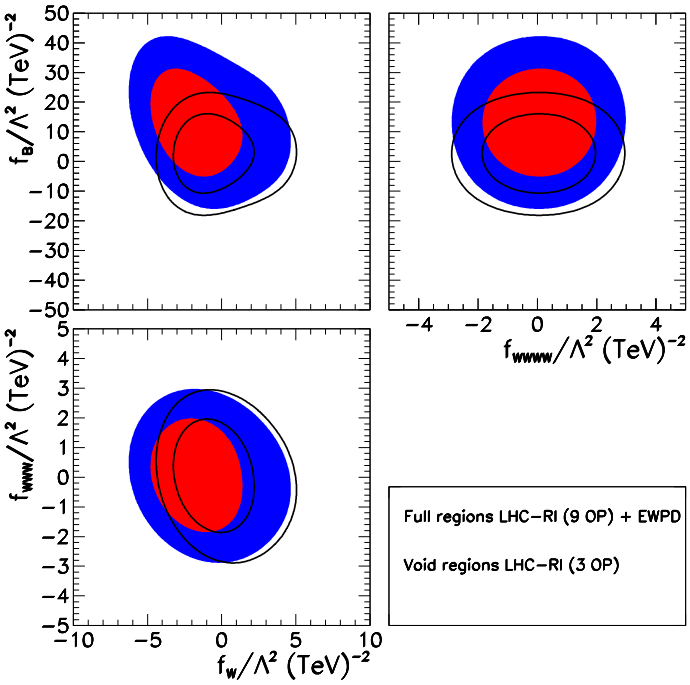

Figure 3.3: 1σ and 95% CL allowed regions in the planes indicated in the axes. Here we considered the W^+W^- and $W^\pm Z$ productions and the EWPD in the analyses. The data set and parameters used are as indicated in the figure.

One salient feature of Figure 3.2 is that the $W^\pm Z$ bounds on the Wilson coefficient f_B/Λ^2 are much looser than the ones on f_W/Λ^2 and f_{WWW}/Λ^2 , as expected, because $\mathcal{O}_B$ does not contribute to the leading term of the growth of the scattering amplitudes; see Eqs. (3.2)–(3.8).

For better comparison of the results obtained with and without including the additional operators we overlay in Fig. 3.3 the 1σ and 95% CL allowed regions

obtained combining all channels and experiments for the two scenarios. As we can see from this figure the addition of more parameters leads to the expansion of the allowed regions, as expected. Moreover, the region of f_B/Λ^2 suffers the largest shift towards positive values of this parameter while there is a small shift in the f_W/Λ^2 direction and there is no appreciable displacement along the f_{WWW}/Λ^2 axis.

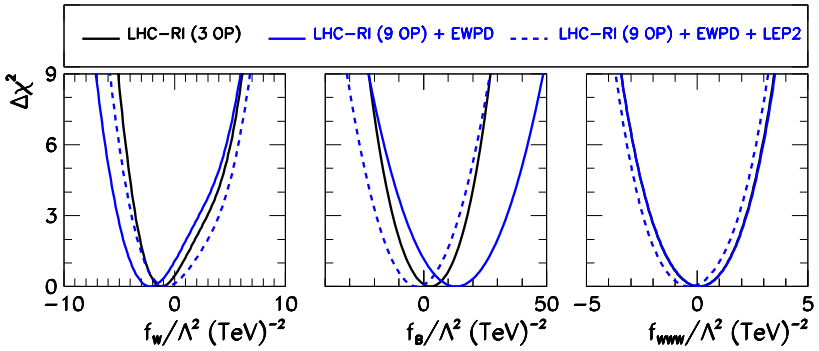

Figure 3.4: $\Delta\chi^2$ dependence on the f_W/Λ^2 (left panel), f_B/Λ^2 (central panel) and f_W/Λ^2 (right panel) parameters after the marginalization over the remaining fit parameters. The solid black line stands for the standard TGC analysis, while the solid blue line represents the 9 parameter fit to the LHC Run 1 data and the EWPD. The dashed blue line differs from the solid ones just by the addition of LEP2 data on TGC.

The corresponding dependence of the $\Delta\chi^2$ for the two analysis with each of the three coefficients is given in Fig. 3.4 and from those we read the 95%CL one-dimensional allowed ranges for each coefficient given in Table 3.2. As seen above, the $\Delta\chi^2$ distribution for f_B/Λ^2 (f_W/Λ^2) broadens and shifts to positive (negative) values when we compare the results considering only the LHC Run 1 data and three canonical parameters (solid black line) with the one containing additional operators also constrained by the EWPD (solid blue line). Quantitatively the effect is slightly larger for f_B/Λ^2 whose allowed range widens by about 30% versus 20% for f_W/Λ^2.

The effect of each of the six additional operators on the extracted range of the three traditional TGC operator coefficients is illustrated in Figure 3.5 where we depict the two-dimensional correlations between the three TGC coefficients and

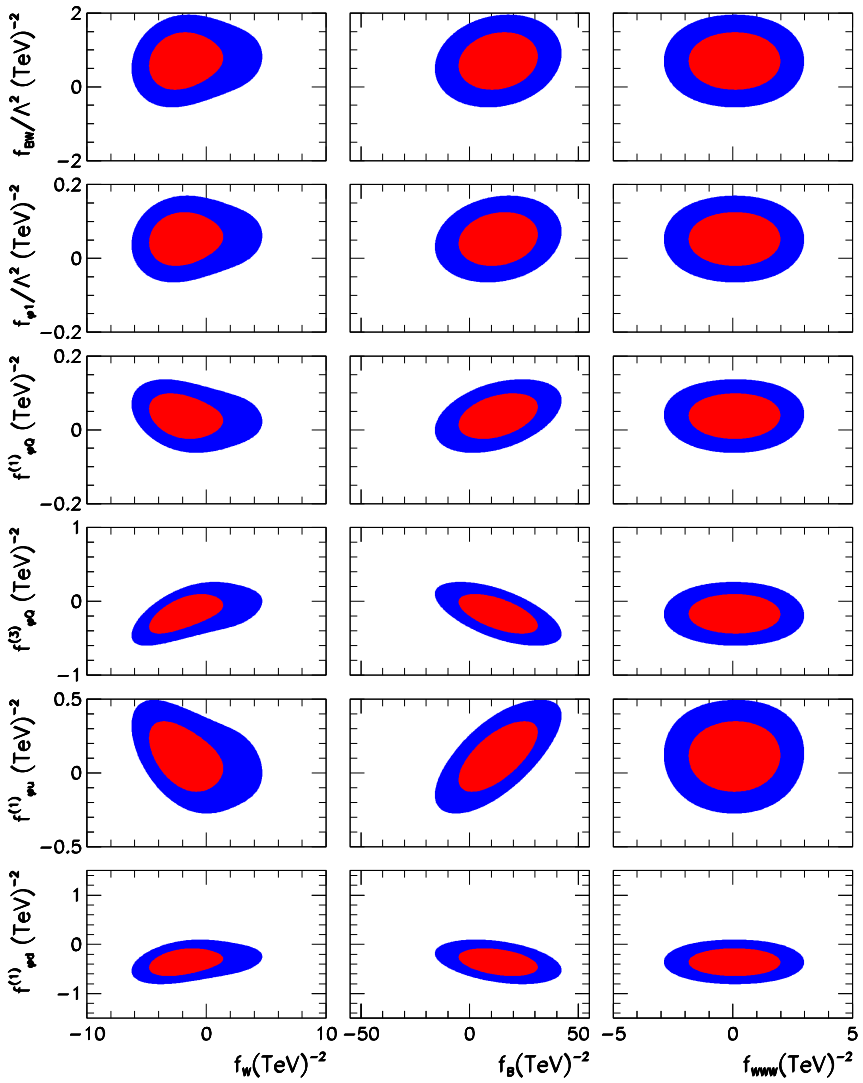

Figure 3.5: 1σ and 95% CL allowed regions in the planes indicated in the axes. Here we considered the W^+W^- and $W^\pm Z$ productions and the EWPD in the analyses.

the additional ones. In each panel of this figure we exhibit the 1σ and 95% CL level (2 dof) allowed regions after marginalizing over the remaining parameters. As we can see, f_B/Λ^2 has a significant correlation only with $f^{(1)}_{\Phi u}/\Lambda^2$ and to a lesser extent is (anti-) correlated with $f^{(1)}_{\Phi Q}/\Lambda^2$ ($f^{(3)}_{\Phi Q}/\Lambda^2$ and $f^{(1)}_{\Phi d}/\Lambda^2$). This is

expected as these are the operator coefficients contributing the growth of the scattering amplitudes into longitudinally polarized gauge bosons (Eqs. (3.2)– (3.8)). In particular the correlion with $f_{\Phi u}^{(1)}/\Lambda^2$ can be understood from the scattering amplitude in Eq. (3.6). Similarly f_W/Λ^2 shows a stronger anti-correlation only with $f_{\Phi u}^{(1)}/\Lambda^2$ and to a smaller degree is correlated with $f_{\Phi Q}^{(3)}/\Lambda^2$ and $f_{\Phi d}^{(1)}/\Lambda^2$. Finally from the third column of this figure we can see that f_{WWW}/Λ^2 shows no correlation with the additional parameters as expected since $\mathcal{O}_{WWW}$ contributes by itself to the energy growth of the scattering amplitudes for transversely polarized gauge bosons.

The impact of the LHC diboson production data on the determination of the parameters directly constrained by the EWPD is illustrated in Fig. 3.6 that depicts the $\Delta\chi^2$ distribution as a function of these parameters where the magenta (blue) line stands for the result obtained using the EWPD (and the LHC Run 1 diboson production data).

The top left and middle panels of this figure show that the addition of the LHC data does not alter the constraints on f_{BW}/Λ^2 and $f_{\Phi 1}/\Lambda^2$ parameters. This is easy to understand since these parameters do not modify the high energy behavior of $q\bar{q} \to VV$ amplitudes; see Eqs. (3.2)–(3.3). This is expected from $\mathcal{O}_{\Phi,1}$ as it only contributes to the amplitudes via finite renormalization effects of the SM parameters. The operator $\mathcal{O}_{BW}$, on the other hand, modifies the TGC directly also, however, its effects on the Z wave-function renormalization cancel the growth with the center–of–mass energy due to the anomalous TGC. From the top right, bottom left and middle panels we can see that the impact of the Run 1 data on $f_{\Phi Q}^{(1)}/\Lambda^2$, $f_{\Phi Q}^{(3)}/\Lambda^2$ and $f_{\Phi u}^{(1)}/\Lambda^2$ is marginal. $f_{\Phi d}^{(1)}/\Lambda^2$ is the only parameter whose $\Delta\chi^2$ distribution gets significantly affected. The EWPD analysis favours non-vanishing value for $f_{\Phi d}^{(1)}/\Lambda^2$ at 2σ, a result driven by the 2.7σ discrepancy between the observed $A_{\rm FB}^{0,b}$ and the SM. On the contrary no significant discrepancy is observed between the observed LHC Run 1 diboson data and the SM. Hence there is a shift towards zero of $f_{\Phi d}^{(1)}/\Lambda^2$ when including the LHC Run 1 data in the analysis. This slight tension results also into the reduction of the globally allowed range.

We finish by comparing our results with the bounds derived from LEP2 diboson data. To do so we plot in Figure 3.7 the two-dimensional 95% CL allowed regions for the three combination of the canonical TGC parameters for the analysis with and without additional operators together with the LEP2 results. As shown in Ref. [32], the limits emanating from the canonical LHC Run 1 diboson data (black solid line) are substantially more stringent than those imposed by LEP2

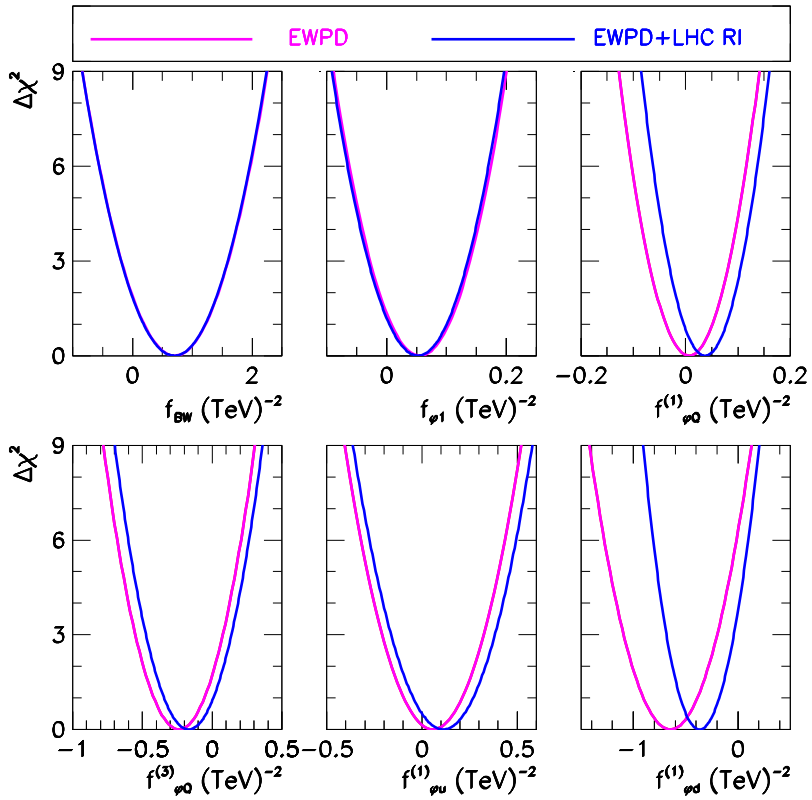

Figure 3.6: $\Delta\chi^2$ dependence on the f_{BW}/Λ^2, $f_{\Phi 1}/\Lambda^2$, $f^{(1)}_{\Phi Q}/\Lambda^2$, $f^{(3)}_{\Phi Q}/\Lambda^2$, $f^{(1)}_{\Phi u}/\Lambda^2$, and $f^{(1)}_{\Phi d}/\Lambda^2$ after the marginalization over the undisplayed parameters. The magenta line stands for the results using only the EWPD while the blue one is obtained considering the EWPD and LHC Run 1 diboson production.

(black dashed line). As seen in this figure, enlarging the number of operators in the LHC analyses, together with the EWPD, does not alter this conclusion despite the growth of the allowed regions (solid blue line). For illustration we also show in the figure the allowed regions obtained by naively combining the general LHC Run 1 + EWPD analysis with the LEP2 information. As seen, including LEP2 data in the approximation used leads to a reduction of the allowed regions in the f_B/Λ^2 direction, as well as to a shift of it towards negative values (see also the dashed blue line in Fig. 3.4).

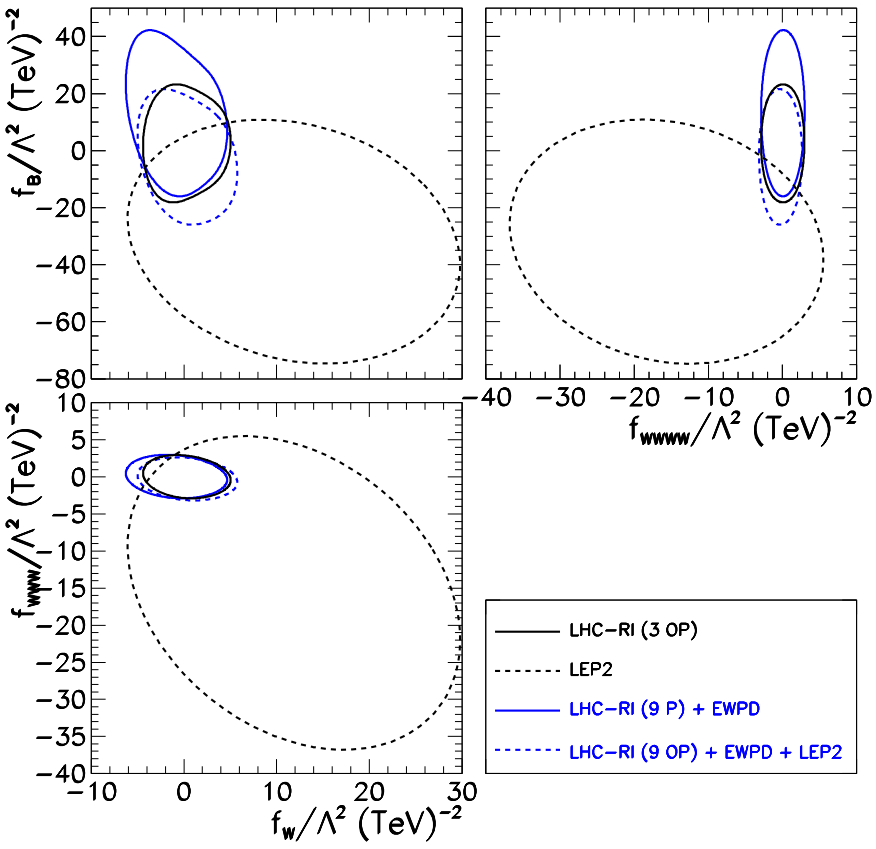

Figure 3.7: Two-dimensional 95% CL allowed regions in the planes indicated in the axes. Here we considered the W^+W^- and $W^\pm Z$ productions, LEP2 data on TGC and the EWPD in the analyses. The lines are as shown in the figure.

3.4 Summary and Conclusions

In this Chapter we have quantified the impact of possible anomalous gauge couplings to quarks on the TGC determination performed using the LHC Run 1 diboson data. In order to carry out a statistically consistent analysis we have included in addition the EWPD to constrain the couplings between quarks and gauge boson as well as the modifications of the gauge boson self energies.

As usual, in order to study any possible deviation from the SM, we worked in model-independent framework of effective lagrangians. In particular, the effective lagrangian for study the effect of the fermionic operators in LHC gauge legacy,

presented in Eq. (3.1), includes 11 dimension–six operators.

As a summary of our findings we present in Table 3.2 the 95% CL globally allowed ranges for the Wilson coefficients of the nine operators that contribute to the LHC Run 1 data considered.

coupling	95% allowed range (TeV^{-2})		
	LHC RI (3 OP)	EWPD	LHC RI (9 OP) + EWPD
f_W	$(-3.9\,,\,3.9)$	—	$(-5.6\,,\,4.0)$
f_B	$(-15\,,\,20)$	—	$(-11\,,\,36)$
f_{WWW}	$(-2.4\,,\,2.5)$	—	$(-2.4\,,\,2.6)$
f_{BW}	—	$(-0.32\,,\,1.7)$	$(-0.33\,,\,1.7)$
$f_{\Phi 1}$	—	$(-0.040\,,\,0.15)$	$(-0.042\,,\,0.15)$
$f_{\Phi Q}^{(1)}$	—	$(-0.083\,,\,0.10)$	$(-0.048\,,\,0.12)$
$f_{\Phi Q}^{(3)}$	—	$(-0.60\,,\,0.12)$	$(-0.52\,,\,0.18)$
$f_{\Phi u}^{(1)}$	—	$(-0.25\,,\,0.37)$	$(-0.19\,,\,0.42)$
$f_{\Phi d}^{(1)}$	—	$(-1.2\,,\,-0.13)$	$(-0.73\,,\,0.023)$

Table 3.2: 95% CL allowed ranges for the Wilson coefficients of the dimension–six operators that contribute to the studied processes in gauge boson pair production at LHC. The ranges for each parameter are obtained after marginalization of the coefficients of all other operators contributing to each analysis. In particular the results given in the third and forth column are obtain after marginalization over $f_{\phi,e}^{(1)}$ and f_{LLLL} as well.

The comparison of the the first and third columns of this table shows that the addition of the new operators modifies the TGC bounds on f_B/Λ^2 and f_W/Λ^2 coming from the LHC Run 1 diboson. Quantitatively the effect is slightly larger for f_B/Λ^2 whose allowed range widens by about 30% versus 20% for f_W/Λ^2. The limits on f_{WWW}/Λ^2, on the contrary, result almost unaffected. Despite these changes, the constraints on these parameters are still dominated by the LHC Run 1 data at large, and are still substantially stronger than those obtained from LEP2 data.

We have also learned from our analyses that the LHC Run 1 diboson data is not precise enough to yield substantial information on the gauge couplings to quarks in addition to what is already known from EWPD; contrast the second and third

columns of Table 3.2. The only apparent exception is $f_{\Phi d}^{(1)}/\Lambda^2$ which in the considered family universal scenario is driven to be non-zero in the EWPD analysis by the discrepancy between the measured $A_{\rm FB}^{0,b}$ at LEP/SLC and the SM while LHC Run 1 data shows no evidence of any deviation with respect to the SM. Nevertheless, these results allow us to foresee that diboson production at the LHC will play an important role in the analyses of anomalous couplings of gauge bosons to quarks as the LHC increases the integrated luminosity. Hence global analysis of LHC and EWPD are becoming a must for consistent determination of the Wilson coefficients of the full set of dimension–six operators.

The end of this chapter points in a clear direction: if we want to include the Higgs observables in our analysis, we definitely need to take into account the fermionic operators. The reason is the following. Operators like $\mathcal{O}_W$ ans $\mathcal{O}_B$ enter in the Higgs observables, like we saw in Chapter 2. If the fermionic operators affect the bounds of the Wilson coefficients of these two operators, then indirectly should have some effect in the other ones contributing to the Higgs interactions. In the next Chapter we shall tackle the question.

Moreover, there is strong take home message, after the analysis of this Chapter. The LHC is getting competitive with LEP, in the sense that what although LHC started as a discovery machine – since higher energies are more easily achieved – now it is also capable of doing precision physics.

Chapter 4

Status after RUN 1 and RUN 2: A Combined Analysis of LHC and Electroweak Precision Data

As we have seen in Chapter 3, the LHC is reaching a precision that for some analyses already surpasses the one of LEP, which makes the fermionic operators relevant for any global analysis of the LHC data in the context of an effective Lagrangian approach. We have seen that within the present LHC statistics, changes in the couplings of gauge bosons to fermions, even within the constraints of EWPD can lead to modifications of the kinematical distributions in gauge boson pair production at LHC of comparable size to the ones stemming from the purely anomalous TGC. Moreover, in Chapter 2, we verified that some operators like $\mathcal{O}_W$ and $\mathcal{O}_B$ contribute to both Higgs interactions and TGC. And so, indirectly the fermionic operators influence the determination of the Wilson coefficients for the operators entering the Higgs observables.

With this aim, in this Chapter we perform an analysis combining the EWPD with all relevant final Run 1 and the most up to date Run 2 Higgs observables in terms of signal strengths or ratios of cross sections and branching ratios, together with the kinematics distributions from both W^+W^- and $W^\pm Z$ production. In this respect, this analysis extends and updates previous partial constrains on Higgs anomalous couplings and TGCs [29–32].

Finally, as we will see in Chapter 5, the constraints derived on all the Wilson coefficients of those non-dipole operators entering the tests of the electroweak gauge boson sector are robust under the inclusion of the light-quark dipole op-

erators. Therefore, without loss of generality, they will not be included in the following global analysis presented in this Chapter. Altogether, the total effective Lagrangian that we consider is

$$\mathcal{L}_{\rm eff} = \mathcal{L}_{\rm SM} + \mathcal{L}_{\rm eff}^{\rm EWPD} + \mathcal{L}_{\rm eff}^{\rm TGC} + \mathcal{L}_{\rm eff}^{\rm Yuk} + \mathcal{L}_{\rm eff}^{\rm HVV} \ , \tag{4.1}$$

where $\mathcal{L}_{\rm eff}^{\rm EWPD}$, $\mathcal{L}_{\rm eff}^{\rm TGC}$, $\mathcal{L}_{\rm eff}^{\rm Yuk}$ and $\mathcal{L}_{\rm eff}^{\rm HVV}$ are given by Eqs. (2.99), (2.100), (2.102), (2.101), respectively.

Before proceeding to the analysis, there is one theoretical interesting aspect that needs to be discussed. In this Thesis, it is the first time that we are including the Higgs observables in our analysis. There is enough experimental information to individually bound the 20 Wilson coefficients but there are still important discrete (quasi-)degeneracies. They can be understood in terms of sign flips of the couplings of the Higgs to gauge bosons and to fermions with respect to the SM. For instance, the coefficient of the $HW_\mu^+ W^{-\mu}$ vertex is

$$\left(\frac{g^2 v}{2}\right)\left[1 - \frac{v^2}{4}\left(\frac{f_{\Phi,1}}{\Lambda^2} + 2\frac{f_{\Phi,2}}{\Lambda^2}\right)\right] \ . \tag{4.2}$$

we anticipate a degeneracy with the SM results for $f_{\Phi,2}/\Lambda^2 = 0$ and around $f_{\Phi,2}/\Lambda^2 = 4/v^2 \sim 65$ TeV^{-2}. These points in parameter space are also nearly degenerate for the vertex $HZ_\mu Z^\mu$.

As for the Higgs couplings to fermions, anomalous interactions can also lead to Yukawa couplings of the order of the SM ones but with a different sign as the coefficient of the $H\bar{f}f$ vertex is now

$$-\frac{m_f}{v}\left[1 - \frac{v^2}{2}\left(\frac{f_{\Phi,2}}{\Lambda^2} + \sqrt{2}\frac{f_f}{\Lambda^2}\right)\right] \tag{4.3}$$

where $f = \mu, \tau, b, t$. Since $f_{\Phi,2}/\Lambda^2$ has two different values compatible with flipping the sign of the SM HVV coupling, we can anticipate that f_f/Λ^2 will have 2×2 degenerate SM-like solutions, two corresponding to $f_f/\Lambda = 0$, and the other two with $f_f/\Lambda = \pm 2\sqrt{2}/v^2 \sim 45$ TeV^{-2}.

A further source of degeneracy is the effective gluon-gluon-Higgs interaction associated to the operator $HG^a_{\mu\nu}G^{a,\mu\nu}$ whose coefficient is

$$-\frac{1}{4}G_{\rm SM}^{gg} - \frac{\alpha_S v}{8\pi}\frac{f_{GG}}{\Lambda^2} \ , \tag{4.4}$$

where $G_{\rm SM}^{gg} \sim -5.3 \times 10^{-2}$ TeV^{-1} summarizes the SM one–loop contribution. Flipping the sign of the SM contribution leads to the existence of a SM-like solution

for $f_{GG}/\Lambda^2 \sim -4\pi/(v\alpha_s)G_{\mathrm{gg,SM}} \sim 25\ \mathrm{TeV}^{-2}$. The equivalent effect is present in the photon-photon-Higgs coupling $HF_{\mu\nu}F^{\mu\nu}$ with a coefficient

$$-\frac{1}{4}G^{\gamma\gamma}_{\mathrm{SM}} + \frac{e^2 v}{4}\frac{f_{WW}+f_{BB}-f_{BW}}{\Lambda^2} \quad , \tag{4.5}$$

where $G^{\gamma\gamma}_{\mathrm{SM}} \sim 3.3\times 10^{-2}\ \mathrm{TeV}^{-1}$, and a SM-like solutions for the $H\gamma\gamma$ decay can be found for $(f_{WW}+f_{BB}-f_{BW})/\Lambda^2 \sim 2/(v\,e^2)G_{\gamma\gamma,\mathrm{SM}} \sim 3\ \mathrm{TeV}^{-2}$. This degeneracy, however, is only approximate because EWPD independently constrains f_{BW} and the measurement of the effective photon-Z-coupling $HF_{\mu\nu}Z^{\mu\nu}$ bounds a different combination of f_{WW}, f_{BB} and f_{BW}. The reason to emphasize the presence of discrete (quasi-)degeneracies in the parameter space of some Wilson coefficients is two folded. First, the marginalization of the profiled binned log-likelihood is computationally very expensive due the high dimensionality of the parameters space, therefore we can test our minimization method by anticipating where are the discrete (quasi-)degeneracies in the parameter space. Second, these degenerate solutions mean that, even with SM-like data, there can still be large NP contributions in the form of these particular operators which cannot be ruled out on the basis of the observations.

4.1 Analysis Framework

In order to constrain the Wilson coefficients of the dimension–six operators in the effective Lagrangian Eq. (4.1), we considered the EWPD, diboson production and Higgs signal strengths.

In the EWPD analysis we take into account the 15 observables of which 12 are Z observables and supplemented by 3 W observables and with those construct χ^2_{EWPD} which is a function of eight Wilson coefficients (see Eq. (3.9)) as discussed in both Sec. 2.3 and 3.2

As described in Chapter 3 the structure of the electroweak triple gauge boson coupling has been the subject of direct scrutiny in gauge boson pair production at LEP2 [53] and the Run 1 of LHC where the ATLAS and CMS collaborations have used their full data samples on W^+W^- [54, 55] and $W^\pm Z$ [56, 57] productions to constrain the possible deviations of TGC's from the SM structure in terms of the effective Lorentz invariant parametrization of Ref. [43] or in terms of coefficients of some of the relevant dimension–six operators. For Run 2, the number of experimental studies aiming at deriving the corresponding limits is still rather sparse. In particular ATLAS [71] has presented some results on bounds on TGC couplings

Channel (a)	Distribution	# bins	Data set	Int Lum
$WW \to \ell^+\ell'^- + \not{E}_T\ (0j)$	$p_T^{\rm leading,lepton}$	3	ATLAS 8 TeV,	20.3 fb^{-1} [54]
$WW \to \ell^+\ell^{(\prime)-} + \not{E}_T\ (0j)$	$m_{\ell\ell^{(\prime)}}$	8	CMS 8 TeV,	19.4 fb^{-1} [55]
$WZ \to \ell^+\ell^-\ell^{(\prime)\pm}$	m_T^{WZ}	6	ATLAS 8 TeV,	20.3 fb^{-1} [56]
$WZ \to \ell^+\ell^-\ell^{(\prime)\pm} + \not{E}_T$	Z candidate $p_T^{\ell\ell}$	10	CMS 8 TeV,	19.6 fb^{-1} [57]
$WW \to e^\pm\mu^\mp + \not{E}_T\ (0j)$	m_T	17	ATLAS 13 TeV,	36.1 fb^{-1} [73]
$WZ \to \ell^+\ell^-\ell^{(\prime)\pm}$	m_T^{WZ}	6	ATLAS 13 TeV,	36.1 fb^{-1} [72]

Table 4.1: Data included in the EWDBD analysis.

from WZ production but still with data collected with 13.3 fb^{-1}. With this limited luminosity, the TGC sensitivity is still below that of Run 1. However, ATLAS has also presented results on their measurements of diboson production at 13 TeV with higher luminosity and this data can be used to set better constraints on TGC. With this aim in here we use the ATLAS results on WZ production [72] and on WW [73] both with 36.1 fb^{-1} as we describe next.

In order to obtain the bounds on the Wilson coefficients in the effective Lagrangian in Eq. (4.1) we study the W^+W^- and $W^\pm Z$ productions in the leptonic channel using the available kinematic distribution that is most sensitive for TGC analysis. More specifically, the channels that we analyze and their kinematical distributions are listed in Table 4.1: For each experiment and channel, we extract from the experimental publications the observed event rates in each bin, $N^a_{i,\rm d}$, as well as the background expectations $N^a_{i,\rm bck}$, and the SM W^+W^- ($W^\pm Z$) predictions, $N^a_{i,\rm sm}$.

The analysis of the Run 1 electroweak diboson data (EWDBD) has been described in Chapter 3. Concerning the Run 2 EWDBD analysis, for the W^+W^- final state we study the transverse mass distribution in the ATLAS 13 TeV ggF sample. We extract from Fig. 4 in Ref. [73] both the data, the non-WW backgrounds, as well as the SM WW contributions in each of the 17 bins in the transverse mass variable

$$m_T \equiv \sqrt{(E_T^{\ell\ell} + E_T^{\rm miss})^2 - |\vec{p}_T^{\,\ell\ell} + \vec{p}_T^{\,\rm miss}|^2} \tag{4.6}$$

with $E_T^{\ell\ell} = \sqrt{|\vec{p}_T^{\,\ell\ell}|^2 + m_{\ell\ell}^2}$ and the transverse momentum (invariant mass) of the lepton pair denoted by $\vec{p}_T^{\,\ell\ell}$ ($m_{\ell\ell}$). The statistical uncertainty is given by $\sqrt{N^{WW}_{i,\rm d}}$ where we combine the contents of the last 3 bins to ensure gaussianity. Theoretical and systematic uncertainties can be found in Tables 5-7 of the same reference. For the 13 TeV $W^\pm Z$ final state, we make the analysis using the transverse mass

distribution in Fig. 4c in Ref. [72] which is presented in terms of $W^{\pm}Z$ signal events in 6 bins covering all values of m_T^{WZ} (last bin containing all data above 600 GeV) and already background subtracted. From the lower panel of the same figure we read the statistical, total experimental and theoretical uncertainties in each bin[1].

With that information the procedure to obtain the relevant kinematical distributions predicted in presence of the dimension–six operators is the same followed for our Run 1 EWDBD analysis in Section 3.1. First we simulate the W^+W^- and $W^{\pm}Z$ productions using MADGRAPH5 [63] with the UFO files for our effective lagrangian generated with FEYNRULES [64, 65]. We employ PYTHIA6.4 [66] to perform the parton shower, while the fast detector simulation is carried out with DELPHES [67]. In order to account for higher order corrections and additional detector effects we simulate SM W^+W^- and $W^{\pm}Z$ productions in the fiducial region requiring the same cuts and isolation criteria adopted by the corresponding ATLAS studies, and normalize our results bin by bin to the experimental collaboration predictions for the kinematical distributions under consideration. Then we apply these correction factors to our simulated WV distributions in the presence of the anomalous couplings.

The statistical confrontation of these predictions with the LHC Run 2 data is made by means of a binned log-likelihood function based on the contents of the different bins in the kinematical distribution of each channel. Besides the statistical errors we incorporate the systematic and theoretical uncertainties added in quadrature to the uncorrelated statistical error in each bin assuming some partial correlation among them which we estimate to range between 30% and 70% with the information provided. Altogether we build the corresponding $\chi^2_{\rm EWDBD}$ with the Run 1 and Run 2 results which we combine with the EWPD bounds so we have

$$\chi^2_{\rm EWPD+EWDBD}(f_B, f_W, f_{WWW}, f_{BW}, f_{\Phi,1}, f^{(3)}_{\Phi,Q}, f^{(1)}_{\Phi,Q}, f^{(1)}_{\Phi,u}, f^{(1)}_{\Phi,d}, f^{(1)}_{\Phi,ud}, f^{(1)}_{\Phi,e}, f_{LLLL}) \,. \qquad (4.7)$$

This represents the extension of Eq. (3.9) including also the results on EWDBD from Run 2.

As for Higgs processes, we use the available data from Runs 1 and 2 from the following sources

[1] Since the data points give the number of WZ signal events after background subtraction their statistical error read from the figure are much larger than $\sqrt{N^{WZ}_{i,\rm d}}$.

Source	Int.Luminosity (fb^{-1})	# Data points
ATLAS+CMS at 7 & 8 TeV [74] [Table 8, Fig 27]	5 & 20	20+1
ATLAS at 13 TeV [75] [Figs. 6,7]	79.8	9
CMS at 13 TeV [76] [Table 3]	35.9	24
ATLAS at 8 TeV [77] (γZ)	20	1
ATLAS at 13 TeV [78] (γZ)	36.1	1
ATLAS at 13 TeV [79] ($\mu^+\mu^-$)	36.1	1

that provide us signal strengths or ratios of cross sections and branching ratios. The first three references above contain information on all production mechanisms and almost all decay channels in the Figures and Tables given in the first column. Moreover, these references also provide the correlation matrix among the observables, as well as statistic and systematic errors (for Ref. [76] the correlation matrix can be found in [80]). The fourth and fifth references contains information on the rare decay mode γZ while the last one on the $\mu^+\mu^-$ channel.

The statistical comparison of our effective theory predictions with the LHC Runs 1 and 2 data is made by means of a $\chi^2_{\rm Higgs}$ function based on these 22 (Run 1) + 35 (Run 2) data points. Adding this to the analysis of EWPD and EWDBD we construct our global 20 dimensional statistical function

$$\chi^2_{\rm EWPD+EWDBD+Higgs}(f_B, f_W, f_{WWW}, f_{BB}, f_{WW}, f_{BW}, f_{GG}, f_{\Phi,1}, f_{\Phi,2}, f^{(3)}_{\Phi,Q}, f^{(1)}_{\Phi,Q}, f^{(1)}_{\Phi,u}, f^{(1)}_{\Phi,d}, f^{(1)}_{\Phi,ud}, f^{(1)}_{\Phi,e}, f_{LLLL}, f_b, f_t, f_\tau, f_\mu)\ . \quad (4.8)$$

4.2 Results

Before presenting the results, we start by summarize the three sets of analyses for the Wilson coefficients, which differ in the data samples included. Our different sets are like layers of an onion, being the EWPD the inner one and constraining the less number of Wilson coefficients. When we start to add the TGC data and the Higgs observables, we go to the most outward layer of the onion, and so more Wilson coefficients are constrained.

We summarize the three different sets of analysis:

- EWPD: $\Delta\chi^2_{\rm EWPD}$ which constrains the 8 coefficients in $\mathcal{L}^{\rm EWPD}_{\rm eff}$, Eq. (2.99). They are given by the green lines in Figs. 4.1 and 4.3. This analysis is performed taking into account only the contributions to the observables that are linear in the anomalous Wilson coefficients; for further detail see Ref. [51].

- EWPD+EWDBD: $\Delta\chi^2_{\rm EWPD+EWDBD}$ which limits the 12 coefficients in $\mathcal{L}^{\rm EWPD}_{\rm eff}$ $+\mathcal{L}^{\rm TGC}_{\rm eff}$, Eqs. (2.99) and (2.100). The results are depicted in Fig. 4.2. In the

evaluation of the predictions for EWDBD we have kept the contribution of the Wilson coefficients up to the quadratic order.

- GLOBAL≡ EWPD+EWDBD+HIGGS: $\Delta\chi^2_{\rm EWPD+EWDBD+HIGGS}$ which constrains the 20 coefficients in $\mathcal{L}_{\rm eff}$ in Eq. (4.1). They are the red, black, and dashed blue curves in Figs. 4.1, 4.3 and 4.4. In the evaluation of the predictions for EWDBD and the Higgs data we have kept the contribution of the Wilson coefficients to the physical observables up to the quadratic order.

4.2.1 Gauge Boson Couplings to Fermions

In Fig. 4.1 we show the bounds of the Wilson coefficients for the operators involving gauge boson and fermion fields and which directly modify the gauge couplings to fermions. As mentioned before, EWPD yields strong bounds on deviations of the SM predictions for the fermion-gauge interactions, and this is quantified in the green curves in the figure. The black (red) curves corresponds to the bounds of the same Wilson coefficients after the inclusion of the LHC data from EWDBD and Higgs observables (now in the larger 20 parameter space) collected at Run 1 (and Run 2).

In the upper left panel of Fig. 4.1, we find the $\Delta\chi^2$ dependence on $f^{(1)}_{\Phi,e}/\Lambda^2$ which is the coefficient of the only operator involving gauge couplings to leptons remaining in the basis after applying the EOM. This operator modifies the Z coupling to right-handed leptons which were precisely tested at LEP. On the contrary, at the LHC observables it enters only via its contribution to the decay rate of the Z boson to leptons in some of the final states considered. Consequently, as seen in the figure, the inclusion of the LHC data does not add any meaningful information about this coefficient.

The central and right upper panels in Fig. 4.1 display the $\Delta\chi^2$ dependence on the coefficients $f^{(1)}_{\Phi,Q}/\Lambda^2$ and $f^{(3)}_{\Phi,Q}/\Lambda^2$, which correspond to operators modifying the couplings of left-handed quarks to Z and W bosons. On the other hand, the left and central lower panels correspond to the dependence on $f^{(1)}_{\Phi,u}/\Lambda^2$ and $f^{(1)}_{\Phi,d}/\Lambda^2$ which give corrections to the u_R and d_R couplings to Z respectively. Comparing the green with the black and red lines we see that the impact of the inclusion of the LHC results is still minor but not negligible, in particular for $f^{(1)}_{\Phi d}/\Lambda^2$. The EWPD analysis favors non-vanishing value for $f^{(1)}_{\Phi d}/\Lambda^2$ at 2σ, a result driven by the 2.7σ discrepancy between the observed $A^{0,b}_{\rm FB}$ and the SM. On the contrary, no significant discrepancy is observed between the relevant LHC observables, in particular in

EWDBD, and the SM predictions. Hence there is a shift towards zero of $f_{\Phi d}^{(1)}/\Lambda^2$ when including the LHC data in the analysis. This slightly smaller tension results also into the reduction of the globally allowed range. This behavior was already observed in Section 3.1 for Run 1 data and the inclusion of Run 2 results adds in this direction.

Finally, in the right lower panel we show the $\Delta\chi^2$ on the coefficient of $\mathcal{O}_{\Phi,ud}^{(1)}$ operator. This operator induces a right-handed coupling of the W boson to quarks. We already discussed how this operator does not interfere with the SM and it effect at the linear level, so the EWPD analysis cannot constrain its Wilson coefficient. Nevertheless, it contributes to the LHC observables which we keep up to the quadratic order (notice that $\Delta\chi^2$ as a function of this coupling is symmetric around zero even though its minimum is not exactly at zero), and so it is possible to obtain the dependence observed in the same figure.

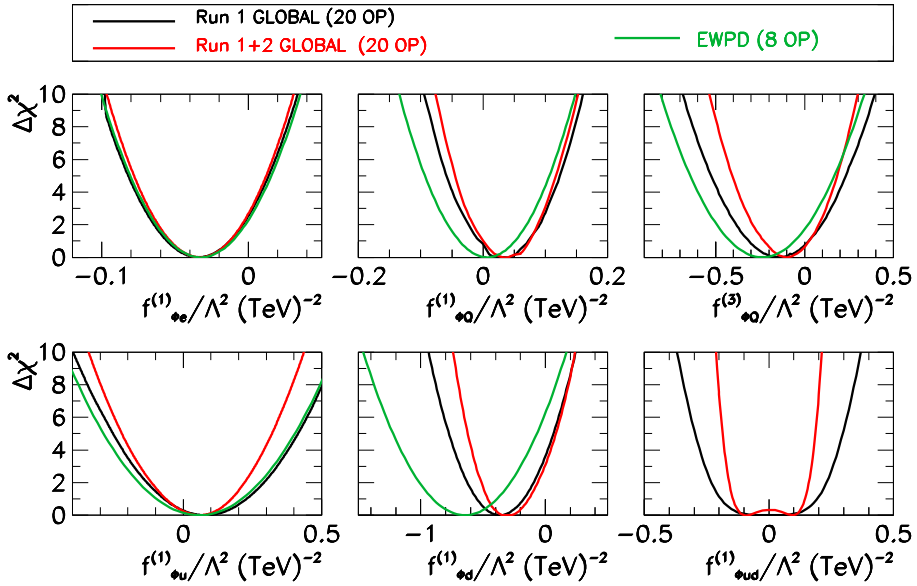

Figure 4.1: $\Delta\chi^2$ as a function of the fermionic Wilson coefficients $f_{\Phi,e}^{(1)}/\Lambda^2$, $f_{\Phi,Q}^{(1)}/\Lambda^2$, $f_{\Phi,Q}^{(3)}/\Lambda^2$, $f_{\Phi,u}^{(1)}/\Lambda^2$, $f_{\Phi,d}^{(1)}/\Lambda^2$, and $f_{\Phi,ud}^{(1)}/\Lambda^2$, as indicated in the panels after marginalizing over the remaining fit parameters. The green solid line stands for the fit of the EWPD that constrains only eight of twenty Wilson coefficients in Eq. (4.1). The black (red) solid line represents the twenty-parameter fit to the LHC Run 1 (and 2) data.

4.2.2 Triple Anomalous Gauge Interactions

For Run 2 the number of experimental studies focused on deriving constraints in the size and structure of TGCs is very limited and makes use only of a small fraction of their collected data [71]. But the ATLAS collaboration has presented results on diboson production in Ref. [72, 73] which we make use to test the TGCs.

The results of our analysis of the ATLAS Run 2 WW and WZ leptonic data [72, 73] together with the EWPD in the twelve-dimensional parameter space

$$\left\{ f_B, f_W, f_{WWW}, f_{BW}, f_{\Phi,1}, f^{(3)}_{\Phi,Q}, f^{(1)}_{\Phi,Q}, f^{(1)}_{\Phi,u}, f^{(1)}_{\Phi,d}, f^{(1)}_{\Phi,ud}, f^{(1)}_{\Phi,e} \right\}$$

are shown in the upper panels in Fig. 4.2, where we plot the one–dimensional $\Delta\chi^2$ distributions for the Wilson coefficients of the canonical TGC operators $\mathcal{O}_B$, $\mathcal{O}_W$ and $\mathcal{O}_{WWW}$ after marginalization over the 11 undisplayed coefficients.

As expected, the WZ channel gives no constraint on $\mathcal{O}_B$ while both WW and WZ contribute with similar precision to the determination of f_W/Λ^2 and f_{WWW}/Λ^2. To illustrate the possible effect of our assumptions on the correlations of the systematic/theoretical uncertainties (labeled as SYS in the figure) among the different bins we show the results obtained with full (zero) correlation among those uncertainties in the dashed (solid) lines. As seen in the figure the effect is small.

In the lower panels we show the impact of adding the Run 2 WW and WZ results to the analysis of the Run 1 diboson data of the last Chapter, which included data on WW and WZ channels from both ATLAS and CMS collected with ~ 20 fb^{-1} at each experiment.

Altogether we find that the combined ATLAS Run 2 diboson data constrains the operator coefficients with a bit better precision to that of the full Run 1 analysis. This is expected from simple statistics of the integrated luminosity and energy scaling. The combination of CMS and ATLAS Run 1 data accounts for about 40 fb^{-1} in each WW and WZ channels which is of the order of the 36 fb^{-1} of ATLAS Run 2 data. Moreover, the total cross section for diboson productions is about twice larger at Run 2 than at Run 1.

In the next section we shall include the Higgs interactions on data set, as a last step to achieve a true global analysis of the LHC data combined with the EWPD. The inclusion of the Higgs data also provides a stringent to the anticipated degeneracies in the parameter space of the couplings between the Higgs and the fermions.

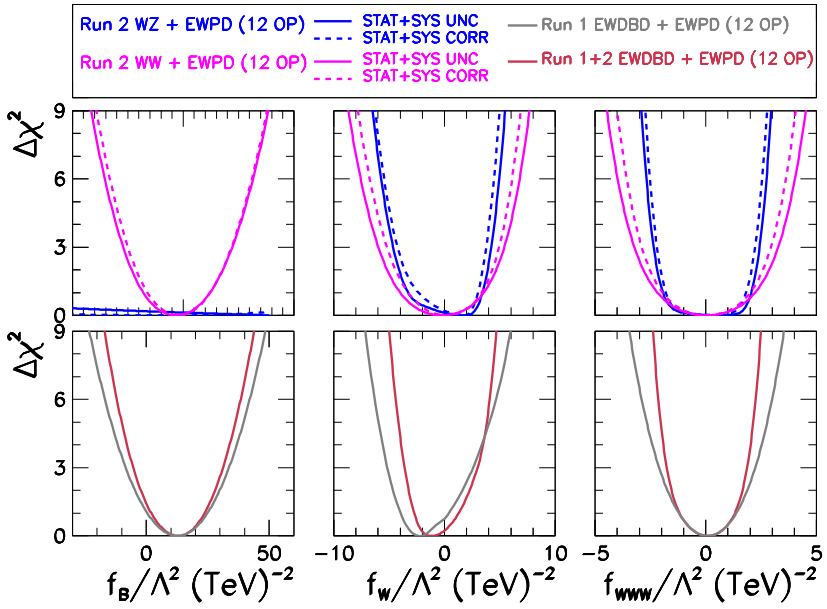

Figure 4.2: $\Delta\chi^2$ dependence on the f_B/Λ^2 (left panel), f_W/Λ^2 (central panel) and f_{WWW}/Λ^2 (right panel) parameters after the marginalization over the 11 undisplayed fit parameters for the analysis of LHC EWDBD and EWPD. The upper panels show the results of our analysis of the ATLAS Run 2 data on WZ [72] and on WW [73] transverse mass distributions. Full lines (dashed) correspond to assuming zero (total) correlation among the non-statistical uncertainties; see text for details. The lower panels show the results of the analysis of the EWDBD from Run 1 of Chapter 3 in combination with EWPD (black lines) and including also the results from ATLAS WW and WZ production at Run 2 (red line).

4.2.3 Higgs Interactions

Besides the introduction of the Run 2 data in the EWDBD, the inclusion of the Higgs observables in the data set is a novel feature of the analysis with respect to the one done in Chapter 3.

Our results concerning the determination of the Wilson coefficients for the operators affecting the interactions of the Higgs field with the gauge bosons and with fermions are shown in Figs. 4.3 and 4.4, respectively. In order to perform the most general analysis of the Higgs boson couplings we use the full data set that we presented in Section 4.1, *i.e.* EWPD, EWDBD and Higgs data, including the effect of the 20 operators in Eq.(4.1).

Figure 4.3 depicts the one–dimensional $\Delta\chi^2$ as a function of the Wilson coefficients of the pure bosonic operators in Eq.(4.1) after fitting the EWPD and Run 1 (and 2) data on Higgs and diboson productions. As expected, the most stringent constraints are those on the oblique operators $\mathcal{O}_{\Phi,1}$ and $\mathcal{O}_{BW}$ that come from the EWPD with very little impact of the LHC data, as we shown in Chapter 3.

The first row of Fig. 4.3 contains the $\Delta\chi^2$ distributions for the coefficients of the canonical TGC operators. As discussed in Chapter 3, only $\mathcal{O}_B$ and $\mathcal{O}_W$ enter both in TGCs and Higgs processes. For completeness we include here the results of our global analysis on f_{WWW}/Λ^2 also but we notice that $\mathcal{O}_{WWW}$ does not involve the Higgs field. As we can see, altogether the inclusion of the Run 2 data improves the bounds on the coefficients of the three canonical TGC operators by a factor $\mathcal{O}(25\%)$. Also comparing the results for these operators to the second row of Fig. 4.2 we learn that the inclusion of the Higgs data set strengthens the bounds on f_B/Λ^2 and f_W/Λ^2 derived from the EWDBD analysis by $\mathcal{O}(10$ –$20\%)$ [46].

We know that the Higgs decay into two photons is a very well measured channel. The operators $\mathcal{O}_{BB}$ and $\mathcal{O}_{WW}$ modify the Higgs decay into two photons with a contribution proportional to $f_{BB}/\Lambda^2 + f_{WW}/\Lambda^2$, therefore, introducing a strong correlation between these operators [29]. This is illustrated in the left panel of Fig. 4.5, where we show the two–dimensional allowed regions from the global analysis for different pairs of Wilson coefficients after marginalizing over the 18 undisplayed parameters in each panel. The strong anti-correlation is still present after combining Run 1 and II data. Also the left panel of the same figure, clearly displays the two quasi-degenerate solutions: the lower one containing the SM solution ($f_{WW} = f_{BB} = 0$) and the upper one with flipped sign of the $H\gamma\gamma$ coupling "displaced" by ~ 3 TeV^{-2}, as it was anticipated in the beginning of this chapter (see Eq.(4.5)).

The lower row of Fig. 4.3 contains the results for f_{GG}/Λ^2 and $f_{\Phi,2}/\Lambda^2$ where we can see the discrete (quasi-) degeneracies, explained in Eqs. (4.4) and (4.2) and resulting from the reversion of the sign of the Hgg and HVV ($V = Z, W$) couplings respectively. Since the f_{GG}/Λ^2 coupling only appears in one vertex, the two solutions are completely equivalent. On the other hand, the operator $\mathcal{O}_{\Phi,2}$ modifies universally all the SM-like Higgs couplings to gauge bosons and fermions, as a consequence of renormalization of the Higgs wave function. For each of them there are two degenerate solutions due to the total reversal of the coupling sign, but they would only lie at exactly the same values of $f_{\Phi,2}/\Lambda^2$ if all the couplings were measured to have the same ratio to their SM value. The quasi-degeneracy in

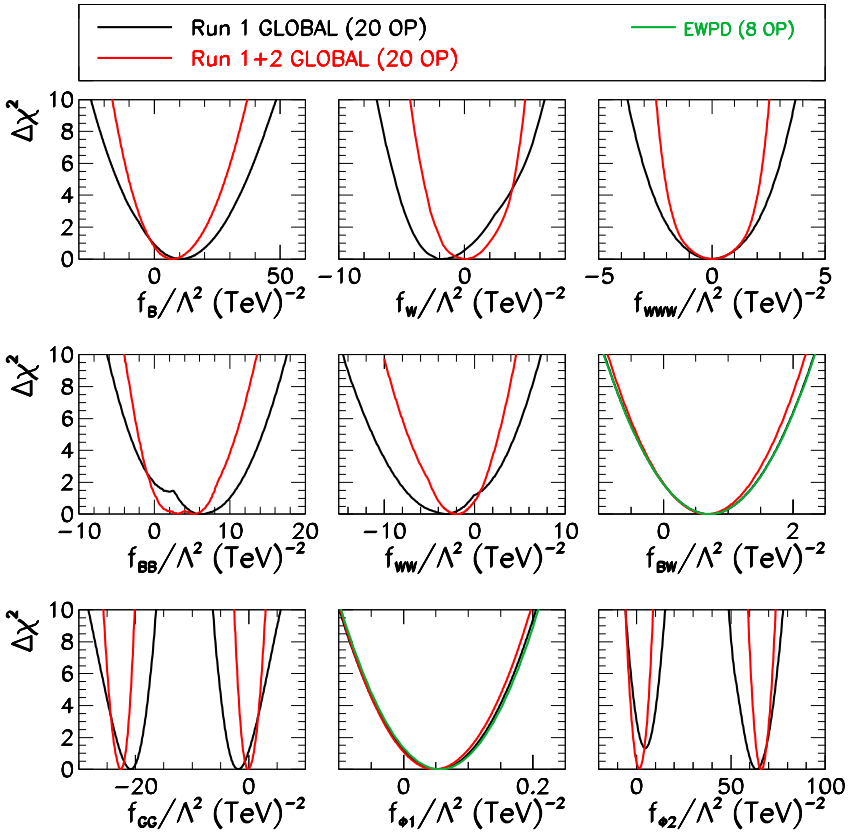

Figure 4.3: $\Delta\chi^2$ dependence on the bosonic Wilson coefficients f_B/Λ^2, f_W/Λ^2, f_{WWW}/Λ^2, f_{BB}/Λ^2, f_{WW}/Λ^2, f_{BW}/Λ^2, f_{GG}/Λ^2, $f_{\Phi,1}/\Lambda^2$, and $f_{\Phi,2}/\Lambda^2$ as indicated in each panel. The black (red) line stands for the results of the twenty-parameter fit using EWPD, EWDBD and Higgs data from LHC Run 1 (and 2). As before, the green line stands for the fit of only the EWPD.

$f_{\Phi,2}/\Lambda^2$ present in our global analysis originates from the lack of tension between the SM predictions and the data for all processes so values around $f_{\Phi,2}/\Lambda^2 \sim 0$ and $f_{\Phi,2}/\Lambda^2 \sim \frac{4}{v^2}$ with all other couplings zero can lead to a good global description of the data. As seen in the figure, the addition of Run 2 data has contributed in this direction.

Finally we display our results on the Wilson coefficients of the operators generating anomalous Yukawa couplings. From Fig. 4.4 we can see that Run 2 (red curve) is essential to better constrain these Wilson coefficients, when compared with the $\Delta\chi^2$ dependence from Run 1 data set (black curve). Once again, it is illustrated the presence of the three discrete solutions, in the parameter space, for

f_b/Λ^2 and f_τ/Λ^2 which originate from Eqs.(4.2)) and (4.3). On the other hand, we would expect the same type of dependence of $\Delta\chi^2$ for each of the Wilson coefficients associated to the operators that generate anomalous couplings. Nevertheless, we see that the data on Higgs decay into muon pairs is still incipient and within the present precision the allowed regions around the three minima merge into a unique allowed range.

Additionally, while displaying the results from the GLOBAL analysis in Fig. 4.4, we contemplate two assumptions for the top-Higgs associate production in Run 2. As described in Ref. [75] both ttH and tH (including tHW and tHj) contribute to the cross section ratio given in Fig. 4.6 of that reference. But with the information provided, it is not possible to determine the relative contribution of tH vs ttH to the reconstructed total cross section ratio. To overcome this issue, we decided to show the results for two extreme assumptions: a ratio of the tH to ttH contribution as predicted by the model (*i.e.* exactly same reconstruction efficiency for both subprocesses), shown as the dashed blue lines in the figure, and a negligible small contribution from tH shown in the red line. For consistency, we see that the results for all non-top Yukawa couplings are exactly the same for the two analyses. For f_t/Λ^2 we find that including a "full" tH contribution results into the total breaking of the degeneracies and eliminates solutions other than the ones around $f_t/\Lambda^2 = 0$. This can also be seen in the right panel in Fig. 4.5 where we show the allowed regions in the plane f_t/Λ^2 vs $f_{\Phi,2}/\Lambda^2$. The void and colored regions of this panel show the four solutions resulting from Eqs. (4.2) and (4.3) which are quasi-degenerated as long as no information on the sign of the ttH coupling is available. On the other hand, the colored regions are the only ones allowed once the information on tH is included in the analysis as described above. This is expected as the tH scattering amplitude receives contributions from the ttH and VVH vertices, therefore, being sensitive to the relative sign of the different diagrams contributing to it [81–83]. In fact, the sign with respect to the SM of the vertices ttH and VVH are the same in the surviving colored regions in Fig. 4.5. This is an important result, since it shows how the data measured from the tH production rate can unambiguously determine the coupling of the Higgs to the top quark. Certainly the sign of the top Yukawa coupling can be corroborated by other channels; see for instance Refs. [31, 84].

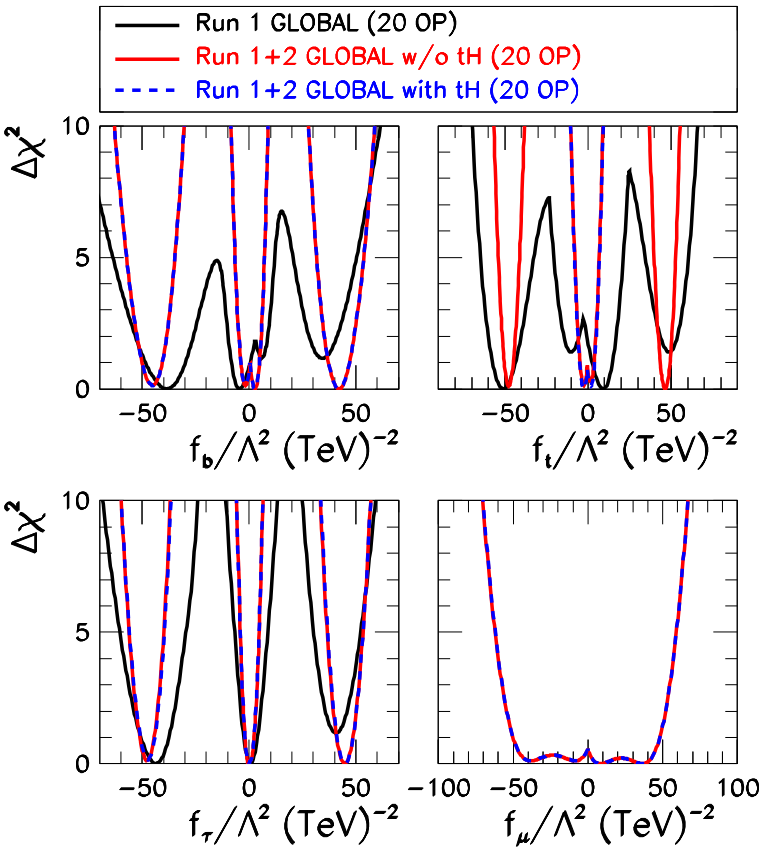

Figure 4.4: $\Delta\chi^2$ dependence on the fermionic Wilson coefficients f_b/Λ^2, f_t/Λ^2, f_τ/Λ^2, and f_μ/Λ^2 as indicated in each panel. The black (blue) line stands for the results of the twenty-parameter fit using EWPD, diboson production and Higgs data from LHC Run 1 (and II). The red line represents that results obtained using EWPD, diboson production and Higgs data from LHC Run 1 and II without the tH contribution to the Higgs top associate production cross section (see text for details).

4.2.4 Results at Linear Order of the Wilson Coefficients

In order to interpret Eq.(2.12) as a systematic expansion in the large mass parameter Λ [85], its contributions to observables at the lowest order $(1/\Lambda)$ are given the interference between anomalous and SM terms. Notwithstanding, in our calculations to get the the BSM cross section we kept the interference between anomalous

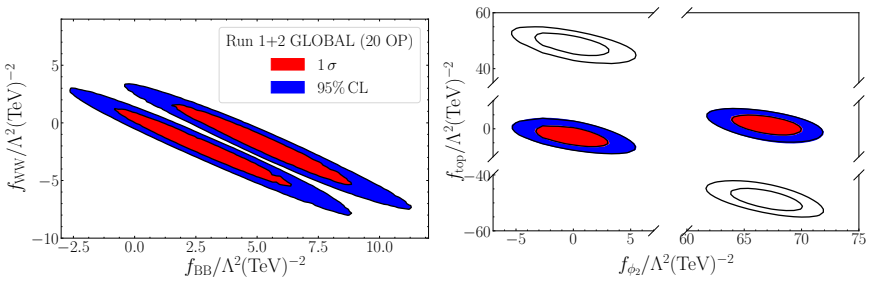

Figure 4.5: 1σ and 95% CL (2dof) allowed regions from the global analysis in the planes indicated in the axes. In the right panel the filled regions are obtained from the global analysis including the tH contribution to the top Higgs associate production data of ATLAS at Run 2 while the void regions are the additional solutions allowed when the tH contribution is not included.

couplings, *i.e.*

$$\sigma_{BSM} \sim \frac{1}{s}\left(|\mathcal{A}_{SM}|^2 + \mathcal{A}^*_{SM}\frac{\mathcal{A}^6_{EFT}}{\Lambda^2} + \frac{|\mathcal{A}^6_{EFT}|^2}{\Lambda^4} + ...\right) \tag{4.9}$$

So, if one keeps the quadratic contributions on the Wilson coefficients of dimension–six operators one should include the interference of dimension–eight operators with the SM as they are of the same order, *i.e.*terms like $\mathcal{A}^*_{SM}\mathcal{A}^8_{EFT}/\Lambda^4$.

Up to this point we consider the effective lagrangian Eq.(4.1) as a straw man that we use to probe the standard model couplings assuming that it contains all information on possible new physics. The results obtained are thus physically meaningful as long as no large cancellations between the dimension–six quadratic terms and the (here absent) linear dimension–eight SM interference are expected. Furthermore, this is a pragmatic approach since there are phase space regions where the lowest order systematic expansion fails [59] that is signaled by the cross section being negative! Notwithstanding, the use of the quadratic contributions of the dimension–six operators is justified if the new physics is strongly interacting; see for instance Refs. [35–37]. Indeed, this result is consequence of Naive Dimensional Analysis [86] and some simple power counting analysis. In any case, Ref. [38] shows that the analysis of the LHC data in terms of dimension–six operators is adequate in almost all realistic weakly coupled scenarios, except in the high energy tails of distributions.

An interesting exercise would be to remake our twenty-parameter fit using only the contributions to the observables at linear order on the Wilson coefficients. By

doing so, we can understand how important are the anomalous quadratic terms in the evaluation of the observables and if with the current amount of available data one can derive strong bounds on the Wilson coefficients. Our results are depicted in Fig. 4.6.

Comparing the results of the dashed curves in Fig. 4.6 with the green curves in Fig. 4.1 we notice that the $\Delta\chi^2$ distributions as a function of (f_{BW}, $f_{\Phi,1}$, $f^{(3)}_{\Phi,Q}$, $f^{(1)}_{\Phi,Q}$, $f^{(1)}_{\Phi,u}$, $f^{(1)}_{\Phi,d}$, $f^{(1)}_{\Phi,e}$, f_{LLLL}) are very much the same as obtained using only the EWPD (see also Table 4.2). This is a clear sign of the influence of the quadratic terms, where the contributions for these particular set of Wilson coefficients due to the diboson and Higgs data arise mainly from the non-linear terms. Moreover, within the input range of variation of the parameters in the analysis, the operator $\mathcal{O}_{\Phi,ud}$ is not bounded if the observables are evaluated using just the linear terms of their Wilson coefficients while $\mathcal{O}_{WWW}$ is only very weakly constrained. This happens because the dominant contributions of these operators are to helicity amplitudes to which the SM does not contribute, as we discussed in Section 3.1.

The results in Fig. 4.6 show that the Higgs data is already precise enough to determine $f_{\Phi,2}/\Lambda^2$ and f_{GG}/Λ^2 in the linear approximation with the quadratic terms being subdominant. Moreover, as expected, at linear order there are no degenerate solutions in these couplings and the allowed regions encompass only the SM. Same applies to the Yukawa-like operators so the corresponding coefficients f_f/Λ^2 have no degenerate solutions. And therefore the f_μ/Λ^2 seems better determined. We also find that at present the Higgs data is precise enough to bound the couplings f_{BB}/Λ^2 and f_{WW}/Λ^2 using the linear evaluation of the observables, however, the size of the 95% CL allowed area increases by a factor of $\simeq 2$. Similarly the bounds on f_B/Λ^2 and f_W/Λ^2 are a factor of $\mathcal{O}(3-4)$ weaker than those obtained when we include the quadratic terms [46]. Nevertheless, this is already very interesting since the diboson production alone does only lead to very mild bounds on these last two couplings when not including the quadratic contributions, which indicates again the relevance of the Higgs observables.

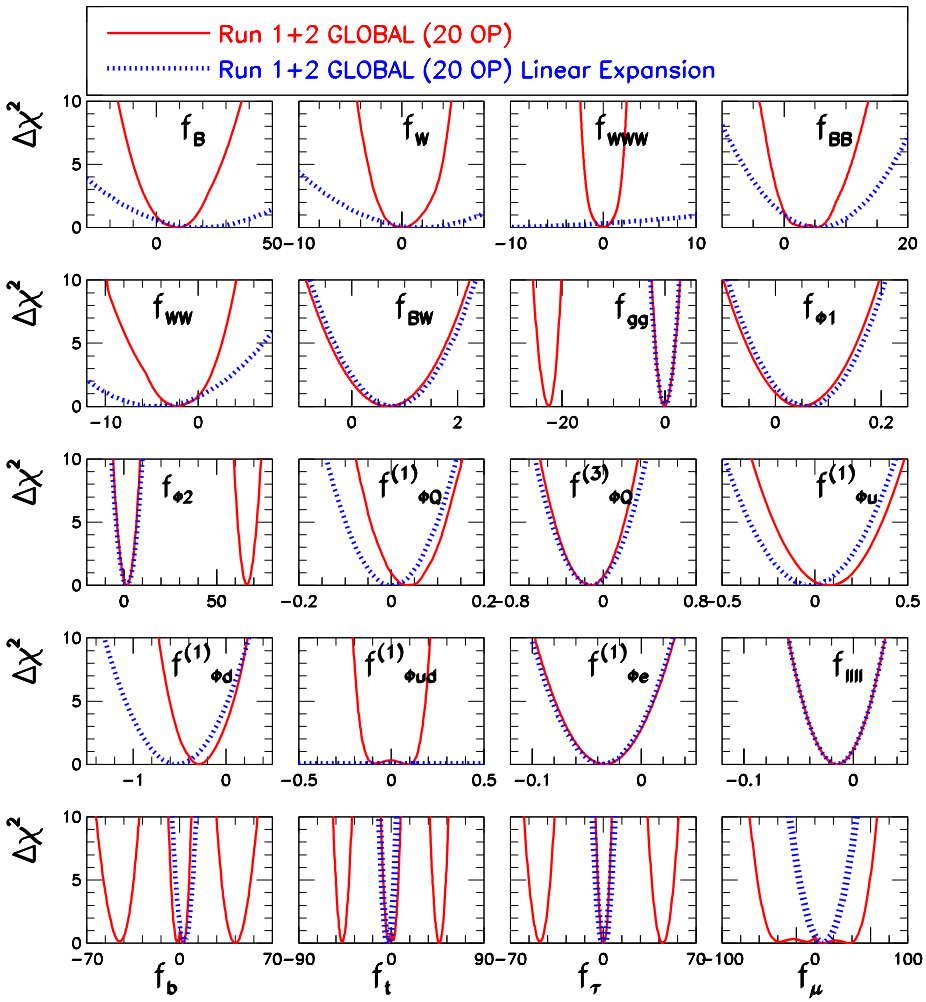

Figure 4.6: $\Delta\chi^2$ dependence on the bosonic Wilson coefficients f/Λ^2 as indicated in each panel. The results using only the linear terms in the anomalous couplings are indicated by the blue dotted curves. The red solid curves stands for the fits keeping the quadratic contributions of the anomalous couplings to the observables. The full data set was used in both cases.

4.2.5 Updated Analysis with the Higgs invisible decay width

The rate for invisible decays of the Higgs boson may be enhanced in the context of NP effects, an effect which was not accounted for in the analysis presented so far. To test the robustness of the results obtained under the inclusion of a possible invisible decay of the Higgs we present in this section the same analysis previously done in this chapter but with one additional parameter, the Higgs boson invisble decay width. We also add the experimental constraint from the latest CMS data on the invisible Higgs decay [87]. As one can see from Fig.4.7, the results show

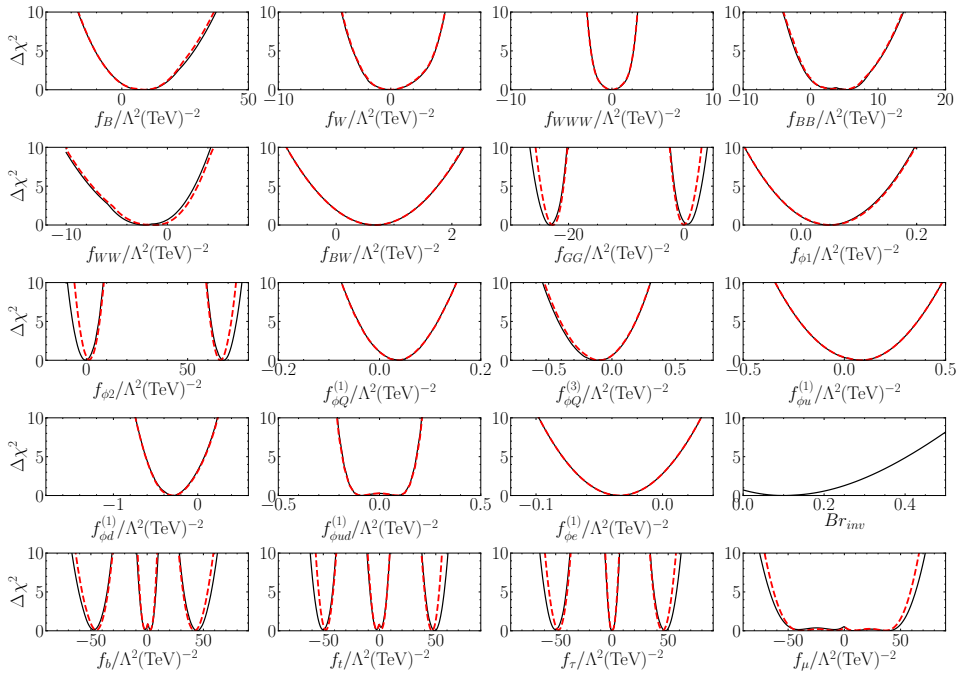

Figure 4.7: $\Delta\chi^2$ dependence on Wilson coefficients f/Λ^2 as indicated in each panel. The results using the Higgs invisible width decay are indicated by the black curves. The red dashed curves stands for the fits without the Higgs invisible width decay. For simplicity we do not plot (but it is included in the fit) the bounds on the coefficient f_{LLLL}.

that the constraints on the Wilson parameters presented in the previous sections are robust when including the invisble width in the fit.

4.3 Summary and Discussion

In this chapter we have performed a comprehensive analysis of the observables related to the electroweak sector, which at present allows for precision tests of the couplings between electroweak gauge bosons and fermions, triple electroweak gauge couplings and the couplings of the Higgs to fermions and gauge bosons. This includes low energy electroweak precision measurements as well as LHC data on gauge boson pair production and Higgs observables. In total, the GLOBAL analysis of EWPD and EWDBD and Higgs results from LHC Run 1 encompasses 64 observables and including Run 1 and 2, 122 observables. By including these three different sets of data and assuming that the new operators do not introduce new tree level sources of flavor violation nor violation of universality of the weak current, the global analysis involves the 20 operators in Eq. (4.1) of which 8 contribute to EWPD (Eq.(2.99)), 4 additional enter in the combination with the LHC EWDBD (Eq.(2.100)), and the 20 operators enter once the Higgs observables are considered.

Altogether the analyses show no statistically significant source of tension with the SM. We find for the SM a $\chi^2_{\rm SM} = 118$ (71.2) for the 122 (64) observables in the GLOBAL analysis of EWPD and EWDBD and Higgs results from LHC Run 1+2 (only Run 1). Including the 20 Wilson coefficients in the fit, we find $\chi^2_{\mathcal{L}_{eff}} = 91$ (52.3). As a consequence, bounds on the Wilson coefficients can be imposed. The 95% allowed ranges for the 20 Wilson coefficients (profiled from the global 9-,12-, or 20-dimensional likelihoods) are listed in Table 4.2. The corresponding allowed 95% CL ranges for the global analysis with Run 1 and Run 1 + 2 EWDBD and Higgs observables are also graphically displayed in Fig. 4.8.

In brief, we find:

- The coefficients of the eight operators contributing to the EWPD are those better determined, as could be anticipated. The inclusion of the LHC EWDBD and Higgs observables has negligible impact on those operators contributing to the couplings of leptons, $\mathcal{O}_{LLLL}$, $\mathcal{O}^{(3)}_{\Phi,e}$, $\mathcal{O}_{\Phi,1}$, and $\mathcal{O}_{BW}$.

- The impact of the inclusion of the LHC results is still minor but not negligible for the EWPD bounded operators involving gauge couplings to quarks. In particular for $f^{(1)}_{\Phi d}/\Lambda^2$, under the assumption of generation universality a non-zero value for this coefficient is favored in the EWPD analysis coming from the 2.7σ discrepancy between the observed $A^{0,b}_{\rm FB}$ and the SM. On the contrary, LHC observables involving this operator, are fully consistent with the SM what results in the shift and reduction of its globally allowed range.

Operator	95% CL f/Λ^2 (TeV^{-2})				
	EWPD	EWPD+EWDBD	GLOBAL Run 1	GLOBAL Run 1+2	GLOBAL Run1+2 Linear
$\mathcal{O}_{LLLL}$	(-0.043, 0.013)	(-0.043, 0.013)	(-0.043, 0.013)	(-0.043, 0.013)	(-0.043, 0.013)
$\mathcal{O}^{(3)}_{\Phi,e}$	(-0.075,0.011)	(-0.075,0.007)	(-0.077,0.009)	(-0.075,0.007)	(-0.077,0.005)
$\mathcal{O}_{\Phi,1}$	(-0.040,0.15)	(-0.040,0.15)	(-0.043,0.15)	(-0.044,0.14)	(-0.034,0.15)
$\mathcal{O}_{BW}$	(-0.32,1.7)	(-0.27,1.7)	(-0.32,1.7)	(-0.30,1.7)	(-0.21,1.8)
$\mathcal{O}^{(3)}_{\Phi,Q}$	(-0.60,0.12)	(-0.45,0.13)	(-0.49,0.11)	(-0.38,0.15)	(-0.41,0.19)
$\mathcal{O}^{(1)}_{\Phi,Q}$	(-0.083,0.10)	(-0.034,0.11)	(-0.049,0.11)	(-0.036,0.11)	(-0.089,0.088)
$\mathcal{O}^{(1)}_{\Phi,d}$	(-1.2,-0.13)	(-0.64,-0.007)	(-0.73,0.02)	(-0.56,0.04)	(-1.0,-0.03)
$\mathcal{O}^{(1)}_{\Phi,u}$	(-0.25,0.37)	(-0.17,0.37)	(-0.22,0.38)	(-0.19,0.33)	(-0.32,0.25)
$\mathcal{O}^{(1)}_{\Phi,ud}$	—	(-0.17,0.17)	(-0.29,0.29)	(-0.18,0.18)	—
$\mathcal{O}_B$	—	(-7.8,34)	(-12,34)	(-8.3,26)	(-31,70)
$\mathcal{O}_W$	—	(-3.9,3.5)	(-5.2,3.5)	(-3.0,3.7)	(-9.5,13)
$\mathcal{O}_{WWW}$	—	(-1.9,2.0)	(-2.6,2.5)	(-1.9,2.0)	(-64,36)
$\mathcal{O}_{BB}$	—	—	(-2.5,13)	(-1.7,10)	(-5.4,16)
$\mathcal{O}_{WW}$	—	—	(-10,3.7)	(-6.7,2.1)	(-15,5.8)
$\mathcal{O}_{GG}$	—	—	(-25,-17)$\cup$(-4.7,2.1)	(-25,-21)$\cup$(-1.7.1,8)	(-1.8,1.7)
$\mathcal{O}_{\Phi,2}$	—	—	(-1.1,10) $\cup$(55,72)	(-3.2,6.2)$\cup$(62,71)	(-3.7,6.9)
$\mathcal{O}_{d\Phi,33}$	—	—	(-62,-20)$\cup$(-12,11)$\cup$(23,45)	(-56,-36)$\cup$(-6.1,6.7)$\cup$(33,52)	(-2.2, 9.2)
$\mathcal{O}_{u\Phi,33}$	—	—	(-64,-35)$\cup$(-19,20)$\cup$(37,59)	(-53,-42)$\cup$[-7.4,6.2]$\cup$(40,52)	(-8.3,2.4)
$\mathcal{O}_{e\Phi,33}$	—	—	(-59,-31) $\cup$(-5.8,7.8)$\cup$(32,50)	(-55,-41)$\cup$(-3.7,4.3)$\cup$(37,52)	(-4.8,5.4)
$\mathcal{O}_{e\Phi,22}$	—	—	—	(-50,57)	(-14,31)

Table 4.2: 95% allowed ranges for the Wilson coefficients for the different analysis performed in this work. For $\mathcal{O}_{u\Phi,33}$ we show in the 5th column the three discrete ranges allowed when no contribution of tH is included in the ATLAS cross section ratio. Including the tH contribution under the assumptions discuss in the text selects the range around zero which we mark with square brackets.

- The operator $\mathcal{O}^{(1)}_{\Phi,ud}$ induces right-handed charged current couplings for quarks and it can only be bound via its quadratic contributions. Including those in the LHC observables its Wilson coefficient can be bounded with precision comparable to that of the other operators affecting gauge-quark couplings.

- We have performed a novel analysis of the Run 2 ATLAS 36.1 fb^{-1} data on transverse mass distribution of W^+W^- and $W^\pm Z$ in the leptonic channel [72, 73] which allows for further tests of the TGC's. The results are shown in Fig. 4.2. We find that the combined ATLAS Run 2 diboson data constrains the operator coefficients with precision similar (a bit better indeed) to that of the full Run 1 analysis.

- Inclusion of the Run 2 results in the global analysis results into a reduction of the allowed range for the coefficients of the bosonic operators $\mathcal{O}_B$, $\mathcal{O}_W$, $\mathcal{O}_{WWW}$, $\mathcal{O}_{BB}$, and $\mathcal{O}_{WW}$ by 20–30%.

- The allowed values for f_{GG}/Λ^2 and $f_{\Phi,2}/\Lambda^2$ present each two discrete ranges originated by the degeneracy (it is a quasi-degeneracy for $f_{\Phi,2}$) associated with the reverse of the sign of the Hgg (Eq.(4.4)) and HXX ($X = f, V$)

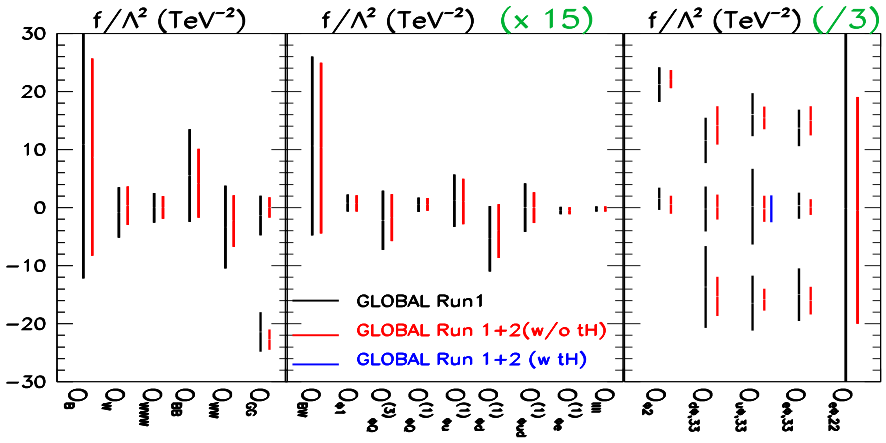

Figure 4.8: Allowed 95% CL ranges for each of the Wilson coefficients from the 20 parameter global analysis. We show results from the global EWPD+LHC analysis including Run 1 EWDB and Higgs observables only (black bars) and including both Run 1 and 2 EWDB and Higgs observables (red line). For the top Yukawa-like operator $\mathcal{O}_{u\Phi,33}$ we show as a blue bar the allowed range when considering the contribution from tHj and tHW in the to the top-Higgs associate production. To help graphical display the ranges in the central (right) panels are multiplied (divide) by a factor 30 (3) as indicated on the top.

(Eqs.(4.2),(4.3)), respectively. Barring that degenerate solutions these are the best determined coefficients for operators not contributing to EWPD.

- The allowed values for the coefficients for the Yukawa-like operators $\mathcal{O}_{d\Phi,33}$ and $\mathcal{O}_{e\Phi,33}$ (f_b, and f_τ), have a two folded degeneracy associated with the reverse of the sign of the corresponding Hff coupling (see Eq.(4.3)) in combination with the reverse of the sign of the HVV coupling. This results into the three discrete allowed ranges in Table 4.2. For the $\mathcal{O}_{e\Phi,22}$ coefficient, f_μ, the data is not precise enough to resolve the three solutions.

- For $\mathcal{O}_{u\Phi,33}$, the inclusion of the incipient tH data can break those degeneracies on f_t, this is, in the determination of the top-Higgs coupling.

- The last column in Table 4.2 shows the allowed ranges when only the terms linear in the Wilson coefficients are kept in the observables. For those operators constrained by EWPD the bounds are just that of the EWPD as at LHC

they are mainly constrained by its quadratic contribution. For the operators without degenerate solutions the bounds become weaker but are still within the same order or magnitude. Exceptions are $\mathcal{O}^{(1)}_{\Phi,ud}$ and $\mathcal{O}_{WWW}$ which become very weakly bounded as their dominant contributions at LHC are to helicity amplitudes which do not interfere with the SM ones. Keeping only the linear contribution to the observables does not allow for the degenerated solutions associated with the sign flip of the Higgs couplings. Consequently f_{GG}/Λ^2, $f_{\Phi,2}/\Lambda^2$, f_B/Λ^2, f_t/Λ^2, f_τ/Λ^2, and f_μ/Λ^2 appear to be better constrained.

- The results show that the fit of all parameters is robust when including the invisble width

- Our results show the importance of the Higgs data to constrain the TGC operators $\mathcal{O}_B$ and $\mathcal{O}_W$ when the LHC observables are evaluated using only the linear terms in the anomalous couplings. This extends the previous results in Refs. [23, 46].

Altogether we find that the increased integrated luminosity gathered at 13 TeV allows us to obtain more stringent bounds on a larger set of anomalous interactions and to perform new tests of the SM. We look forward for the release of the complete data set accumulated at Run 2.

Chapter 5

Light-Quark Dipole Operators at LHC

In Chapter 3 we studied the effect on the diboson production at LHC of a class of operators affecting the SM-like couplings of the gauge-bosons to fermions and which are constrained by the EWPD. We concluded that LHC processes are becoming competitive with the EWPD in the precision attainable to detect effects associated with those operators. This prompted us to the need of a combined analysis of EWPD and all relevant LHC observables to study in the most generality the EWSB sector, which we presented in Chapter 4.

As mentioned in the introduction of Chapter 4, in the analysis presented we left out a class of operators which also affect the gauge boson couplings to fermions, those generating dipole-like couplings, (2.19) which also enter in the LHC diboson processes. In this Chapter we proceed analyize the effect of including these dipole operators in our analysis. So, as we assume no family mixing and the Wilson coefficients to be generation independent, the relevant dimension–six contributions in the electroweak gauge-boson pair production depend upon 16 Wilson coefficients:

$$\mathcal{L}_{\rm eff} = \mathcal{L}_{\rm SM} + \mathcal{L}_{\rm eff}^{\rm EWPD} + \mathcal{L}_{\rm eff}^{\rm TGC} + \mathcal{L}_{\rm eff}^{\rm DIP} \ , \tag{5.1}$$

where $\mathcal{L}_{\rm eff}^{\rm EWPD}$, $\mathcal{L}_{\rm eff}^{\rm TGC}$ and $\mathcal{L}_{\rm eff}^{\rm DIP}$ are given by Eqs. (2.99), (2.100) and (2.103), respectively.

First by studying electroweak diboson production in Sec. 5.1 we will be able to test the possible effect of the dipole operators on the extracted information on the gauge boson self-couplings and indirectly on the global analysis presented in Chapter 4. The light-quark electroweak dipole operators have been previously studied using EWPD [60, 61], as well as deep inelastic scattering results from HERA [61],

leading to constraints on their Wilson coefficients of the order of 10 TeV^{-2}. So in Sec. 5.1 we compare the constrains on the Wilson coefficients of the light-quark electroweak dipole operators imposed by the the diboson (W^+W^-, $W^\pm Z$) production at the LHC Run 1 and 2 with the ones stemming from the EWPD analysis. Finally in Sec. 5.3 we consider also the information attainable from the analysis of Drell-Yan processes.

5.1 Effects in Electroweak Diboson Production

As mentioned before, deviations of TGC and gauge bosons interactions with quarks from the SM ones modify the high energy behavior of the scattering of quark pairs into two electroweak gauge bosons. We explicitly show in Eqs. (3.2)–(3.8) the leading scattering amplitudes in the helicity basis are for the W^+W^- and $W^\pm Z$ channels generated by the operators which modify the SM-like couplings of the gauge bosons to fermions. The corresponding leading scattering amplitudes in the helicity basis generated by the new operators that were not taken into account in the previous analysis, namely $\mathcal{O}^{(1)}_{\Phi ud}$, $\mathcal{O}_{uW,ij}$, $\mathcal{O}_{uB,ij}$, $\mathcal{O}_{dW,ij}$ and $\mathcal{O}_{dB,ij}$ [50, 51] read:

$$
\begin{aligned}
A(d_+\bar{u}_- \to W_0^- Z_0) &= -i\frac{s}{\Lambda^2}\sin\theta\sqrt{2}f^{(1)}_{\Phi ud}\,, && (5.2)\\
A(d_-\bar{d}_- \to W_0^+ W_+^-) &= -A(d_+\bar{d}_+ \to W_-^+ W_0^-) = -\frac{s}{\Lambda^2}\sin\theta\, g\, f_{dW} \\
&= -\frac{s}{\Lambda^2}\sin\theta\, e\, \left(s_W F_{d\gamma} + c_W F_{dZ}\right)\,, && (5.3)\\
A(u_-\bar{u}_- \to W_0^+ W_+^-) &= -A(u_+\bar{u}_+ \to W_-^+ W_0^-) = -\frac{s}{\Lambda^2}\sin\theta\, g\, f_{uW} \\
&= -\frac{s}{\Lambda^2}\sin\theta\, e\, \left(s_W F_{u\gamma} + c_W F_{uZ}\right)\,, && (5.4)\\
A(d_-\bar{u}_- \to W_0^- Z_+) &= \frac{s}{\Lambda^2}\sin\theta\frac{g}{\sqrt{2}c_W}\left\{s_W^2 f_{uB} + c_W^2 f_{uW}\right\} \\
&= \frac{s}{\Lambda^2}\sin\theta\frac{e}{\sqrt{2}}\left\{2c_W F^R_{udW} - F_{uZ}\right\}\,, && (5.5)\\
A(d_-\bar{u}_- \to W^- Z_0) &= -\frac{s}{\Lambda^2}\sin\theta\frac{g}{\sqrt{2}}f_{uW} = -\frac{s}{\Lambda^2}\sin\theta\frac{e}{\sqrt{2}}F^R_{udW}\,, && (5.6)\\
A(d_+\bar{u}_+ \to W_0^- Z_-) &= -\frac{s}{\Lambda^2}\sin\theta\frac{g}{\sqrt{2}c_W}\left\{s_W^2 f_{dB} - c_W^2 f_{dW}\right\} \\
&= \frac{s}{\Lambda^2}\sin\theta\frac{e}{\sqrt{2}}\left\{2c_W F^L_{udW} - F_{dZ}\right\}\,, && (5.7)\\
A(d_+\bar{u}_+ \to W_+^- Z_0) &= -\frac{s}{\Lambda^2}\sin\theta\frac{g}{\sqrt{2}}f_{dW} = -\frac{s}{\Lambda^2}\sin\theta\frac{e}{\sqrt{2}}F^L_{udW}\,, && (5.8)
\end{aligned}
$$

where s stands for the center-of-mass energy and θ is the polar angle in the center-of-mass frame.

In the limit of vanishing light-quark masses, the dipole operators contribute to different diboson helicity amplitudes than the SM or any of the other operators in Eq. (5.1) due to their tensor structure. Therefore, there is no interference between the contributions coming from the dipole operators and the SM and other dimension-six operators in Eq. (3.1), which by other words means that the dipole operators only contribute to these observables at the quadratic level.

As for the data considered in the analysis we will consider the same channels and kinematical distributions as Sec. 4.1 and listed in Table 4.1. The procedure to obtain the prediction of the relevant kinematical distributions in presence of the additional dimension–six operators is also similar to the one used in Chapter 3. We simulate W^+W^- and $W^\pm Z$ events within the experimental fiducial regions by applying the same cuts and isolation criteria adopted by the corresponding experimental analysis. This is carried out by using MADGRAPH5 [63] with the UFO files for our effective Lagrangian generated with FEYNRULES [64,65]. We employ PYTHIA6.4 [66] to perform the parton shower, while the fast detector simulation is done with DELPHES [67].

The higher order corrections and additional effects are taken into account in the usual way: we simulate the corresponding SM W^+W^- and $W^\pm Z$ events and normalize our results bin by bin to the SM predictions provided by the experimental collaborations. Then we apply these correction factors to our simulated WV distributions in the presence of the anomalous couplings.

The statistical confrontation of these predictions with the LHC data is made by means of a binned log-likelihood function based on the contents of the different bins in the kinematical distribution of each channel. Besides the statistical errors we incorporate the systematic and theoretical uncertainties including also their corresponding correlations. With this, we build $\chi^2_{\rm EWDBD}$

$$\chi^2_{\rm EWDBD}(f_B, f_W, f_{WWW}, f_{BW}, f_{\Phi,1}, f^{(3)}_{\Phi,Q}, f^{(1)}_{\Phi,Q}, f^{(1)}_{\Phi,u}, f^{(1)}_{\Phi,d}, f^{(1)}_{\Phi,ud}, f^{(1)}_{\Phi,e}, f_{LLLL}, f_{uB}, f_{uW}, f_{dB}, f_{dW}) \ . \quad (5.9)$$

We also include the information from EWPD, in particular from Z and W pole measurements,

$$\chi^2_{\rm EWPD}(f_{BW}, f_{\Phi,1}, f^{(3)}_{\Phi,Q}, f^{(1)}_{\Phi,Q}, f^{(1)}_{\Phi,u}, f^{(1)}_{\Phi,d}, f^{(1)}_{\Phi,ud}, f^{(1)}_{\Phi,e}, f_{LLLL}, f_{uB}, f_{uW}, f_{dB}, f_{dW}) \ , \quad (5.10)$$

where we have include the EWPO discussed in Chapter 2, *i.e.*twelve Z observables and three W observables. In building $\chi^2_{\rm EWPD}$ we incorporate the correlations among the above observables from Ref. [68] and the SM predictions and their uncertainties from [70].

In order to single out the possible effect of the dipole operators in the EWDBD analysis we make a combined analysis in which we include their effect in EWPBD but not in the EWPD observables. First, we make a fit to EWDBD+EWPD in terms of 16 operator coefficients using

$$\begin{aligned}
&\chi^2_{\rm EWDBD+EWPD}(f_B, f_W, f_{WWW}, f_{BW}, f_{\Phi,1}, f^{(3)}_{\Phi,Q}, f^{(1)}_{\Phi,Q}, f^{(1)}_{\Phi,u}, f^{(1)}_{\Phi,d}, f^{(1)}_{\Phi,ud}, f^{(1)}_{\Phi,e}, \\
&\qquad\qquad f_{LLLL}, f_{uB}, f_{uW}, f_{dB}, f_{dW}) \\
&= \chi^2_{\rm EWDBD}(f_B, f_W, f_{WWW}, f_{BW}, f_{\Phi,1}, f^{(3)}_{\Phi,Q}, f^{(1)}_{\Phi,Q}, f^{(1)}_{\Phi,u}, f^{(1)}_{\Phi,d}, f^{(1)}_{\Phi,ud}, f^{(1)}_{\Phi,e}, f_{LLLL}, \\
&\qquad\qquad f_{uB}, f_{uW}, f_{dB}, f_{dW}) \\
&\quad + \chi^2_{\rm EWPD}(f_{BW}, f_{\Phi,1}, f^{(3)}_{\Phi,Q}, f^{(1)}_{\Phi,Q}, f^{(1)}_{\Phi,u}, f^{(1)}_{\Phi,d}, f^{(1)}_{\Phi,ud}, f^{(1)}_{\Phi,e}, f_{LLLL}, \\
&\qquad\qquad f_{uB}=0, f_{uW}=0, f_{dB}=0, f_{dW}=0)
\end{aligned} \tag{5.11}$$

We then compare the allowed parameter ranges for the coefficients with those obtained from the a combined analysis in which the dipole operators are set to zero in the analysis of EWDBD as well.

The results of these analyses are shown in Fig. 5.1 where we display one-dimensional projections of the $\Delta\chi^2$ for both analysis. In each panel, χ^2 has been marginalized over all other 15 (or 11) coefficients. This figure clearly illustrates that the constraints on the 12 coefficients f_B, f_W, f_{WWW}, f_{BW}, $f_{\Phi,1}$, $f^{(3)}_{\Phi,Q}$, $f^{(1)}_{\Phi,Q}$, $f^{(1)}_{\Phi,u}$, $f^{(1)}_{\Phi,d}$, $f^{(1)}_{\Phi,ud}$, $f^{(1)}_{\Phi,e}$, and f_{LLLL} from the combined analysis of EWDBD at LHC and EWPD are robust independently of the inclusion of the dipole operators in the analysis. The impact of these dipole operators in the previous analyses is minimal.

5.2 Comparison with EWPD Bounds

From Figure. 5.1 it is possible to verify how the high energy of LHC data plays an important role in the diboson production to impose strong constraints on the electroweak dipole couplings of the light quarks. We quantify how much these bounds improve over the ones from EWPD in Fig. 5.2 where we show in the red line the constraints from the above analysis together with those obtained from Z- and W-pole EWPD exclusively (black lines).

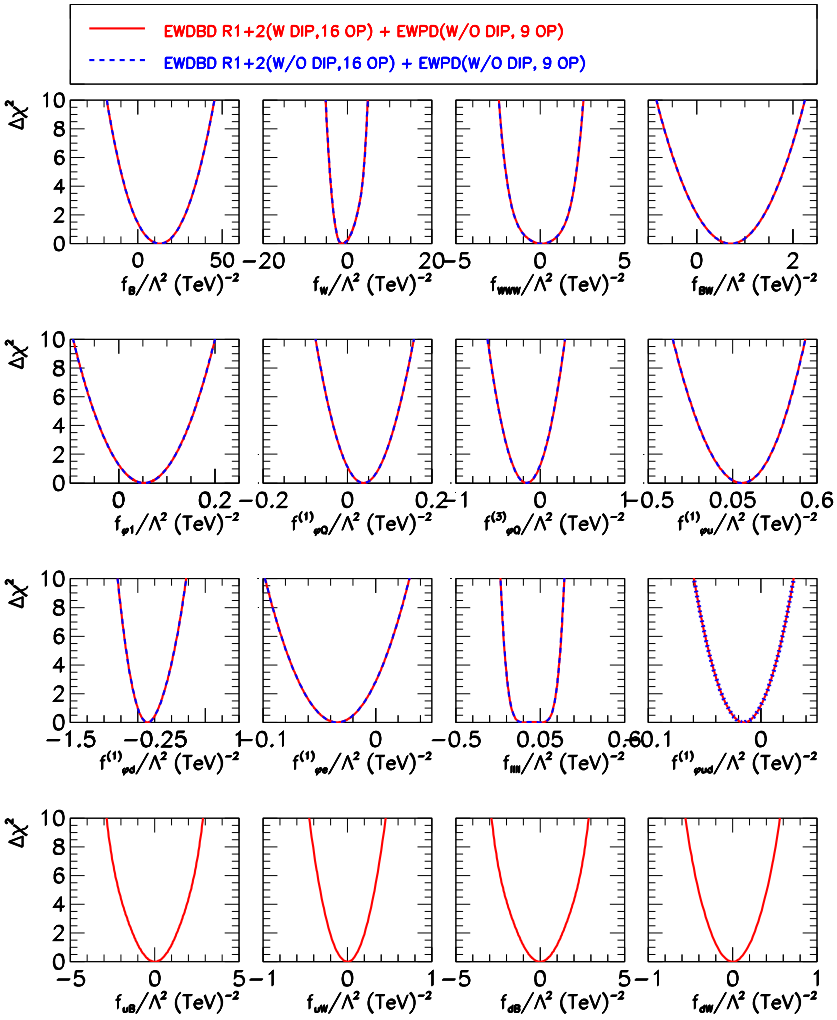

Figure 5.1: $\Delta\chi^2$ dependence on the Wilson coefficients of 16 operators (after marginalization in each panel over the undisplayed ones) entering the analysis of EWDBD from LHC Run 1 and 2 in combination with the EWPD. The red line includes the effect of light-quark dipole operators in diboson production but does not include then in the from EWPD (see Eq. (5.11) . The blue dashed lines are the results of the corresponding analysis without including the light-quark dipole operators (see text for details).

Moreover, to check if the EWPD bounds are suitable of changes in the presence of other operators, we show also the results when the coefficients of all non-dipole operators are set to zero (the black dashed line in Fig. 5.2). As expected the bounds

are only a bit stronger (about a factor O(30%)) when no other contribution is included.

As already mentioned, dipole operators enter quadratically in EWPD observables so we expect that their contribution cannot cancel against that of any other dimension six-operator. As a matter of fact, the presence of dimension–eight operators could led to a contribution that cancels against the one from the dipole operators, nevertheless we assume that does not happen in the derived bounds.

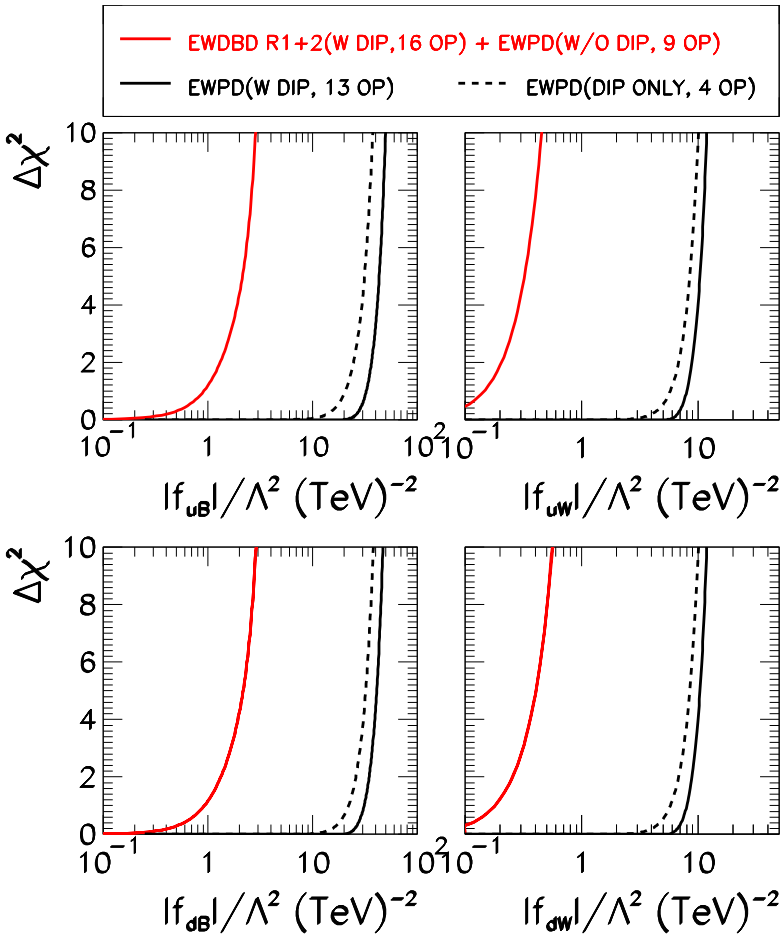

Figure 5.2: $\Delta\chi^2$ dependence on the four fermionic Wilson coefficients of the dipole operators from the combined analysis of diboson data and EWPD after marginalizing over the 15 undisplayed coefficients (full red lines), EWPD after marginalizing over the 12 undisplayed parameters (full black lines) and EWPD with only the four quark dipole operator after marginalizing over the 3 undisplayed coefficients (black dashed line).

As seen in figure. 5.2, the bounds from EWPD are weaker than those from LHC EWDBD by more than an order of magnitude. The reason for this is two folded. First, the EWPD constraints are mainly driven by the Z hadronic observables which bound the combinations F_{qZ}/Λ^2 in Eq. (2.95) which means that there is a large degeneracy between the constraints on f_{qW}/Λ^2 and $\tan^2\theta_W f_{qB}/\Lambda^2$. The degeneracy is broken only by the data on the W width which is much less precisely known. Second, the contributions from dipole operators to EWDBD grow as s, as seen in Eqs. (5.3)- (5.8), and hence the lever arm of the high energy of LHC to constrain them. It is interesting to see that these results are pointing in the same direction of the ones in Chapter 3 : LHC is reaching the high precision frontier thanks to its COM high energy and high luminosity.

This is explicitly displayed in Fig. 5.4 where we show the strong correlations in the 95% allowed region from the EWPD analysis in the plane f_{qW}/Λ^2 vs f_{qB}/Λ^2. Also shown are the corresponding rotated projection of the allowed region on F_{qZ}/Λ^2 vs $F_q\gamma/\Lambda^2$ and clearly illustrate how the EWPD bounds on the electric dipole coupling $F_{q\gamma}/\Lambda^2$ are visibly weaker. On the contrary, as seen in Eqs. (5.3)- (5.8), the production of pairs of electroweak gauge bosons receives independent contributions from different combinations of the effective light-quark dipole couplings to Z, W, and γ and that help breaking the degeneracy and allow for constraining both the Z and γ dipole couplings with similar precision. This is explicitly shown in Fig. 5.5 where we plot the 95% allowed region from the EWDBD analysis in both planes f_{qW}/Λ^2 vs f_{qB}/Λ^2 and F_{qZ}/Λ^2 vs $F_q\gamma/\Lambda^2$.

5.3 On Including the Drell-Yan Data

The Drell-Yan process is a source of lepton pairs at high energy and is measured with great precision at the LHC. Light quark dipole operators contribute to this process in the production vertex of the intermediate Z and γ, and hence, can be constrained by these precise LHC results. Furthermore, the dipole operators also lead to a mild energy growth in the corresponding helicity amplitudes $q\bar{q} \to \ell^-\ell^+$

which at high energy behave as

$$\begin{aligned} A(q_+\bar{q}_+ \to \ell^-_-\ell^+_+) &= A(q_-\bar{q}_- \to \ell^-_-\ell^+_+) \\ &= \frac{e^2 v}{\sqrt{2}}\sqrt{s}\sin\theta\left[-\frac{F_{q\gamma}}{\Lambda^2}+\frac{-1+2s_W^2}{2c_W s_W}\frac{F_{qZ}}{\Lambda^2}\right], \quad (5.12) \\ A(q_+\bar{q}_+ \to \ell^-_+\ell^+_-) &= A(q_-\bar{q}_- \to \ell^-_+\ell^+_-) \\ &= \frac{e^2 v}{\sqrt{2}}\sqrt{s}\sin\theta\left[\frac{F_{q\gamma}}{\Lambda^2}-\frac{s_W}{c_W}\frac{F_{qZ}}{\Lambda^2}\right], \quad (5.13) \end{aligned}$$

where θ is the center-of-mass polar scattering angle.

Both ATLAS and CMS have published in Refs. [88] and [89] respectively, the final results of the Run 1 Drell-Yan measurements in the form of differential Drell-Yan cross section as a function of the invariant mass of the lepton pair after correction for detector effects and also giving a very detail account of the systematic and theoretical uncertainties after the unfolding of detector effects. This data allow us a very straightforward comparison with the invariant mass differential cross section predictions including the effect of the dipole couplings.

As for Run 2, CMS has also presented the corresponding differential cross section results but only for a small integrated luminosity [90]. However, both collaboration performed a search for high-mass phenomena in dilepton final states using larger Run 2 samples [91,92]. These data can also be analyzed to study the effect of dipole operators. In this case, we follow a procedure similar to that sketched in last section for the analysis of EWDBD. We simulate the e^+e^- and $\mu^+\mu^-$ invariant mass differential distributions within the cuts of the experimental searches using the packages MADGRAPH5 [63], PYTHIA6.4 [66] and DELPHES [67]. The SM predictions from this procedure are then normalized bin by bin to the predictions provided by the experimental collaborations and the obtained correction factors are subsequently applied to the predicted distributions in presence of the dipole operators.

In summary, we include the following data samples in our Drell-Yan analysis[1]:

	Int.Luminosity (fb^{-1})	$m_{\ell\ell}$	# Data points
ATLAS 13 TeV [91]	36 fb^{-1}	250–6000 GeV	6+6
CMS 13 TeV [92]	36 fb^{-1}	200–3000 GeV	6+6
ATLAS 8 TeV [88]	20.3 fb^{-1}	200–1500 GeV	8
CMS 8 TeV [89]	19.7 fb^{-1}	200-2000 GeV	11

[1]We only consider in the analysis the bins with invariant mass above $\sim$ 200 GeV where the dipole operator contribution is potentially more relevant. Also for better statistical significance, we have combined in one bin the data for the last three invariant mass bins in Ref. [91].

and with those and the information provided by the experiments on the systematic and theoretical uncertainties and correlations we build a binned log-likelihood function

$$\chi^2_{\rm DY}(f_{uB}, f_{uW}, f_{dB}, f_{dW}) \ , \tag{5.14}$$

where for simplicity we have set to zero the coefficients of all other operators contributing to the process.

As discussed in the previous section, the amplitudes generated by dipole operators do not interfere neither with the SM ones nor with those generated by the other dimension-6 operators in Eq. (2.99) and, therefore, no cancellation of their effects is possible. So as it was the case in the analysis of EWDBD and of EWPD, the constraints from DY on the Wilson coefficients of dipole operators can only be marginally affected by the inclusion of other operators in the analysis.

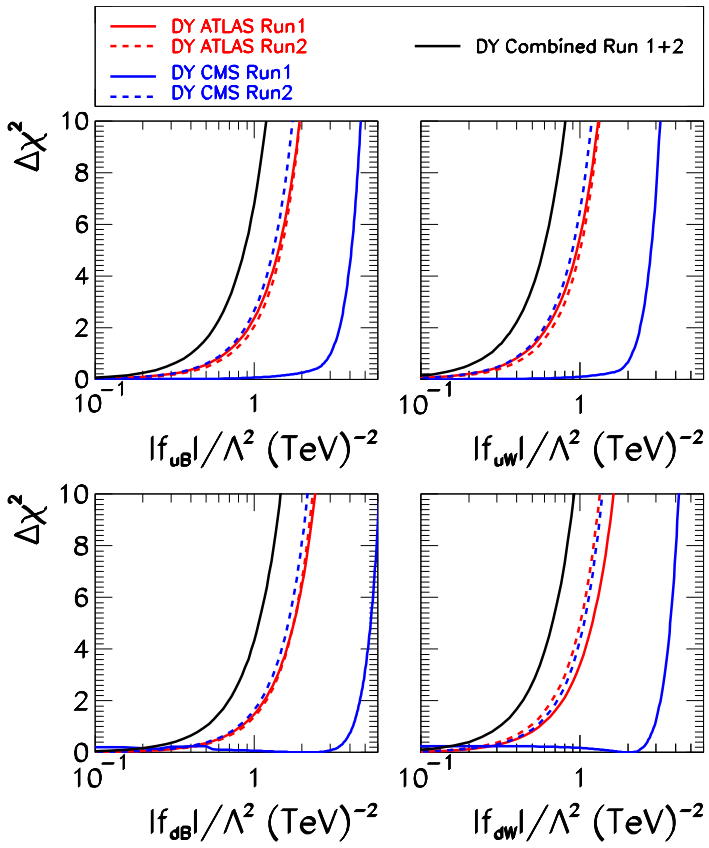

Figure 5.3: $\Delta\chi^2$ dependence on the four fermionic Wilson coefficients of the dipole operators for the analysis of DY data (see text for details).

The results for the DY analysis are depicted in Fig. 5.3 where we display one-dimensional projections of the $\Delta\chi^2_{\rm DY}$ as a function of the Wilson coefficient of each dipole operator after marginalizing over the other three. We show the results using each of the data samples separately and the combination. As seen in the figure, the constraints imposed with the analysis of the ATLAS 8 Run 1 DY results are substantially stronger than those obtained from the analysis of the corresponding CMS Run 1 data.

We trace this difference to the fact that the ATLAS results are slightly lower than the SM predictions in all bins included in the analysis (see Table 12 in Ref. [93]) which results in bounds which are about a twice stronger than the expected sensitivity from data centered in the SM predictions. On the contrary, CMS finds a mild excess of events with respect to the SM predictions for invariant masses between 200-500 GeV where the data is most precise (see Fig. 3 in Ref. [89]). This weakens their constraints by about 20%. The analysis of the Run 2 data yields bounds very much within the expected sensitivity from measurements compatible with the SM.

Comparing the results in Fig. 5.3 with those from EWDBD analysis in Fig. 5.1, we find that the combined analysis of the Drell-Yan data can yield slightly stronger (weaker) bounds on the coefficients of the quark dipole operators $\mathcal{O}_{qB}$ ($\mathcal{O}_{qW}$). However, as seen in Fig. 5.5 DY results totally resolve the light-quark dipole couplings to Z and γ and, consequently, yield stronger constraints over those projections.

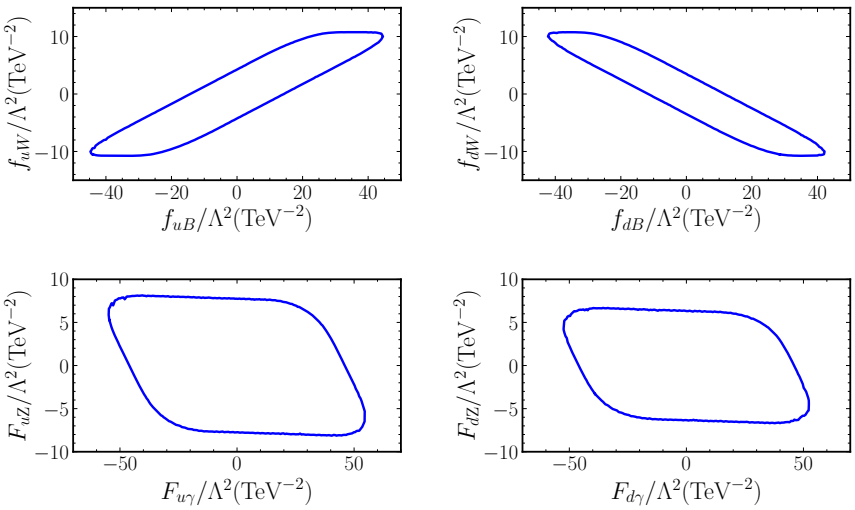

Figure 5.4: 95% allowed region from the EWPD analysis in planes f_{qW}/Λ^2 vs f_{qB}/Λ^2 and F_{qZ}/Λ^2 vs $F_q\gamma/\Lambda^2$.

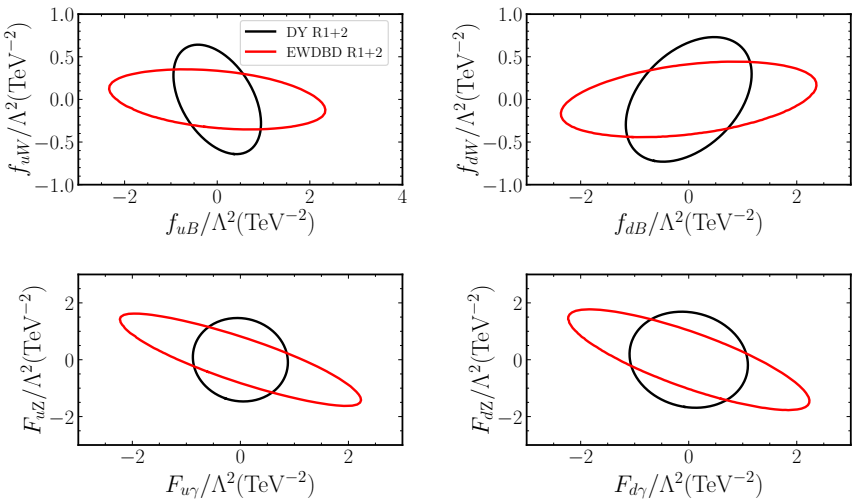

Figure 5.5: 95% allowed regions from the combined EWDBD analysis (red lines) and the combined DY data analysis (black lines) in the planes f_{qW}/Λ^2 vs f_{qB}/Λ^2 and F_{qZ}/Λ^2 vs $F_q\gamma/\Lambda^2$.

5.4 Conclusions

In this Chapter we have studied the power of the high energy LHC data to reveal the effects associated to electroweak dipole couplings of the light quarks. We have focused on two type of processes: pair production of electroweak gauge bosons and Drell-Yan lepton pair production. Because of their different tensor structure, the amplitudes induced by these couplings do not interfere with the SM ones nor with those generated by the other dimension-six operators that modify the gauge boson couplings to fermions and TGCs. Consequently, we find that the constraints derived on all the Wilson coefficients of those non-dipole operators entering the tests of the electroweak gauge boson sector are robust under the inclusion of the light-quark dipole operators.

Dipole couplings of the light quarks to the weak gauge bosons have been explored in the past using the precise data of the on-shell Z and W couplings to fermions. Our results show that analyses of LHC data improves over those by more than one order of magnitude. This is explicitly quantified in Table 5.1 where we constrast the resulting constraints from the analysis of the data on EWDBD and DY at LHC with those from the pole measurements. The improvement is driven both by the growth of the dipole contribution with energy, and because LHC data

	95% CL $\|f\|/\Lambda^2$ (TeV^{-2})		
	EWPD	EWDBD+EWPD	DY
f_{uB}	41	1.9	0.78
f_{uW}	10	0.29	0.53
f_{dB}	38	1.9	0.96
f_{dW}	10	0.36	0.60
$F_{u\gamma}$	51	1.8	0.78
F_{uZ}	7.0	1.3	1.2
$F_{d\gamma}$	48	1.8	0.91
F_{dZ}	5.8	1.4	1.4

Table 5.1: Comparison of the 95% upper bounds for the Wilson coefficients of the light-quark dipole operators for the different analysis performed in this work.

is sensitive to the dipole couplings to Z and γ's with similar weight. Consequently, as seen in this table, the LHC bounds on the combinations entering on the dipole couplings to the Z and the photon are comparable.

It is important to stress that the constraints derived with LHC data are obtained in the asymptotic free regime for the light quarks. So in this respect, the information provided by LHC complements the more model-dependent limits on the dipole couplings of the light quarks which can be derived from measurements of the anomalous magnetic moments of hadrons [94].

In summary, so far we have studied EWSB process using effective Lagrangian and different sources of data like the diboson production and the Higgs observables at LHC. This is arguable a safe way of doing analysis of physics BSM, by looking for the effects of NP at the precision level. Nevertheless these studies can be complemented with searches of new resonances, and in the next Chapter we move to the study of the direct search for new particles.

Chapter 6

A Model Dependent Search for New States: Type III See–Saw for Neutrino Masses with Minimal Flavour Violation

As mentioned in the Introduction, one of main drawbacks of the SM is that within the symmetries of the model neutrinos are strictly massless. The experimental observation of neutrino masses and mixing is therefore an unambiguous evidence of physics BSM.

At first sight, a straightforward solution to explain neutrino masses would consist in the addition of three right-handed singlet fields $\nu_{R,i}$ with null hypercharge. With those the extra terms in the Yukawa Lagrangian read:

$$-\mathcal{L}_Y = ... + (Y_\nu)_{\alpha\beta}\,\overline{L}_{L,\alpha}\tilde{\Phi}\,\nu_{R,\beta} + h.c.\,. \tag{6.1}$$

After the EWSB this generates the so call "Dirac mass" for the neutrinos in total analogy to the mass generation for all other fermions. To explain the smallness of neutrino masses $\left(\lesssim 1 \text{ eV}\right)$, the term $\frac{v}{\sqrt{2}}\,(Y_\nu)_{\alpha\beta}\,\overline{L}_{L,\alpha}\,\nu_{R,\beta}$ needs to be unnaturally small when compared to the other fermion couplings. In this simple extension, all fermion masses have the same origin but neutrinos seem to be such an outsider in the picture. Dirac mass terms for neutrinos are not natural according to the 't Hooft criterium [95]. This could be a clue of an alternative mass generation mechanism for the neutrinos' mass. Notice also that by rotating the lepton fields to the mass eigenstates (now one can not use the same transformation for the charged lepton

fields and for the neutrino fields), the charged current interaction in the lepton sector can now become not flavour diagonal and it is possible to generate physical flavour mixing in the leptonic sector.

Contrary to the other fermions of the SM, neutrinos do not have conserved charges (color and electric). This difference leads to new possibilities for neutrino masses, all of which involve physics beyond the SM. In particular, one can build a so-called "Majorana mass term" involving only the left-handed doublets:

$$\mathcal{L}_{\text{Majorana}} = -\frac{1}{2} M_\nu \left(\overline{\nu_L}\, \nu_L^C + H.c. \right). \tag{6.2}$$

The overall factor of $1/2$ compared to the general Dirac Lagrangian is usual for selfconjugate fields, preventing the double counting of independent fields when obtaining the equations of motion for Majorana neutrinos.

The Eq.(6.2) is Lorentz invariant since ν_L^C transforms as ν_L under a Lorentz transformation. We do not need any addition of right-handed neutrino fields, since ν_L^C behaves like a right-handed field. Nevertheless, it is impossible to have this Majorana term either as a result of nonperturbative effects or in loop corrections since it violates the lepton number [1] ($\Delta L = 2$), and therefore, the B - L symmetry. The Majorana mass term can be understood as a perturbation to an effective Lagrangian which generates transitions $\Delta L = 2$. Furthermore, since the left-handed neutrinos are components of a $SU(2)$ doublet, there is no field in the SM with the required electroweak assignments to produce an invariant term containing the interaction $\overline{L_L^C}\ L_L$ and also renormalizable [2], *i.e.*an isospin scalar triplet with hypercharge $Y = 1$.

The solution to the previous problem goes in the direction of what has been discussed in this Thesis: let us just consider the SM as an effective theory, valid at low-energy, whereas the real theory becomes manifest only at energies of the order of a new high-energy scale Λ. If we forgo the requirement of renormalizability of the theory at low energies, the lowest order non-renormalizable operator, which generates Majorana neutrino masses after EWSB, is the unique dimension–five

[1] When performing a global gauge transformation $\nu_L \rightarrow e^{i\alpha}\nu_L$, for the conjugated field we have $\nu_L^C \rightarrow e^{-i\alpha}\nu_L^C$, so it is obvious that the mass term (6.2) is not invariant under the gauge transformations. Thus, in the case of the Majorana mass term, there is no global gauge invariance.

[2] The right-handed neutrinos are allowed to have Majorana masses, $M_D \overline{\nu_R^C}\ \nu_R + H.c.$ where C is the Dirac charge-conjugation matrix. Because ν_R are singlets under the SM gauge group, M_D can appear as a bare mass term in the Lagrangian or be generated by interactions with a singlet scalar field.

Weinberg operator [33]:

$$\begin{aligned}\mathcal{L}^{d=5}_{\text{Weinberg}} &= -\frac{f_5^{\alpha\beta}}{\Lambda_{LN}}\left(\overline{L}_{L,\alpha}\tilde{\Phi}\right)\ C\ \left(\overline{L}_{L,\beta}\tilde{\Phi}\right)^T + h.c. \\ &\overset{EWSB}{\longrightarrow} -\frac{1}{2}\left(M_\nu\right)_{\alpha\beta}\overline{\nu}_{L,\alpha}\ \nu^C_{L,\beta} + h.c.,\end{aligned} \tag{6.3}$$

where $\left(M_\nu\right)_{\alpha\beta} = \frac{v^2}{\Lambda_{LN}} f_5^{\alpha\beta}$ is the 3×3 effective neutrino mass matrix, Λ_{LN} is the new high-energy physics cutoff scale and $f_5^{\alpha\beta}$ are complex numbers.

Neutrino masses turn out to be very small when compared to the rest of the fermions, if a large enough scale Λ_{LN} is considered. This is entirely in agreement with the 't Hooft criterium, since the new mass parameters are naturally small and, if we take the limit $m_\nu \to 0$, we recover the lepton number conservation.

In the simplest UV completions, it is possible to obtain the Weinberg operator at low energies, without breaking the SM gauge group, through the see–saw mechanism. This can be accomplished with the introduction of new heavy degrees of freedom and allowing the violation of the lepton number in the high energy theory. These new heavy particles, with a mass taken to be of the order of Λ_{LN}, decouple from the theory at low energy scale.

There are three types of see–saw mechanisms on the literature. For each see–saw mechanism type, the dimension–five Weinberg operator arises after integrating out the heavy degrees of freedom from tree-level interactions, in which they are exchanged. These interactions reduce to four-point interactions at low energies, containing only the light degrees of freedom. Next we briefly describe each see–saw type mechanism:

- See–saw Type-I mechanism [96–99] results from the addition of three heavy right-handed neutrinos into the SM. One is also free to add the Majorana mass term (6.2) for the right-handed fields as they are singlets of the SM. The lepton number is violated by the right-handed neutrinos' Majorana mass term.

- See–saw Type-II mechanism [100–104] results from adding one heavy Higgs triplet Δ with hypercharge $Y = 1$ into the SM. The lepton number is violated by the presence of interactions of both the lepton doublet and the Higgs doublet with the Higgs triplet.

- See–saw Type-III [105], three heavy triplet fermions Σ_i with null hypercharge are added into the SM and again the lepton number is violated by the new triplets' Majorana mass term.

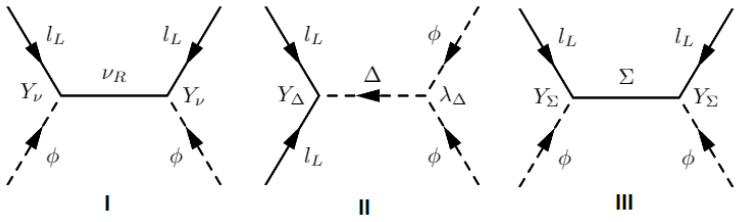

Figure 6.1: see–saw Types I and III correspond to the exchange of fermion ν_R and Σ, respectively, while the Type II see–saw mechanism is implemented through the exchange of scalar fields Δ.

It is possible to get the unique dimension–five Weinberg operator of neutrino masses, after integrating out the heavy degrees of freedom, for each four-point interaction:

$$-\mathcal{L}^{d=5}_{\text{Weinberg}} = \begin{cases} \frac{1}{2}\,\left(Y_\nu\, M_D^{-1}\, Y_\nu^T\right)_{\alpha\beta}\, \bar{l}_{L,\alpha}\, \tilde{\Phi}\, \tilde{\Phi}^T\, l^C_{L,\beta} + H.c. & \text{Type I} \\ -\frac{\lambda_\Delta}{M_\Delta}\,(Y_\Delta)_{\alpha\beta}\, \bar{l}_{L,\alpha}\, \tilde{\Phi}\, \tilde{\Phi}^T\, l^C_{L,\beta} & \text{Type II} \\ \frac{1}{2}\,\left(Y_\Sigma\, M_\Sigma^{-1}\, Y_\Sigma^T\right)_{\alpha\beta}\, \bar{l}_{L,\alpha}\, \tilde{\Phi}\, \tilde{\Phi}^T\, l^C_{L,\beta} + H.c. & \text{Type III} \end{cases} \tag{6.4}$$

After the EWSB we are left with the effective Majorana mass term, M_ν in eq. (6.2), for three light neutrinos:

$$M_\nu = \begin{cases} -\frac{1}{2}\, Y_\nu\, \frac{v^2}{M_D}\, Y_\nu^T & \text{Type I} \\ \lambda_\Delta Y_\Delta \frac{v^2}{M_\Delta} & \text{Type II} \\ -\frac{1}{2}\, Y_\Sigma\, \frac{v^2}{M_\Sigma}\, Y_\Sigma^T & \text{Type III} \end{cases} \tag{6.5}$$

The smallness of M_ν can be attributed to the largeness of M_D, M_Δ and M_Σ in each see–saw mechanism. Besides these three standard cases, we can find in the literature hybrid scenarios combining more than one realization [106–108].

Given the energy range of the neutrino experiments it is clear that if the NP scale is beyond $\sim$ GeV it is not possible to clarify its origin within the oscillation neutrino experiments themselves. On the other hand, the high energy frontier is currently being explored by the LHC which has been running for 10 years with a reach to NP at the TeV scale. Our interest lies in the possible observation of one of these heavy states or any observable effect at LHC. If one considers a neutrino mass of $\mathcal{O}(1)$ eV, and a coupling f_5 also of $\mathcal{O}(1)$, the relation implies that $\Lambda_{LN} \sim 10^{14}$ GeV, which clearly out of the LHC reach. The last statement is a common feature of the three scenarios. Therefore, to use the full discovery potential of LHC, we need to find a way of putting the NP scale accessible in the TeV region.

Nothing prevents that the new states have TeV scale masses. In the literature there exist many models trying to analyze and predict signatures of the neutrino mass generation states with TeV scale masses at the LHC [109–111]. On the other hand, while presenting very interesting phenomenological aspects, from the theoretical point of view some of these models are unable to justify a technically unnatural low scale mass M for the heavy states: you always pay the price of tuning the size of the Yukawa couplings to account for the tiny neutrino masses.

The type of models which can overcome this limitation can be foreseen by looking at the effective operators associated to the presence of neutrino masses. As mentioned above, Majorana neutrino masses imply breaking of the total lepton number symmetry. Neutrino masses also imply that the charged current of the leptons is not-diagonal in flavour space but a leptonic mixing matrix is generated, in analogy to the CKM matrix for the quarks. This means that lepton flavours are also non-conserved. In terms of effective operators, LNV is introduced at dimension–five via the Weinberg operator. But LFV without LNV can be introduced at dimension–six via four-lepton operators. So generically neutrino mass models generate at sufficiently low energy

$$\mathcal{L} = \mathcal{L}_{SM} + \frac{f_5}{\Lambda_{\rm LN}}\mathcal{O}_5 + \sum_i \frac{f_{6,i}}{\Lambda^2_{\rm LFV}}\mathcal{O}_{6,i} + \dots \quad , \tag{6.6}$$

where $\mathcal{O}_5$ is the Weinberg's operator, *i.e.* the one responsible for the neutrino masses, and where we have denoted with $\mathcal{O}_{6,i}$ the dimension–six flavor–changing, but total lepton number conserving, operators.

We can then think of models for which the high energy scale of this tiny LNV may be separated from the NP effects associated to LFV. So if the scale of LFV is made low enough the models are able to give observable effects at the LHC. And so, the most attractive models are the ones where it is possible to relate the mass of the new states $M \sim \Lambda_{\rm LFV} \sim \mathcal{O}$ (TeV), but still keep $\Lambda_{\rm LN} \gg \Lambda_{\rm LFV}$ to explain the smallness of the neutrino mass.

No clear evidence of NP has been observed at LHC which bears implications for such models constructed to explain the neutrino masses containing new states at the TeV scale. Therefore, in this Chapter our main purpose will be to explore the possibility of detecting or constraining this class of models using results of existing LHC searches.

One essential point in the dectectabiliy of the new states, besides their mass and gauge couplings is their decay modes which are determined by the flavour structure of their yukawa couplings. A priory, the decay channels are arbitrary in

most Type–I and Type–III see–saw models, making difficult to derive unambiguous constraints on the NP scale in these scenarios [112, 113]. For example searches for triplet leptons of the Type–III see–saw models have been performed both by CMS [114–117] and ATLAS [118, 119] collaborations, however, most of these searches have been carried out within the context of simplified models such as Ref. [120] and the derived bounds can be evaded depending on which is the dominant decay mode of the triplet leptons.

The only exception are see–saw models which extend the principle of minimal flavour violation to the leptonic sector. This principle was first introduced for quarks [121–123] as a way to explain the absence of NP effects in flavour changing processes in meson decays. The basic assumption is that the only source of flavour mixing in the full theory is the same as in the SM, *i.e.*the quark Yukawa couplings. This idea was latter on extended for leptons [124, 125] and in particular to TeV scale see–saw models [124–127].

From the point of view of LHC phenomenology MLFV see–saw models are attractive, mainly for two reasons: the new states can be light enough to be produced at LHC and their signatures are fully determined by the neutrino parameters. As discussed in Ref. [126] scalar (Type-II) see–saw with light doublet-triplet mixing is a light scale MLFV model by construction (for early study of their observability see for example [128, 129]). In Ref. [126] simple MLFV models for fermionic see–saw were also presented.

From now on we shall focus on the Type-III see–saw MLFV. The Type-III see–saw fermions are $SU(2)_L$ triplets with weak-interaction pair-production cross section, and consequently, having the potential to allow for tests of the hypothesis of MLFV. With Type–I see–saw the picture is completely different. The new states are singlets under the SM gauge group, and therefore, they can only be produced via their mixing with the SM neutrinos. This leads to small production rates which makes the model only marginally testable at LHC.

The Chapter is organized as it follows. We first summarize in Sec. 6.1 the basics of the MLFV Type-III see–saw model and we quantify the allowed range of the relevant couplings controlling the triplet decay modes as derived from the present analysis of neutrino oscillation data from Ref. [131]. Section 6.2 describes our simulation of signal events by the reaction $pp \to ll'jj\nu\nu$ with $l^{(\prime)} = e$ or μ in the context of the MLFV Type-III see–saw model. The quantification of the bounds is presented in Sec. 6.3. In doing so we have put special emphasis and we have quantified how the information on flavour and charge of the produced leptons

is important for maximal sensitivity to MLFV.

6.1 MLFV Type-III See–Saw Model

In Ref. [130] it was introduced the simplest MLFV Type-III see–saw model which was adapted from the Type-I one presented in Ref. [126]. For completeness we summarize here its main features.

The particle contents of model is that of the SM extended with two fermion triplets $\vec{\Sigma} = (\Sigma_1, \Sigma_2, \Sigma_3)$ and $\vec{\Sigma}' = (\Sigma_1', \Sigma_2', \Sigma_3')$, each one formed by three right-handed Weyl spinors of zero hypercharge. Hence, the Lagrangian is

$$\mathcal{L} = \mathcal{L}_{SM} + \mathcal{L}_K + \mathcal{L}_Y + \mathcal{L}_\Lambda \tag{6.7}$$

with

$$\mathcal{L}_K = \quad i\left(\overline{\vec{\Sigma}}\not{D}_\mu\vec{\Sigma} + \overline{\vec{\Sigma}'}\not{D}_\mu\vec{\Sigma}'\right) \ , \tag{6.8}$$

$$\mathcal{L}_Y = \quad -Y_\beta^\dagger\overline{L_{L\beta}^w}\left(\vec{\Sigma}\cdot\vec{\tau}\right)\tilde{\Phi} - \epsilon Y_\beta'^\dagger\overline{L_{L\beta}^w}\left(\vec{\Sigma}'\cdot\vec{\tau}\right)\tilde{\Phi} + h.c. \ , \tag{6.9}$$

$$\mathcal{L}_\Lambda = \quad -\frac{\Lambda}{2}\left(\overline{\vec{\Sigma}^c}\vec{\Sigma}' + \overline{\vec{\Sigma}'^c}\vec{\Sigma}\right) - \frac{\mu}{2}\overline{\vec{\Sigma}'^c}\vec{\Sigma}' - \frac{\mu'}{2}\overline{\vec{\Sigma}^c}\vec{\Sigma} + h.c. \ . \tag{6.10}$$

Here $\vec{\tau}$ are the Pauli matrices, the gauge covariant derivative is defined as $D_\mu = \partial_\mu + ig\vec{T}\cdot\vec{W}_\mu$, where $\vec{T}$ are the three-dimensional representation of the $SU(2)_L$ generators, Φ stands for the SM Higgs doublet field, and $L_\beta^w = (\nu_\beta^w, \ell_\beta^w)^T$ are the three weak eigenstate lepton doublets of the SM. The parameters ϵ, μ and μ' are flavour-blind and *small*, *i.e.*, the scales μ and μ' are much smaller than Λ and v while $\epsilon \ll 1$.

The Lagrangian in Eq. (6.7) breaks total lepton number due to the simultaneous presence of the Yukawa terms Y_i and $\epsilon Y_i'$ as well as to the existence of the μ and μ' terms. Thus in the limit $\mu, \mu', \epsilon \to 0$ it is possible to define a conserved total lepton number by assigning $L(L^w) = L(\Sigma) = -L(\Sigma') = 1$. Without any loss of generality one can work in a basis in which Λ is real while both Y and Y' are complex. In general the parameters μ and μ' would be complex, but for the sake of simplicity we take them to be real in what follows though it is straight forward to generalize the expression to include the relevant phases [132].

After electroweak symmetry breaking, in the unitary gauge, the leptonic mass

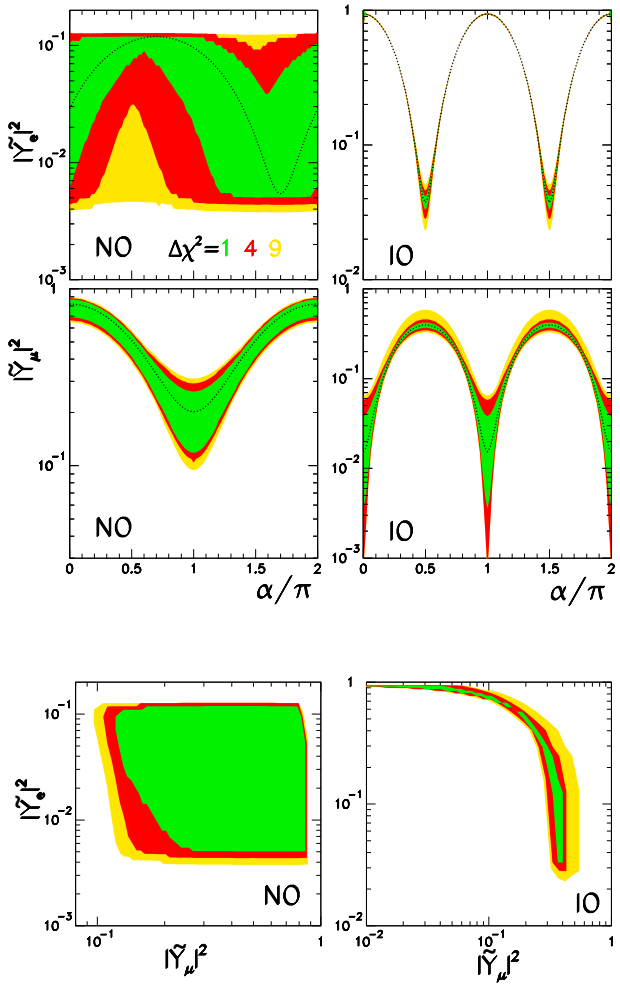

Figure 6.2: Allowed ranges of the Yukawa couplings $|\tilde{Y}_e|^2 \equiv |Y_e|^2/y^2$ and $|\tilde{Y}_\mu|^2 \equiv |Y_\mu|^2/y^2$ obtained from the global analysis of neutrino data in Ref. [131]. The upper four panel shows the values of the couplings as a function of the unknown Majorana phase α. The correlation between the two couplings is shown in the two lower panels. The (left) [right] panels correspond to (normal) [inverted] ordering (NO) [IO]. The dotted line corresponds to the best fit values. The ranges in the filled green, red and yellow areas are shown at 1σ, 2σ, and 3σ with 1 dof ($\Delta\chi^2 = 1, 4, 9$ respectively).

matrices are

$$\mathcal{L}_m = -\frac{1}{2}\left(\overline{\vec{\nu}_L^{\,c}}\ \overline{\tilde{N}_R}\ \overline{\tilde{N}'_R}\right) M_0 \begin{pmatrix} \vec{\nu}_L \\ \tilde{N}^c_R \\ \tilde{N}'^c_R \end{pmatrix} - \left(\overline{\vec{\ell}_L}\ \overline{E_L}\ \overline{E'_L}\right) M_\pm \begin{pmatrix} \vec{\ell}_R \\ E_R \\ E'_R \end{pmatrix} + h.c. \tag{6.11}$$

with

$$M_0 = \begin{pmatrix} 0 & \frac{v}{\sqrt{2}}Y^T & \epsilon\frac{v}{\sqrt{2}}Y'^T \\ \frac{v}{\sqrt{2}}Y & \mu' & \Lambda \\ \epsilon\frac{v}{\sqrt{2}}Y' & \Lambda & \mu \end{pmatrix} \quad \text{and} \quad M_\pm = \begin{pmatrix} \frac{v}{\sqrt{2}}Y^\ell & vY^\dagger & \epsilon v Y'^\dagger \\ 0 & \mu' & \Lambda \\ 0 & \Lambda & \mu \end{pmatrix}, \tag{6.12}$$

where Y^ℓ are the charged lepton Yukawa couplings of the SM. $\vec{\nu}^w$ and $\vec{\ell}^w$ are column vectors containing respectively the three neutrinos and charged leptons of the SM in the weak basis. The charge eigenstates Dirac fermions E and E' and the neutral Majorana fermions $\tilde{N}$ and $\tilde{N}'$ are defined in terms of the triplet states, $\Sigma_\pm^{(\prime)} = \frac{1}{\sqrt{2}}\left(\Sigma_1^{(\prime)} \mp i\Sigma_2^{(\prime)}\right)$, and $\Sigma_0^{(\prime)} = \Sigma_3^{(\prime)}$, as

$$E^{(\prime)} = \Sigma_-^{(\prime)} + \Sigma_+^{(\prime)^c} \qquad \tilde{N}^{(\prime)} = \Sigma_0^{(\prime)} + \Sigma_0^{(\prime)^c}\,. \tag{6.13}$$

The mass basis is composed of:

- Three light Majorana neutrinos ν_i (with the lightest one being massless) and three light charged leptons leptons ℓ_i with masses

$$m_\nu^{diag} = V^{\nu T}\left[-\frac{v^2}{2\Lambda}\epsilon\left[\left(Y' - \frac{1}{\epsilon}\frac{\mu}{2\Lambda}Y\right)^T Y + Y^T\left(Y' - \frac{1}{\epsilon}\frac{\mu}{2\Lambda}Y\right)\right]\right]V^\nu\,, \tag{6.14}$$

$$m_\ell^{diag} = \frac{v}{\sqrt{2}}V^{\ell\dagger}_R Y^{\ell\dagger}\left[1 - \frac{v^2}{2\Lambda^2}Y^\dagger Y\right]V_L^\ell\,, \tag{6.15}$$

  where V^ν and $V^\ell_{L,R}$ being 3×3 unitary matrices and in general, one can choose the flavour basis such that $V_L^\ell = V_R^\ell = I$.

- Two charged heavy leptons, E_1^- and E_2^+, both with masses $M \simeq \Lambda(1 \mp \frac{\mu+\mu'}{2\Lambda})$.

- Two heavy Majorana neutral leptons and two charged heavy leptons also with masses $M \simeq \Lambda(1 \mp \frac{\mu+\mu'}{2\Lambda})$ with which we build a quasi-Dirac heavy state N.

The relation between the weak and mass eigenstate to first order in the small

parameters μ, μ' and ϵ is:

$$\nu_L^w = V^\nu \nu_L + \frac{v}{\sqrt{2}\Lambda} Y^\dagger N_L + \frac{v}{\sqrt{2}\Lambda}\left(\epsilon Y'^\dagger - \left(\frac{3\mu+\mu'}{4\Lambda}\right) Y^\dagger\right) N_R^c, \quad (6.16)$$

$$\ell_L^w = \ell_L + \frac{v}{\Lambda} Y^\dagger E_{1L}^- + \frac{v}{\Lambda}\left(\epsilon Y'^\dagger - \left(\frac{3\mu+\mu'}{4\Lambda}\right) Y^\dagger\right) E_{2R}^{+c}, \quad (6.17)$$

$$\ell_R^w = \ell_R\,, \quad (6.18)$$

$$\tilde{N}_L = N_R^c - \left(\frac{\mu-\mu'}{4\Lambda}\right) N_L - \frac{v}{\sqrt{2}\Lambda}\left(\epsilon Y' - \frac{\mu}{\Lambda} Y\right) V^\nu \nu_L\,, \quad (6.19)$$

$$\tilde{N}'_L = N_L + \left(\frac{\mu-\mu'}{4\Lambda}\right) N_R^c - \frac{v}{\sqrt{2}\Lambda} Y V^\nu \nu_L\,, \quad (6.20)$$

$$E_L = E_{2R}^{+c} - \left(\frac{\mu-\mu'}{4\Lambda}\right) E_{1L}^- - \frac{v}{\Lambda}\left(\epsilon Y' - \frac{\mu}{\Lambda} Y\right) \ell_L\,, \quad (6.21)$$

$$E_R = E_{1R}^- - \left(\frac{\mu-\mu'}{4\Lambda}\right) E_{2L}^{+c}\,, \quad (6.22)$$

$$E'_L = E_{1L}^- + \left(\frac{\mu-\mu'}{4\Lambda}\right) E_{2R}^{+c} - \frac{v}{\Lambda} Y \ell_L\,, \quad (6.23)$$

$$E'_R = E_{2L}^{+c} + \left(\frac{\mu-\mu'}{4\Lambda}\right) E_{1R}^-\,. \quad (6.24)$$

From the above relations it follows that the neutral weak interactions of the light states take the same form as that on the SM and the charged current interactions involve a 3x3 unitary matrix $U_{LEP} = V^\nu$ which after phase redefinition of the light charged leptons, can be chosen

$$U_{LEP} = \begin{pmatrix} 1 & 0 & 0 \\ 0 & c_{23} & s_{23} \\ 0 & -s_{23} & c_{23} \end{pmatrix} \begin{pmatrix} c_{13} & 0 & s_{13} e^{-i\delta_{\rm CP}} \\ 0 & 1 & 0 \\ -s_{13} e^{i\delta_{\rm CP}} & 0 & c_{13} \end{pmatrix} \begin{pmatrix} c_{21} & s_{12} & 0 \\ -s_{12} & c_{12} & 0 \\ 0 & 0 & 1 \end{pmatrix} \begin{pmatrix} e^{-i\alpha} & 0 & 0 \\ 0 & e^{i\alpha} & 0 \\ 0 & 0 & 1 \end{pmatrix}, \quad (6.25)$$

where $c_{ij} \equiv \cos\theta_{ij}$ and $s_{ij} \equiv \sin\theta_{ij}$. The angles θ_{ij} can be taken without loss of generality to lie in the first quadrant, $\theta_{ij} \in [0, \pi/2]$ and the phases $\delta_{\rm CP},\ \alpha \in [0, 2\pi]$. The leptonic mixing matrix contains only one Majorana phase because there are only two heavy triplets and consequently only two light neutrinos are massive while the lightest one remains massless. Also notice that unitarity violation in the charged current and flavour mixing in the neutral current of the light leptons in generated at higher order [132–134].

This model is MLFV because one can fully reconstruct the neutrino Yukawa coupling Y and the combination $\widehat{Y'} = Y' - \frac{1}{\epsilon}\frac{\mu}{2\Lambda} Y$ from the neutrino mass ma-

trix [126] up to two real normalization factors y and $\hat{y}'$ as follows:

NO ($m_1 = 0 < m_2 < m_3$)	IO ($m_3 = 0 < m_1 < m_2$)
$r = \frac{\Delta m^2_{21}}{\Delta m^2_{32}}$	$r = -\frac{\Delta m^2_{21}}{\Delta m^2_{31}}$
$\rho = \frac{\sqrt{1+r}-\sqrt{r}}{\sqrt{1+r}+\sqrt{r}}$	$\rho = \frac{\sqrt{1+r}-1}{\sqrt{1+r}+1}$
$m_{2,3} = \frac{\epsilon y \widehat{y'} v^2}{\Lambda}(1 \mp \rho)$	$m_{1,2} = \frac{\epsilon y \widehat{y'} v^2}{\Lambda}(1 \mp \rho)$
$Y_\beta = \frac{y}{\sqrt{2}}\left(\sqrt{1+\rho}\, U^*_{\beta 3} + \sqrt{1-\rho}\, U^*_{\beta 2}\right)$	$Y_\beta = \frac{y}{\sqrt{2}}\left(\sqrt{1+\rho}\, U^*_{\beta 2} + \sqrt{1-\rho}\, U^*_{\beta 1}\right)$
$\widehat{Y'}_\beta = \frac{\widehat{y'}}{\sqrt{2}}\left(\sqrt{1+\rho}\, U^*_{\beta 3} - \sqrt{1-\rho}\, U^*_{\beta 2}\right)$	$\widehat{Y'}_\beta = \frac{\widehat{y'}}{\sqrt{2}}\left(\sqrt{1+\rho}\, U^*_{\beta 2} - \sqrt{1-\rho}\, U^*_{\beta 1}\right)$

(6.26)

In writing Eq. (6.26) we follow the notation of using greek index β to denote lepton flavour index $\beta, \gamma = e, \mu, \tau$. And in what follows we will use roman index $i, j = 1, 2, 3$ to denote the light neutrino mass index.

We plot in Fig. 6.2 the ranges of the Yukawa couplings $|\tilde{Y}_e|^2 \equiv |Y_e|^2/y^2$ and $|\tilde{Y}_\mu|^2 \equiv |Y_\mu|^2/y^2$ obtained by projecting the allowed ranges of oscillation parameters from the global analysis of neutrino data [131] using Eqs. (6.26). In the first and second rows we plot the ranges of the Yukawa couplings as a function of the unknown Majorana phase α while the lower row shows the correlation between the electron and muon Yukawa couplings. This figure illustrates the quite different allowed ranges and correlation of the electron and muon Yukawa couplings in the two orderings. As a curiosity we notice that in NO the dependence of the range of $|Y_e|$ on α is driven by the present hint of $\delta_{\rm CP} \sim 270^\circ$ in the oscillation data analysis [131] because α enters via $\mathrm{Re}(U_{e3}U^*_{e2}) \propto \cos(\alpha + \delta_{\rm CP})$.

In what respects the interactions of the heavy states, as discussed in Ref. [130], lepton number violating couplings appear due to $\mathcal{O}(\epsilon, \mu/\Lambda, \mu'/\Lambda)$ mixings and mass splittings in the heavy states, that are, by hypothesis, very suppressed in MLFV models. This renders the lepton number violating processes involving heavy fermions unobservable at LHC, at a difference with the non MLFV scenarios for Type–III see–saw for which $\Delta L = 2$ final states constitute a smoking gun [135, 136]. Consequently in what follows we concentrate in the lepton conserving interaction Lagrangian with $\Lambda = M$ being the common mass of the heavy

states:

$$\mathcal{L}_W = -g\left(\overline{E_1^-}\gamma^\mu N W_\mu^- - \overline{N}\gamma^\mu E_2^+ W_\mu^-\right) + h.c.$$
$$-g\left(\frac{1}{\sqrt{2}}K_\beta\overline{\ell_{\beta L}}\gamma^\mu N_L W_\mu^- + \overline{K}_i\overline{\nu_{iL}}\gamma^\mu E_{2L}^+ W_\mu^-\right) + h.c. \quad (6.27)$$
$$\mathcal{L}_Z = gC_W\left(\overline{E_1^-}\gamma^\mu E_1^- Z_\mu - \overline{E_2^+}\gamma^\mu E_2^+ Z_\mu\right)$$
$$+\frac{g}{2\sqrt{2}C_W}\left(\frac{1}{\sqrt{2}}\overline{K}_i\overline{\nu_{iL}}\gamma^\mu N_L Z_\mu + K_\beta\overline{\ell_{\beta L}}\gamma^\mu E_{1L}^- Z_\mu\right) + h.c. \quad (6.28)$$
$$\mathcal{L}_\gamma = e\left(\overline{E_1^-}\gamma^\mu E_1^- A_\mu - \overline{E_2^+}\gamma^\mu E_2^+ A_\mu\right) \quad (6.29)$$
$$\mathcal{L}_{h^0} = \frac{gM}{\sqrt{2}M_W}\left(\frac{1}{\sqrt{2}}\overline{K}_i\overline{\nu_{iL}}N_R + K_\beta\overline{\ell_{\beta L}}E_{1R}^-\right) + h.c.\,. \quad (6.30)$$

where c_W stands for the cosine of the weak mixing angle and the lepton number conserving couplings of the heavy triplet fermions are

$$K_\beta = -\tfrac{v}{\sqrt{2}M}Y_\beta{}^* \quad , \qquad \overline{K}_i = \sum_{\beta=e,\mu,\tau}(U_{LEP}^*)_{\beta i}K_\beta\,, \quad (6.31)$$

which verify

$$\sum_{\beta=e,\mu,\tau}|K_\beta|^2 = \sum_{i=1}^{3}|\overline{K}_i|^2 = \frac{y^2v^2}{2M^2}\,. \quad (6.32)$$

Notice that flavour structures of the couplings K and $\overline{K}$ are fully determined by the low energy neutrino parameters and fully determined by the oscillation data up to the Majorana phase α. Their strengths are, however, arbitrary as they are controlled by the normalization factor yv/M while it is the combination $\epsilon\widehat{yy'}/M$ what is fixed by the neutrino masses.

6.1.1 Signatures

In line with what was discussed about the advantage of using a Type-III see–saw model instead of Type-I, the fermion triplet gauge interactions lead to the following production process

$$pp \to E^+E^- \quad , \quad pp \to E_i^\pm N \quad (6.33)$$

for $i = 1, 2$. From the interactions in Eqs. (6.27),(6.28), (6.30) we can obtain the decay widths of the heavy states [137], which are well known functions of the mass

of the new states:

$$\begin{aligned}
\Gamma\left(N \to \ell_\beta^- W^+\right) &= \frac{g^2}{64\pi}|K_\beta|^2 \frac{M^3}{M_W^2}\left(1-\frac{M_W^2}{M^2}\right)\left(1+\frac{M_W^2}{M^2}-2\frac{M_W^4}{M^4}\right) , \\
\Gamma\left(N \to \nu_i Z\right) &= \frac{g^2}{128\pi c_w^2}|\overline{K}_i|^2 \frac{M^3}{M_Z^2}\left(1-\frac{M_Z^2}{M^2}\right)\left(1+\frac{M_Z^2}{M^2}-2\frac{M_Z^4}{M^4}\right) , \\
\Gamma\left(N \to \nu_i h^0\right) &= \frac{g^2}{128\pi}|\overline{K}_i|^2 \frac{M^3}{M_W^2}\left(1-\frac{M_{h^0}^2}{M^2}\right)^2 , \\
\Gamma\left(E_2^+ \to \nu_i W^+\right) &= \frac{g^2}{32\pi}|\overline{K}_i|^2 \frac{M^3}{M_W^2}\left(1-\frac{M_W^2}{M^2}\right)\left(1+\frac{M_W^2}{M^2}-2\frac{M_W^4}{M^4}\right) , \\
\Gamma\left(E_1^- \to \ell_\beta^- Z\right) &= \frac{g^2}{64\pi c_W^2}|K_\beta|^2 \frac{M^3}{M_Z^2}\left(1-\frac{M_Z^2}{M^2}\right)\left(1+\frac{M_Z^2}{M^2}-2\frac{M_Z^4}{M^4}\right) , \\
\Gamma\left(E_1^- \to \ell_\beta^- h^0\right) &= \frac{g^2}{64\pi}|K_\beta|^2 \frac{M^3}{M_W^2}\left(1-\frac{M_{h^0}^2}{M^2}\right)^2 .
\end{aligned} \tag{6.34}$$

Therefore, using Eq. (6.32) the total decay widths for the three triplet fermions $F = N, E_1^-, E_2^+$ are

$$\Gamma_F^{\text{TOT}} = \frac{g^2 M^3}{64\pi M_W^2}\frac{y^2 v^2}{M^2}(1+\mathcal{F}_F(M)) \tag{6.35}$$

where $\mathcal{F}_F(M) \to 0$ for $M \gg m_{h^0}, M_Z, M_W$. Consequently, the arbitrary y factor cancels out in the branching ratios. Furthermore the branching ratio in a final state with a charge lepton of flavour α or a neutrino state i produced in the vertex of the heavy state decay is proportional to $|\tilde{Y}_\alpha|^2$ and $|\sum_\beta \tilde{Y}_\beta (U_{LEP})_{\beta i}|^2$) times a kinematic factor depending solely on the heavy mass M.

Unlike in a general Type–III see–saw model for which the branching ratio of N or $E_i^\pm$ into a light lepton of a given flavour can be negligibly small, for the MLFV Type–III see–saw model the branching ratios in the different light lepton flavours are fixed by the neutrino physics and are non-vanishing as can be seen from Fig. 6.2 and Eqs. (6.34). This makes the flavour composition of the final states in any decay chain of the heavy leptons to be fully determined given a neutrino mass ordering. Consequently in the narrow width approximation the only free parameters in the model are the mass of the states and the Majorana phase α, making the model more unambiguously testable. Conversely, as discussed in Ref. [130] in this MLFV Type-III model the values of the neutrino masses imply a lower bound on the total decay width of the triplet fermions as a consequence of the hierarchy between the L-conserving and L-violating y and $\epsilon\widehat{y'}$ constants. So their decay length is too short to produce a detectable displaced decay vertex signature [138, 139] at difference with other see–saw models [128, 135, 136, 140].

In summary, a key point for the observation of the MLFV nature of the model is the determination of the flavor of the leptons decaying from the fermion triplets. Therefore, in order to be able to tag the flavor of the leptons, we need to consider processes where the new fermions have two-body decays exhibiting charged leptons,

$$pp \to F(\to \ell_a X) F'(\to \ell_b X') \ , \tag{6.36}$$

for F,$F' = N, E_i$ and with $X, X' = Z, W, h$. Using the narrow width approximation, the production cross sections of these processes can be calculated using

$$\sigma \left[pp \to F(\to l_a X) F'(\to l_b X') \right] \propto |\tilde{Y}_a|^2 |\tilde{Y}_b|^2 \ , \tag{6.37}$$

where $\tilde{Y}_a \equiv \frac{Y_a}{y}$. It turns out that the number of events expected for final states with different combinations of charged lepton flavors can be fully determined in terms of the low–energy neutrino parameters.

In the next section we shall use the available data from LHC, to constrain a specific case of this type of models, *i.e.*to find a bound for the triplet mass where it is possible to unambiguously rule out this scenario.

6.2 Case Study: $pp \to l\, l'\, \nu\, \nu$

In order to study the sensitivity of LHC Run 1 to MLFV Type–III see–saw signatures we will use the event topologies studied by ATLAS in Ref. [118] which contain two charged leptons (either electron or muons), two jets from a hadronically decaying W boson and large missing transverse momentum. ATLAS used these topologies to search for heavy fermions in the context of the simplified Type–III see–saw model as implemented in Ref. [120]. They presented their results as number of events for the six different flavour and charge lepton pair combinations: same sign (SS) and opposite sign (SS) ee, $\mu\mu$ and $e\mu$. Using those they obtain bounds on the triplet mass which depend on the decay branching ratio into the different flavours. In particular for triplets decaying mostly into τ's no bound can be derived.

On the contrary, as stressed in the previous section, in the MLFV scenario the flavour and lepton number of the final states produced in the heavy fermion decay chain is very much constrained. Thus having the final states classified in the different flavour and charge combinations makes the result in Ref. [118] best suited for testing the MLFV scenario as we quantify next.

Finally, we have implemented the Lagrangian in Eqs. (6.27)–(6.30) using the package FeynRules [64, 65]. This will allow us to simulate the expected signals in this MLFV Type–III. We have made available the corresponding model files at the corresponding URL [141].

6.2.1 Contributing subprocesses

Let us start by listing the possible subprocesses contributing to the different flavour and charge combinations in the MLFV Type–III see–saw model. They all proceed by the production of a pair of heavy triplet states and their subsequent decay. The pair production of the fermion triplets takes place via gauge interactions, and, therefore, it depends exclusively upon the mass of the new states. On the other hand, the branching ratios of these fermions into the final states described in the previous section depend upon the Yukawa couplings $\tilde{Y}_\beta$ which vary in the different subprocesses:

- $pp \to E_1^- \tilde{N}$, $(E_1^- \to l_\beta^- Z$, $Z \to \nu_i \nu_i)$ $(\tilde{N} \to l_\gamma^+ W^-$, $W^- \to jj)$:

  Using interactions in (6.27)–(6.28) it is easy to show that the production cross section for this process (after summing over neutrino states i) is proportional to $|K_\beta|^2\,|K_\gamma|^2$. Therefore, as discussed in the previous section, in the narrow width approximation the production cross section for this process and its charge conjugated one can be factorized as

  $$\sigma^{(1)}_{\beta\gamma}\ |\tilde{Y}_\beta|^2\,|\tilde{Y}_\gamma|^2. \tag{6.38}$$

- $pp \to E_2^+ \tilde{N}$, $(E_2^+ \to \nu_i W^+$, $W^+ \to jj)$ $(\tilde{N} \to l_\beta^+ W^-$, $W^- \to l_\gamma^- \nu_\gamma)$:

  whose production cross section is proportional to $|K_\beta|^2 |\overline{K}_i|^2$. So in the narrow width approximation and after summing over the ν_i states using Eq. (6.32) the cross section for this process and its charge conjugated one can be written as

  $$\sigma^{(2a)}_{\beta\gamma}\ |\tilde{Y}_\beta|^2\ . \tag{6.39}$$

- $pp \to E_2^+ \tilde{N}$, $(E_2^+ \to \nu_i W^+$, $W^+ \to l_\gamma^+ \nu_\gamma)$ $(\tilde{N} \to l_\beta^+ W^-$, $W^- \to jj)$:

  and the respective charge conjugate process possess a cross section proportional to $|K_\beta|^2 |\overline{K}_i|^2$. As before, in the narrow width approximation and after summing over the ν_i states we parametrize the production cross section as

  $$\sigma^{(2b)}_{\beta\gamma}\ |\tilde{Y}_\beta|^2\ . \tag{6.40}$$

- $pp \to E_2^+ \tilde{N}\,,\, (E_2^+ \to \nu_i W^+\,,\, W^+ \to jj)\; (\tilde{N} \to \nu_j Z\,,\, Z \to l_\beta^- l_\beta^+)$:

  and its charge conjugate process with cross section proportional to $|\overline{K}_i|^2|\overline{K}_j|^2$ that after summing over the neutrino states i and j reads

$$\sigma_{\beta\beta}^{(2c)}\ . \tag{6.41}$$

- $pp \to E_1^+ E_1^-\,,\, (E_1^+ \to l_\beta^+ Z\,,\, Z \to jj) \quad (E_1^- \to l_\gamma^- Z\,,\, Z \to \nu_i\,\nu_i)\,,$
  $pp \to E_1^+ E_1^-\,, \quad (E_1^+ \to l_\beta^+ Z\,,\, Z \to \nu_i\nu_i) \quad (E_1^- \to l_\gamma^- Z\,,\, Z \to jj)$:

  with cross section

$$\sigma_{\beta\gamma}^{(3)}\ |\tilde{Y}_\beta|^2|\tilde{Y}_\gamma|^2\ . \tag{6.42}$$

Altogether the cross section of each OS flavour channel is given by:

$$\begin{aligned}
\sigma_{ee}^{OS} &\equiv \left[\sigma_{ee}^{(1)} + \sigma_{ee}^{(3)}\right]|\tilde{Y}_e|^4 + \sigma_{ee}^{(2a)}|\tilde{Y}_e|^2 + \sigma_{ee}^{(2c)}\,,\\
\sigma_{e\mu}^{OS} &\equiv \left[\sigma_{e\mu}^{(1)} + \sigma_{\mu e}^{(1)} + \sigma_{e\mu}^{(3)} + \sigma_{\mu e}^{(3)}\right]|\tilde{Y}_e|^2|\tilde{Y}_\mu|^2\\
&\quad + \sigma_{e\mu}^{(2a)}|\tilde{Y}_e|^2 + \sigma_{\mu e}^{(2a)}|\tilde{Y}_\mu|^2\,,\\
\sigma_{\mu\,\mu}^{OS} &\equiv \left[\sigma_{\mu\mu}^{(1)} + \sigma_{\mu\mu}^{(3)}\right]|\tilde{Y}_\mu|^4 + \sigma_{\mu\mu}^{(2a)}|\tilde{Y}_\mu|^2 + \sigma_{\mu\mu}^{(2c)}\,,
\end{aligned} \tag{6.43}$$

while for SS lepton final state

$$\begin{aligned}
\sigma_{ee}^{SS} &\equiv \sigma_{ee}^{(2b)}|\tilde{Y}_e|^2\,,\\
\sigma_{e\mu}^{SS} &\equiv \sigma_{e\mu}^{(2b)}|\tilde{Y}_e|^2 + \sigma_{\mu e}^{(2b)}|\tilde{Y}_\mu|^2\,,\\
\sigma_{\mu\mu}^{SS} &\equiv \sigma_{\mu\mu}^{(2b)}|\tilde{Y}_\mu|^2\,.
\end{aligned} \tag{6.44}$$

We notice that in Eq. (6.38)– (6.44) the $\sigma_{\beta\gamma}^{(1)}$,$\sigma_{\beta\gamma}^{(2a)}$, $\sigma_{\beta\gamma}^{(2b)}$, $\sigma_{\beta\gamma}^{(2c)}$, and $\sigma_{\beta\gamma}^{(3)}$ factors are primarely functions of the heavy mass M and their flavour dependence enters only via the difference response of the e and μ to the selection cuts. Conversely the normalized yukawas $\tilde{Y}_\beta$ contain the dominant dependence on the lepton flavour and are functions of the parameters determined by the neutrino oscillation data and the unknown Majorana phase α give in Eq. (6.26).

6.2.2 Signal simulation: procedure and expected event rates

In our analysis, we first simulated the above parton level signal processes with MadGraph 5 [63]. We then used PYTHIA 6.4 [66] to generate the parton shower and hadronization. Finally we performed a fast detector simulation with DELPHES

3 [67] with jets being reconstructed using the anti-k_T algorithm with a radius $R = 0.4$ with the package FASTJET [142].

In order to reproduce the ATLAS event selection corresponding to the searches in Ref. [118] we required that the events contain exactly two leptons (muons and/or electrons), a minimum of two jets and no b-tagged jet. In the case of OS (SS) leptons the leading lepton must have transverse momentum (p_T) in excess of 100 (70) GeV with the next-to-leading lepton p_T larger than 25 (40) GeV. In addition we imposed the invariant mass of the two leptons to be larger than 130 and 90 GeV for OS and SS events respectively. We also demanded the p_T of two leading jets to be larger than 60 (40) and 30 (25) GeV for the OS (SS) final state. Moreover, to characterize the presence of a hadronically decaying W in the event the invariant mass of the leading jet pair was required to be between 60 and 100 GeV, and for OS events we require the two leading jets to satisfy $\Delta R_{jj} < 2$. Finally, we only selected events presenting missing transverse energy in excess of 110 (100) GeV for OS (SS) events. We implement the above selection in MadAnalysis5 [143].

In order to tune our calculations we first simulated the signal for the Type-III see–saw model of Ref. [120] which is the one used in the ATLAS analysis. By comparing our number of expected events with the ones obtained by ATLAS in Fig. 2 of [118] for the OS and SS final states presenting ee, $e\mu$ and $\mu\mu$ pairs, we extract overall multiplicative correction factors for each of these final states such that our fast simulation agrees with the one of ATLAS. To validate our procedure we verified that our tuned Monte Carlo reproduces the missing transverse momentum distribution presented in Fig. 1 of [118]. We then apply these correction factors in the evaluation of the expected number of events of the MLFV type-III see–saw model.

Concerning backgrounds, the dominant contribution comes from the production of dibosons (WW,WZ,ZZ), Z plus jets, top pairs and single top in association with a W. In addition there are also background events that stems from misidentification of leptons. In our analysis we directly use the background rates estimated by ATLAS [118].

Figure 6.3 depicts the resulting cross section factors σ_1, σ_{2a}, σ_{2b}, and σ_3 introduced in Eqs. (6.38)–(6.42), for the events passing the selection cuts and after applying the tuning correction factors. The results are shown as a function of the new fermion mass and for the different lepton flavor combinations and a center-of-mass energies of 8 TeV [3] . From this figure we can see that the four possible

[3] σ_{2c} is vanishing small since the event selection vetoes the presence of on-shell Z's.

leptonic final states (ee, $\mu\mu$, $e\mu$, and μe) have similar cross section factors for masses larger than 300 GeV, however, closer to the threshold the detection and acceptance efficiencies induce differences among the leptonic final states. In the case of σ_{2a} both leptons originate from the decay of a single triplet fermion, therefore reducing the acceptance at small masses due to the OS lepton pair invariant mass cut.

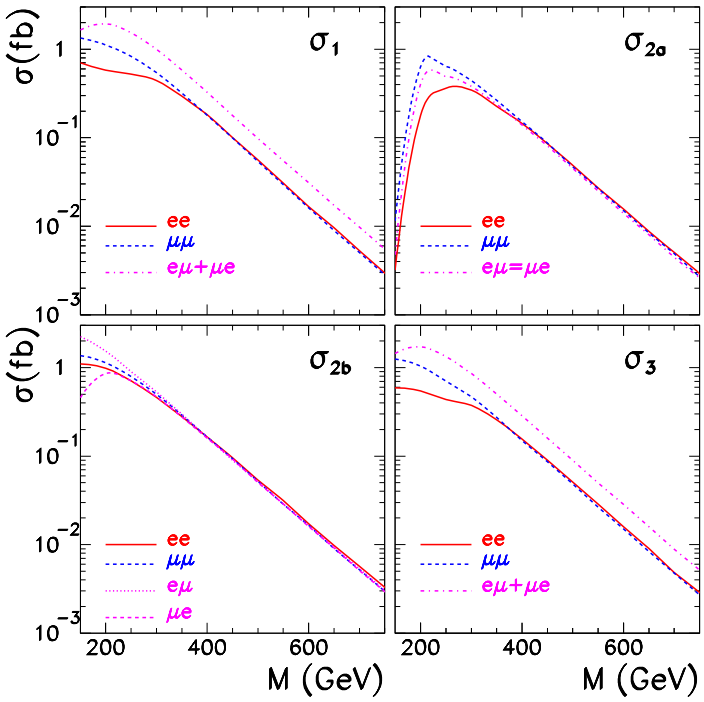

Figure 6.3: Cross section factors for the different contributions to the event topologies as a function of the triplet mass M as defined in Eqs. (6.38)–(6.42) after inclusion of our simulation of the selections of Ref. [118] (see text for details).

Weighting these cross section factors with the different combination of Yukawa couplings as in Eqs. (6.43) and (6.44) and times the luminosity we predict the signal event rates in the different flavour and charge combinations of the final lepton pair. For example in Figs. 6.4 and 6.5 we present the event rate prediction as a function of the unknown Majorana phase α for a triplet mass of 300 GeV, an integrated luminosity of 20.3 fb^{-1} and normal ordering and inverted ordering respectively. As seen in Fig. 6.4 for NO, the expected number of ee events is very small for both OS and SS channels. Nevertheless, a considerable number of events

containing muons is expected except for α/π around 1. This is so because for NO $|\tilde{Y}_\mu|$ is much larger than $|\tilde{Y}_e|$ as can be seen from Fig. 6.2. For IO we see in Fig. 6.5, as could be anticipated from Fig. 6.2, that the expectations in all flavor channels vary appreciably with the Majorana phase α. However, the strong correlation between $|\tilde{Y}_e|$ and $|\tilde{Y}_\mu|$ in IO – depicted in the right bottom panel of Fig. 6.2 – guarantees a sizable number of events for almost the entire α range with the signal being dominated by the channels $e\mu$ and $\mu\mu$ for OS leptons and the channel $e\mu$ for SS leptons.

6.3 Analysis and Results

In order to quantify the bounds on the MLFV Type–III see–saw scenario we build the likelihood function using the six data points associated to the events with ee, $e\mu$ and $\mu\mu$ leptons of either SS or OS. As discussed in the previous section, we make direct use of the corresponding background estimate by ATLAS which we read from Fig. 2 and Table I of Ref. [118] and that summarize here for completeness:

	OS ee	SS ee	OS $\mu\mu$	SS $\mu\mu$	OS $e\mu$	SS $e\mu$	total OS	total SS
N^{dat}	9	3	3	1	13	0	25	4
N^{bck}	8.5	1	9.5	0.5	13	1.65	31.0 ± 7.7	3.15 ± 0.8

According to Ref. [118] the reported background errors in the table and figure include both the statistical and systematic uncertainties. Comparing the read out of these uncertainties for each of the six individual channels with the total reported in the table we conclude that the $\sim 25\%$ background uncertainty is strongly correlated among the different channels as the total background uncertainty comes to be very close to the arithmetic sum of the individual ones, while if they were totally uncorrelated one would expect it to be the quadratic sum.

So we build the likelihood function as

$$-2\mathcal{L}_{6d} = \chi^2_{6d} = \min_{\xi} \left\{ 2 \sum_{i=1,6} \left[(1+\xi) N_i^{bck} + N_i^{mod} - N_i^{dat} \log \frac{N_i^{dat}}{(N_i^{bck} + N_i^{mod})} \right] + \frac{\xi^2}{0.25^2} \right\} \tag{6.45}$$

where we account for the background uncertainty by introducing a unique pull ξ with an uncertainty of 25%[4]. N_i^{mod} is the predicted contribution to the number

[4] We have verified that including several pulls for the different source of background and smaller

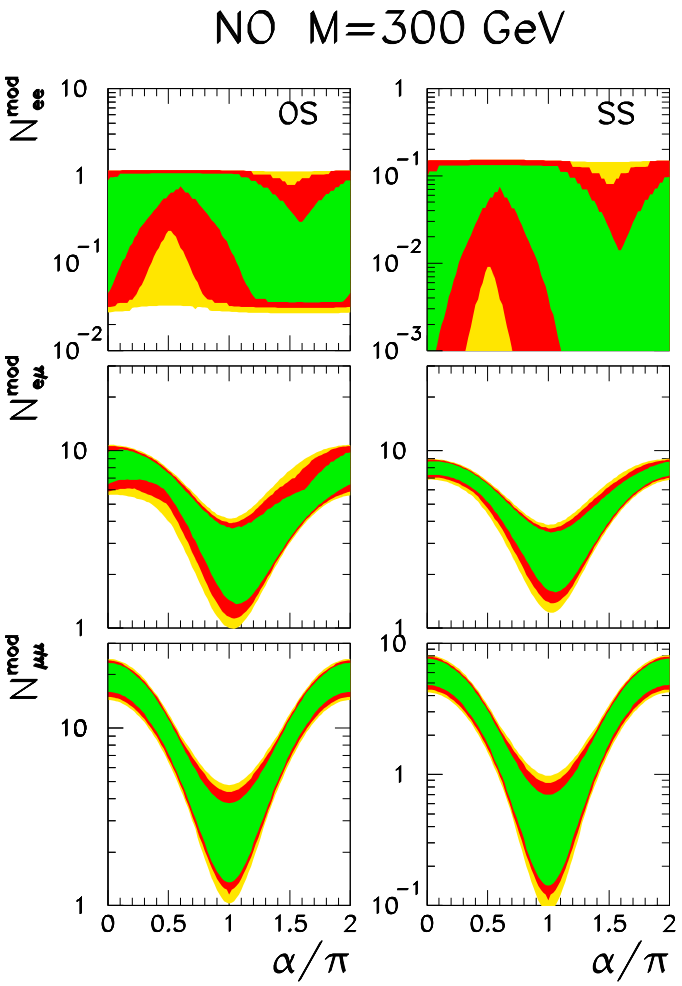

Figure 6.4: Expected number of signal events at $\sqrt{s} = 8$ TeV and an integrated luminosity of 20.3 fb^{-1}, in each of the six flavour-charge combinations for a triplet mass of $M = 300$ GeV and for neutrino parameters corresponding to the NO. The conventions are the same as in Fig.1.

of events in channel i from the triplet production and decays which depends on the triplet mass and the neutrino parameters as discussed in the previous section. In building the likelihood (6.45) we have used Poisson statistics to account for the small number of events in each channel.

We plot as full lines in Fig. 6.6 the dependence of χ^2_{6d} on the triplet mass after marginalization over the neutrino parameters (including the unknown Majorana

uncertainties each does not have any significant impact in the results.

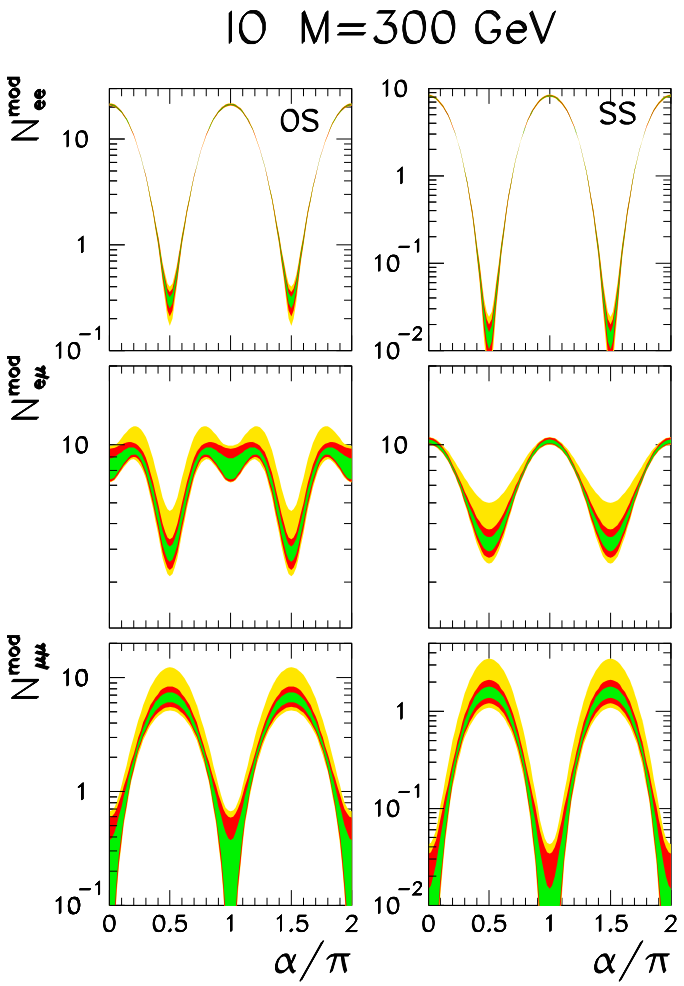

Figure 6.5: Same as Fig. 6.5 for IO.

phase α) over the 95% CL allowed values from the neutrino oscillation analysis for either NO or IO. First thing to notice is that in the SM (N_i^{mod}=0, which can be inferred from the large M limit in the figure) we find $\chi^2_{6d,SM} = 11.8$ which is a bit high for 6 data points. This is mostly driven by the OS $\mu\mu$ channel for which 3 events are observed when about 10 are expected in the SM. From this figure we also read that requiring $\chi^2_{6d} - \chi^2_{6d,SM} < 4$ we can infer an absolute bound on the triplet mass of 300 GeV (375 GeV) for NO (IO) light neutrino masses.

In order to stress the importance of the flavour and charge information on the possibility of imposing this bound, we have constructed the corresponding likelihood function summing the information from all the channels. As in this case the

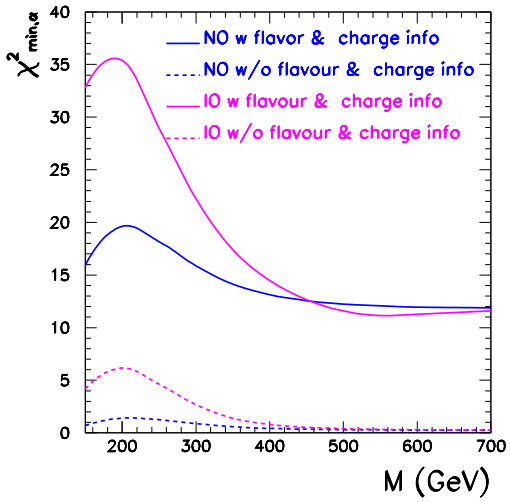

Figure 6.6: Triplet mass dependence of the χ^2 functions of the analysis of $pp \to ll'jj\nu\nu$ events with l, l' being either e or μ of either charge observed in the LHC Run 1 in ATLAS [118] when analyzed in the context of MLFV Type–III see–saw model. The full lines correspond to the likelihood function constructed including the full information given on flavour and charge of the final states (see Eq. (6.45)) while the dashed lines are obtained from the analysis of the total data summing over charge and flavour. The triplet couplings have been marginalized within the ranges allowed at 95% CL by the neutrino oscillation data analysis in Ref. [131] for NO (blue lines) and IO (purple lines) and for any value of the Majorana phase α.

total number of observed events is large enough, we assume gaussianity. So we define:

$$\chi^2_{tot} = \frac{(N^{tot,bck} + N^{tot,mod} - N^{tot,dat})^2}{N^{tot,dat} + (0.25N^{tot,bck})^2} \ . \tag{6.46}$$

The dependence of χ^2_{tot} on the triplet mass after marginalization over the neutrino parameters (including the unknown Majorana phase α) over the 95% CL allowed values from the neutrino oscillation analysis ($\Delta\chi^2_{osc} \leq 4$) for either NO or IO is shown as dashed lines in Fig. 6.6. As the deficit in OS $\mu\mu$ is compensated by the slight excesses in other channels, we find that in this case the SM gives a perfect description of the total observed event rates ($\chi^2_{tot,SM}$=0.25). The figure clearly illustrates the relevance of flavour and charge information, as in this case the condition $\chi^2_{tot} - \chi^2_{tot,SM} < 4$ does result into no bound on the triplet mass for

NO neutrino masses while it rules out only $M < 260$ for IO.

The dependence of the bounds on the unknown phase α is displayed in Fig. 6.7. The full red regions are excluded values of triplet masses in the MLFV scenario at 95% CL ($\chi^2_{6d} - \chi^2_{6d,SM} > 4$) when marginalizing over the oscillation parameters within the 95% CL allowed values by the oscillation analysis in NO (left) and IO (right) for each value of α. The α marginalized bound discussed above correspond to the lightest allowed masses in these panels which for NO ($M > 300$ GeV) correspond to $\alpha = \pi$ while for $\alpha = 0, 2\pi$ the bound strengthens to $M > 480$ GeV. For IO the dependence of the bound on α is weaker. The marginalized bound $M > 380$ GeV corresponds to $\alpha \sim 3\pi/4, 3\pi/2$ but it is close to that value for almost all values of alpha. The strongest bound of $M > 430$ GeV corresponds also to $\alpha = 0, 2\pi$.

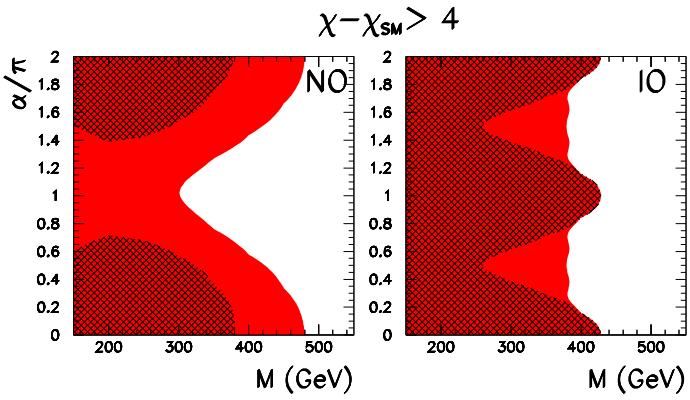

Figure 6.7: 95% excluded triplet mass in the MLFV Type–III see–saw scenario as a function of the unknown phase α from the analysis of $pp \to ll'jj\nu\nu$ events with l, l' being either e or μ of either charge observed in the LHC Run 1 in ATLAS [118]. The full regions correspond to the likelihood function constructed including the full information given on flavour and charge of the final states (see Eq. (6.45)) while the hatched ones are obtained from the analysis of the total data summing over charge and flavour (see Eq. (6.46)). The triplet couplings have been marginalized within the ranges allowed at 95% CL by the neutrino oscillation data analysis in Ref. [131] for NO (left) and IO (right).

The hatched regions are the corresponding constraints obtained using only the information on the total number of events ($\chi^2_{tot} - \chi^2_{tot,SM} > 4$) summed over flavour and charge of the final leptons. This figure illustrates again how using the flavour and charge information allows to impose stronger bounds on this scenario,

in particular allowing to rule out triplet masses irrespective of α for both orderings while for NO no bound can be imposed for $70^\circ \lesssim \alpha \lesssim 250^\circ$ if only the total number of events is considered.

6.4 Conclusions

In this Chapter we have discussed a complementary analysis to the ones using EFT to look for footprints of NP at LHC. Instead of assuming that the new states are too heavy to be seen at LHC and the only way to see their effects is to look for desviations in the SM couplings, we made a direct search to look for new sates. In the particular model-dependent study presented we used as motivation the origin of neutrinos' mass, which is one of the open question in the SM.

We analyzed a consistent TeV model for the generation of the neutrino masses that could lead, in addition, to measurable LHC signals. The MLFV type–III see–saw model contains fermion triplets that could live at the TeV scale, while the neutrino masses are related to the tiny total lepton number violation that has a very high energy scale associated. Due to the MLFV hypothesis, a highly predictive flavor composition of the heavy partner couplings to the SM, so at LHC we should look for testable flavor signals. We did it for a specific case, where the final state at LHC contains two charged leptons (either electron or muons of equal or opposite sign), two jets from a hadronically decaying W boson and large missing transverse momentum. In this scenario the flavor structure of the couplings of the triplet fermions to the SM leptons can be reconstructed from the neutrino mass matrix and lepton number violation is very suppressed.

In summary, we have shown how the analysis of the events containing two charged leptons (either electron or muons), two jets from a hadronically decaying W boson in the Run 1 with the ATLAS detector [118] can be used to impose constraints on the MLFV Type III see–saw scenario. Because of MLFV, the expected event rates in the different flavour and charge combinations of the two leptons are constrained by the existing neutrino data so the bounds cannot be evaded. For this reason it is possible to use this data to rule out these scenario with triplet masses lighter than 300 GeV at 95% CL irrespective of the neutrino mass ordering and of the value of the unknown Majorana phase parameter. The same analysis allows to rule out triplet masses masses up to 480 GeV at 95% CL for NO and $\alpha = 0, \pi$. We have stressed and quantified how the information on flavour and charge information of the produced leptons is important for maximal sensitivity to MLFV. In

particular we showed that in the absence of information on charge and flavour of the final leptons it is not possible to obtain unambiguous limits on the mass of the new triplet fermions.

We finish by commenting that extended sensitivity to MLFV with heavier triplets should be attainable with the data already accumulated from Run 2 in the same or other event topologies. For example by the analysis of the multilepton final states in CMS in Ref. [115] which, so far, has been performed only in the context of the simplified Type–III see–saw model. Nevertheless, as previously stressed to do so it is important to make use of the flavour and charge of final state leptons which has not been made public yet.

Chapter 7

Conclusions

We are living in an era where experiments play an important role in unveiling any signs of physics BSM. While writing this Thesis, we believe that colliders can guide us towards the answers of some open questions in Particle Physics. At 2012, the last missing ingredient of the SM was found at LHC, just two years after the start of the operation. The particles physics community was feeling enthusiastic about looking for new resonances at LHC, since the COM energy was still at half of the its full potential. For the first time, we were able to access the EWSB scale and to search for new resonances at the TeV scale.

The discovery was followed by a large number of analysis in order to determine if the observed particle was indeed the SM Higgs. After finishing the Run 1 and its complete analysis, several studies point to SM-like picture. In addition, there was not any sign of a new resonance, even after many preliminary analyses from Run 2, with a COM energy of 14 TeV. This is a clear motivation to the work done in the first part of this Thesis, which includes Chapter 2 to Chapter 5, in which we adopted an atheist perspective of NP, which is laying in some higher scale. We do not know what happens at that scale, but whichever NP, it can leave footprints at low energy scale in the form of effective operators of dimension higher than four. So, in a completely model-independent approach, we make use of such effective Lagrangian to look for deviations from the SM at the EWSB scale.

We started in Chapter 2 by introducing what is an EFT and how the SM can be seen as an EFT at low energies. We presented an effective Lagrangian describing the physics relevant to the EWSB sector at the TeV scale. We assumed that the Higgs boson is part of an $SU(2)_L$ doublet so the $SU(3)_C \otimes SU(2)_L \otimes U(1)_Y$ is realized linearly. The possible deviations from the SM are parametrized by a set of new higher dimension operators. We followed a bottom–up approach, in which we

assume our ignorance about the nature of the theory at high energy scale, with a choice of the operator basis which is driven by the experimental information available. This way the theoretical bias was maximally reduced, so that as many UV completions as possible can be confronted with the data. In the same Chapter we show how these operators change some interactions and observables relevant for our analyses: the triple gauge couplings, the Higgs couplings to both fermions and gauge bosons, and the couplings of the gauge bosons to fermions. We considered all the Lorentz–structures implied by the new operators, many of which are not induced in the SM at tree level. The importance of taking into account different experimental sets is highlighted in the correlated structures between Higgs–gauge and triple gauge couplings. We finished the Chapter by presenting the final basis of operators used in this Thesis. The chosen basis has the advantage of avoiding blind directions, *i.e.*the nonexistence of any combination of the anomalous operators whose contribution at tree level to any of the considered observables cancels out.

In Chapter 3 we have studied the effect of the fermionic operators in the analysis of the TGCs, using the LHC Run 1 diboson data. Traditionally, the analysis of TGCs was done assuming the so called TGC dominance, where NP effects other than anomalous TGC were considered negligible. In this Chapter, we have shown that changes in the couplings between quarks and gauge bosons, even within the constrains from EWPD, lead to modifications of the kinematical distributions in gauge boson pair production of comparable size to the ones stemming from the purely anomalous TGC. The effects from fermionic operators are thus amplified with the increase of the COM energy at LHC. To perform a consistent analysis on constraining the Wilson coefficients from the new operators, we built a χ^2 function including both kinematic distributions from diboson production and LEP data on the triple gauge boson couplings. Besides obtaining the allowed ranges for the Wilson coefficients of the operators that contribute to the LHC Run 1 data considered, we also learned that the LHC Run 1 diboson data is not precise enough to yield substantial information on the gauge couplings to quarks in addition to what is already known from EWPD but it is not that far off. Thus the results are a clear sign that LHC is getting competitive in terms of precision with LEP, so that diboson production at the LHC will play an important role in the analyses of anomalous couplings of gauge bosons to quarks as the LHC increases the integrated luminosity. Hence, any analysis of LHC observables should also include these fermionic operators, and therefore combine also the information from EWPD for a consistent

determination of the Wilson coefficients of the full set of dimension–six operators.

In Chapter 4 we performed a global analysis of all the relevant observables related to the electroweak sector, which at present allows for precision tests of the couplings between electroweak gauge bosons and fermions, triple electroweak gauge couplings and the couplings of the Higgs to fermions and gauge bosons. Moreover, as we have seen in Chapter 3, the effects of the fermionc operators in diboson analysis can also lead indirectly to changes in the Higgs couplings, due to the correlation between triple gauge vertices and Higgs–gauge vertices. Therefore, our analysis includes low energy electroweak precision measurements as well as LHC data on gauge boson pair production and Higgs observables. In total, the global analysis of EWPD and EWDBD and Higgs results from LHC Run 1 encompassed 64 observables and including Run 1 and 2, 122 observables. By including these three different sets of data and assuming that the new operators do not introduce new tree level sources of flavor violation nor violation of universality of the weak current, the global analysis involved the 20 operators of which 8 contribute to EWPD, 4 additional enter in the combination with the LHC EWDBD, and the 20 operators enter once the Higgs observables are considered. Altogether the analyses show no statistically significant source of tension with the SM. We also saw that the inclusion of the Run 2 data, with an increased integrated luminosity gathered at 13 TeV allows us to obtain more stringent bounds on a larger set of anomalous interactions and to perform new tests of the SM. Nevertheless we also identified set of four discrete quasi-degeneracies in the large parameter space which allows for large deviations from the SM predictions in the corresponding Wilson coefficients without any tension with the data. Finally we also presented a comparative quantification of the dependence of the extracted information on the Wilson coefficients of the twenty operators on the order of the truncation of the effective series.

In Chapter 5 we moved to the analysis of a different set of dimension–six operators that were not included before: the light-quark dipole operators. The light-quark electroweak dipole operators had been previously studied using EWPD and as well as deep inelastic scattering results from HERA. Due to its structure, these operators contribute to any process at the LHC initiated by the quark and antiquark components of the colliding protons, in particular to the electroweak diboson production without interfering with the SM amplitudes. The first part of the analysis has shown us that the determination of the gauge boson self-couplings from electroweak diboson production at LHC is robust under the inclusion of those quark dipole operators even when let them totally unconstrained in the analysis. There-

fore leaving these operators out of the global analysis of Chapter 4 was justified. We also use the analysis to determine the bounds imposed on the light quark dipole operators by LHC EWDBD together with Drell-Yan lepton pair production. Our results show that these analyses of LHC data improve over the bounds obtained from the EWPD by more than one order of magnitude, further stressing the reach of the precision frontier by LHC.

In this Thesis we also followed a different approach, a more model-dependent one where we can study direct searches at LHC for some SM completion, instead of just looking for subdominant effects at low energy coming from some high scale theory, unreachable at our current experiments. The chosen motivation was the origin of neutrino masses, since it is clearly the most undoubtful proof that the SM picture is not complete.

In Chapter 6 our prescription to study the potential of the LHC to address the question of neutrino mass generation was to find a consistent model with observable and maximally predictable signals at the TeV scale. The MLFV Type–III see–saw was such a suitable model due to its interesting TeV phenomenology. The heavy partners, two charged heavy leptons and one quasi–Dirac neutral heavy state, are light enough to be produced at LHC and their decay length is too short to produce a detectable displaced decay vertex signature, contrary to other see–saw models. Also, any lepton number violating process is really suppressed in this model. One other interesting feature of MLFV Type–III see–saw was the fact that the the couplings of the new heavy leptons to the SM charged leptons and neutrinos can be predicted, up to irrelevant normalization constants, from the low energy neutrino parameters. We obtain the bounds on the NP scale of this scenario that originates from the ATLAS searches in the final state topology containing two charged leptons (electrons and/or muons), two jets compatible with a hadronically decaying W and missing transverse momentum. We made use of the fact that this ATLAS search classified the final states in the different flavour and charge combinations, which made possible to exploit the predictions of the MLFV Type-III see–saw model.

In summary, in this Thesis, we started by studying the possible presence of NP in the electroweak sector using a model-independent approach, an effective Lagrangian. By doing so, we simultaneously tested the SM for possible deviations and also the nature of the Higgs particle. With the current LHC, already working at the 13 TeV with an integrated luminosity around 20 fb^{-1}, the SM is surviving to this plethora of tests, without any sign of weakness, barring the effect of the remaining quasi-degeneracies in some of the couplings, the picture seems to be

SM-like. Nevertheless we foresee that, as the LHC increases the integrated luminosity, some effects could be enhanced and unveil hints for NP. This also could be the case of a new resonance, capable of explaining the origin of neutrino masses.

After providing a better understanding of the EWSB, colliders are still our best option to access unexplored energy scales and to enlighten us with answers to the open mysteries in Particle Physics.

List of Figures

List of Tables

Bibliography

[1] A. Alves, N. Rosa-Agostinho, O. J. P. Eboli and M. C. Gonzalez–Garcia, Phys. Rev. D **98**, no. 1, 013006 (2018) [arXiv:1805.11108 [hep-ph]].

[2] E. da Silva Almeida, A. Alves, N. Rosa Agostinho, O. J. P. Eboli and M. C. Gonzalez-Garcia, Phys. Rev. D **99**, no. 3, 033001 (2019) [arXiv:1812.01009 [hep-ph]].

[3] E. da Silva Almeida, N. Rosa-Agostinho, O. J. P. Eboli and M. C. Gonzalez-Garcia, arXiv:1905.05187 [hep-ph].

[4] N. R. Agostinho, O. J. P. Eboli and M. C. Gonzalez-Garcia, JHEP **1711**, 118 (2017) [arXiv:1708.08456 [hep-ph]].

[5] S. Chatrchyan *et al.* [CMS Collaboration], Phys. Lett. B **716** (2012) 30 [arXiv:1207.7235 [hep-ex]].

[6] G. Aad *et al.* [ATLAS Collaboration], Phys. Lett. B **716** (2012) 1 [arXiv:1207.7214 [hep-ex]].

[7] F. Englert and R. Brout, Phys.Rev.Lett. **13**, 321 (1964).

[8] P. W. Higgs, Phys.Rev.Lett. **13**, 508 (1964).

[9] P. W. Higgs, Phys.Lett. **12**, 132 (1964).

[10] G. Guralnik, C. Hagen, and T. Kibble, Phys.Rev.Lett. **13**, 585 (1964).

[11] P. W. Higgs, Phys.Rev. **145**, 1156 (1966).

[12] T. Kibble, Phys.Rev. **155**, 1554 (1967).

[13] M. C. Gonzalez-Garcia and M. Maltoni, Phys. Rept. **460**, 1 (2008) [arXiv:0704.1800 [hep-ph]].

[14] J. F. Donoghue, E. Golowich and B. R. Holstein, Dynamics of the Standard Model (Cambridge University Press, 1992).

[15] W. Buchmuller and D. Wyler, Nucl.Phys. **B268**, 621 (1986).

[16] C. N. Leung, S. Love, and S. Rao, Z.Phys. **C31**, 433 (1986).

[17] A. De Rujula, M. Gavela, P. Hernandez, and E. Masso, Nucl.Phys. **B384**, 3 (1992).

[18] K. Hagiwara, S. Ishihara, R. Szalapski, and D. Zeppenfeld, Phys.Rev. **D48**, 2182 (1993).

[19] K. Hagiwara, R. Szalapski, and D. Zeppenfeld, Phys.Lett. **B318**, 155 (1993), arXiv:hep-ph/9308347.

[20] K. Hagiwara, S. Matsumoto, and R. Szalapski, Phys.Lett. **B357**, 411 (1995), arXiv:hep-ph/9505322.

[21] K. Hagiwara, T. Hatsukano, S. Ishihara and R. Szalapski, Nucl. Phys. B **496**, 66 (1997) [hep-ph/9612268].

[22] M. Gonzalez-Garcia, Int.J.Mod.Phys. **A14**, 3121 (1999), arXiv:hep-ph/9902321;

[23] F. de Campos, M. C. Gonzalez-Garcia and S. F. Novaes, Phys. Rev. Lett. **79**, 5210 (1997) [hep-ph/9707511];

[24] M. C. Gonzalez-Garcia, S. M. Lietti and S. F. Novaes, Phys. Rev. D **57**, 7045 (1998) [hep-ph/9711446];

[25] O. J. P. Eboli, M. C. Gonzalez-Garcia, S. M. Lietti and S. F. Novaes, Phys. Lett. B **434**, 340 (1998) [hep-ph/9802408];

[26] M. C. Gonzalez-Garcia, S. M. Lietti and S. F. Novaes, Phys. Rev. D **59**, 075008 (1999) [hep-ph/9811373];

[27] O. J. P. Eboli, M. C. Gonzalez-Garcia, S. M .Lietti and S. F. Novaes, Phys. Lett. B **478**, 199 (2000) [hep-ph/0001030].

[28] G. Passarino, Nucl. Phys. B **868**, 416 (2013) [arXiv:1209.5538 [hep-ph]].

[29] T. Corbett, O. J. P. Eboli, J. Gonzalez-Fraile and M. C. Gonzalez-Garcia, Phys. Rev. D **86**, 075013 (2012) [arXiv:1207.1344 [hep-ph]].

[30] T. Corbett, O. J. P. Eboli, J. Gonzalez-Fraile and M. C. Gonzalez-Garcia, Phys. Rev. D **87**, 015022 (2013) [arXiv:1211.4580 [hep-ph]].

[31] T. Corbett, O. J. P. Eboli, D. Goncalves, J. Gonzalez-Fraile, T. Plehn and M. Rauch, JHEP **1508**, 156 (2015) [arXiv:1505.05516 [hep-ph]].

[32] A. Butter, O. J. P. Eboli, J. Gonzalez-Fraile, M. C. Gonzalez-Garcia, T. Plehn and M. Rauch, JHEP **1607**, 152 (2016) [arXiv:1604.03105 [hep-ph]].

[33] S. Weinberg, Phys. Rev. Lett. **43** (1979) 1566.

[34] B. Grzadkowski, M. Iskrzynski, M. Misiak and J. Rosiek, JHEP **1010**, 085 (2010) [arXiv:1008.4884 [hep-ph]].

[35] A. Biekotter, A. Knochel, M. Kramer, D. Liu and F. Riva, Phys. Rev. D **91**, 055029 (2015) [arXiv:1406.7320 [hep-ph]].

[36] R. Contino, A. Falkowski, F. Goertz, C. Grojean and F. Riva, JHEP **1607**, 144 (2016) [arXiv:1604.06444 [hep-ph]].

[37] A. Falkowski, M. Gonzalez-Alonso, A. Greljo, D. Marzocca and M. Son, JHEP **1702**, 115 (2017) [arXiv:1609.06312 [hep-ph]].

[38] J. Brehmer, A. Freitas, D. Lopez-Val and T. Plehn, Phys. Rev. D **93**, no. 7, 075014 (2016) [arXiv:1510.03443 [hep-ph]].

[39] H. D. Politzer, Nucl. Phys. B **172**, 349 (1980);

[40] H. Georgi, Nucl. Phys. B **361**, 339 (1991);

[41] C. Arzt, Phys. Lett. B **342**, 189 (1995) [hep-ph/9304230];

[42] H. Simma, Z. Phys. C **61**, 67 (1994) [hep-ph/9307274].

[43] K. Hagiwara, R. Peccei, D. Zeppenfeld, and K. Hikasa, Nucl. Phys. **B282**, 253 (1987).

[44] M. Tanabashi *et al.* [Particle Data Group], Phys. Rev. D **98**, no. 3, 030001 (2018).

[45] I. Brivio, T. Corbett, O. J. P. Eboli, M. B. Gavela, J. Gonzalez-Fraile, M. C. Gonzalez-Garcia, L. Merlo and S. Rigolin, JHEP **1403**, 024 (2014) [arXiv:1311.1823 [hep-ph]].

[46] T. Corbett, O. J. P. Eboli, J. Gonzalez-Fraile and M. C. Gonzalez-Garcia, Phys. Rev. Lett. **111**, 011801 (2013) [arXiv:1304.1151 [hep-ph]].

[47] M. E. Peskin and T. Takeuchi, Phys. Rev. Lett. **65**, 964 (1990).

[48] LEP Electroweak Working Group [ALEPH and CDF and D0 and DELPHI and L3 and OPAL and SLD Collaborations and LEP Electroweak Working Group and Tevatron Electroweak Working Group and SLD Electroweak and Heavy Flavour Groups], arXiv:1012.2367 [hep-ex].

[49] S. Alam, S. Dawson and R. Szalapski, Phys. Rev. D **57**, 1577 (1998) [hep-ph/9706542].

[50] T. Corbett, O. J. P. Eboli and M. C. Gonzalez-Garcia, Phys. Rev. D **91**, no. 3, 035014 (2015) [arXiv:1411.5026 [hep-ph]].

[51] T. Corbett, O. J. P. Eboli and M. C. Gonzalez-Garcia, Phys. Rev. D **96**, no. 3, 035006 (2017) [arXiv:1705.09294 [hep-ph]].

[52] J. Elias-Miro, J. R. Espinosa, E. Masso and A. Pomarol, JHEP **1311**, 066 (2013) [arXiv:1308.1879 [hep-ph]].

[53] The LEP collaborations and The LEP TGC Working group LEPEWWG/TGC/2003-01

[54] G. Aad *et al.* [ATLAS Collaboration], JHEP **1609**, 029 (2016) [arXiv:1603.01702 [hep-ex]].

[55] V. Khachatryan *et al.* [CMS Collaboration], Eur. Phys. J. C **76**, no. 7, 401 (2016) [arXiv:1507.03268 [hep-ex]].

[56] G. Aad *et al.* [ATLAS Collaboration], Phys. Rev. D **93**, no. 9, 092004 (2016) [arXiv:1603.02151 [hep-ex]].

[57] V. Khachatryan *et al.* [CMS Collaboration], Eur. Phys. J. C **77**, no. 4, 236 (2017) [arXiv:1609.05721 [hep-ex]].

[58] Z. Zhang, Phys. Rev. Lett. **118**, no. 1, 011803 (2017) [arXiv:1610.01618 [hep-ph]].

[59] J. Baglio, S. Dawson and I. M. Lewis, Phys. Rev. D **96**, no. 7, 073003 (2017) [arXiv:1708.03332 [hep-ph]].

[60] R. Escribano and E. Masso, Nucl. Phys. B **429**, 19 (1994) [hep-ph/9403304].

[61] G. Kopp, D. Schaile, M. Spira and P. M. Zerwas, Z. Phys. C **65**, 545 (1995) [hep-ph/9409457].

[62] A. Buckley, C. Englert, J. Ferrando, D. J. Miller, L. Moore, M. Russell and C. D. White, JHEP **1604**, 015 (2016) [arXiv:1512.03360 [hep-ph]].

[63] J. Alwall *et al.*, JHEP **1407**, 079 (2014) [arXiv:1405.0301 [hep-ph]].

[64] N. D. Christensen and C. Duhr, Comput. Phys. Commun. **180**, 1614 (2009) [arXiv:0806.4194 [hep-ph]].

[65] A. Alloul, N. D. Christensen, C. Degrande, C. Duhr and B. Fuks, Comput. Phys. Commun. **185**, 2250 (2014) [arXiv:1310.1921 [hep-ph]].

[66] T. Sjostrand, S. Mrenna and P. Z. Skands, JHEP **0605**, 026 (2006) [hep-ph/0603175].

[67] J. de Favereau *et al.* [DELPHES 3 Collaboration], JHEP **1402**, 057 (2014) [arXiv:1307.6346 [hep-ex]].

[68] S. Schael *et al.* [ALEPH and DELPHI and L3 and OPAL and SLD Collaborations and LEP Electroweak Working Group and SLD Electroweak Group and SLD Heavy Flavour Group], Phys. Rept. **427**, 257 (2006) doi:10.1016/j.physrep.2005.12.006 [hep-ex/0509008].

[69] C. Patrignani *et al.* [Particle Data Group], Chin. Phys. C **40**, no. 10, 100001 (2016). doi:10.1088/1674-1137/40/10/100001

[70] M. Ciuchini, E. Franco, S. Mishima, M. Pierini, L. Reina and L. Silvestrini, Nucl. Part. Phys. Proc. **273-275**, 2219 (2016) [arXiv:1410.6940 [hep-ph]].

[71] The ATLAS collaboration [ATLAS Collaboration], ATLAS-CONF-2016-043.

[72] The ATLAS collaboration [ATLAS Collaboration], ATLAS-CONF-2018-034.

[73] M. Aaboud *et al.* [ATLAS Collaboration], Eur. Phys. J. C **78**, no. 1, 24 (2018) [arXiv:1710.01123 [hep-ex]].

[74] G. Aad *et al.* [ATLAS and CMS Collaborations], JHEP **1608**, 045 (2016) [arXiv:1606.02266 [hep-ex]].

[75] The ATLAS collaboration [ATLAS Collaboration], ATLAS-CONF-2018-031.

[76] A. M. Sirunyan *et al.* [CMS Collaboration], Eur. Phys. J. C **79**, no. 5, 421 (2019) [arXiv:1809.10733 [hep-ex]].

[77] G. Aad *et al.* [ATLAS Collaboration], Eur. Phys. J. C **76**, no. 1, 6 (2016) [arXiv:1507.04548 [hep-ex]].

[78] M. Aaboud *et al.* [ATLAS Collaboration], JHEP **1710**, 112 (2017) [arXiv:1708.00212 [hep-ex]].

[79] The ATLAS collaboration [ATLAS Collaboration], ATLAS-CONF-2018-026.

[80] A. M. Sirunyan *et al.* [CMS Collaboration], Eur. Phys. J. C **79**, no. 5, 421 (2019) [arXiv:1809.10733 [hep-ex]].

[81] V. Barger, M. McCaskey and G. Shaughnessy, Phys. Rev. D **81**, 034020 (2010) [arXiv:0911.1556 [hep-ph]].

[82] J. Chang, K. Cheung, J. S. Lee and C. T. Lu, JHEP **1405**, 062 (2014) [arXiv:1403.2053 [hep-ph]].

[83] S. Biswas, E. Gabrielli, F. Margaroli and B. Mele, JHEP **1307**, 073 (2013) [arXiv:1304.1822 [hep-ph]].

[84] D. Goncalves, F. Krauss, S. Kuttimalai and P. MaierhÃ¶fer, Phys. Rev. D **92**, no. 7, 073006 (2015) [arXiv:1509.01597 [hep-ph]].

[85] S. Weinberg, Physica A **96**, no. 1-2, 327 (1979).

[86] A. Manohar and H. Georgi, Nucl. Phys. B **234**, 189 (1984).

[87] A. M. Sirunyan *et al.* [CMS Collaboration], Phys. Lett. B **793**, 520 (2019) [arXiv:1809.05937 [hep-ex]].

[88] G. Aad *et al.* [ATLAS Collaboration], JHEP **1608**, 009 (2016) [arXiv:1606.01736 [hep-ex]].

[89] V. Khachatryan *et al.* [CMS Collaboration], Eur. Phys. J. C **75**, no. 4, 147 (2015) [arXiv:1412.1115 [hep-ex]].

[90] A. M. Sirunyan *et al.* [CMS Collaboration], [arXiv:1812.10529 [hep-ex]].

[91] M. Aaboud *et al.* [ATLAS Collaboration], JHEP **1710**, 182 (2017) [arXiv:1707.02424 [hep-ex]].

[92] A. M. Sirunyan *et al.* [CMS Collaboration], JHEP **1806**, 120 (2018) [arXiv:1803.06292 [hep-ex]].

[93] Measurement of the double-differential high-mass Drell-Yan cross section in pp collisions at $\sqrt{s} = 8$ TeV with the ATLAS detector. https://atlas.web.cern.ch/Atlas/GROUPS/PHYSICS/PAPERS/STDM-2014-06/

[94] L. Brekke and J. L. Rosner, Comments Nucl. Part. Phys. **18**, no. 2, 83 (1988).

[95] G. 't Hooft, NATO Sci. Ser. B **59**, 135 (1980).

[96] P. Minkowski, Phys. Lett. **67B**, 421 (1977).

[97] T. Yanagida, Conf. Proc. C **7902131**, 95 (1979).

[98] M. Gell-Mann, P. Ramond and R. Slansky, Conf. Proc. C **790927**, 315 (1979) [arXiv:1306.4669 [hep-th]].

[99] R. N. Mohapatra and G. Senjanovic, Phys. Rev. Lett. **44**, 912 (1980). doi:10.1103/PhysRevLett.44.912

[100] W. Konetschny and W. Kummer, Phys. Lett. **70B**, 433 (1977). doi:10.1016/0370-2693(77)90407-5

[101] T. P. Cheng and L. F. Li, Phys. Rev. D **22**, 2860 (1980). doi:10.1103/PhysRevD.22.2860

[102] G. Lazarides, Q. Shafi and C. Wetterich, Nucl. Phys. B **181**, 287 (1981). doi:10.1016/0550-3213(81)90354-0

[103] J. Schechter and J. W. F. Valle, Phys. Rev. D **22**, 2227 (1980). doi:10.1103/PhysRevD.22.2227

[104] R. N. Mohapatra and G. Senjanovic, Phys. Rev. D **23**, 165 (1981). doi:10.1103/PhysRevD.23.165

[105] R. Foot, H. Lew, X. G. He and G. C. Joshi, Z. Phys. C **44**, 441 (1989).

[106] E. Ma, Phys. Rev. Lett. **81**, 1171 (1998) [hep-ph/9805219].

[107] B. Bajc and G. Senjanovic, JHEP **0708**, 014 (2007) [hep-ph/0612029].

[108] P. Fileviez Perez, Phys. Lett. B **654**, 189 (2007) [hep-ph/0702287].

[109] M. C. Chen and J. Huang, Mod. Phys. Lett. A **26**, 1147 (2011) [arXiv:1105.3188 [hep-ph]].

[110] J. Kersten and A. Y. Smirnov, Phys. Rev. D **76**, 073005 (2007) [arXiv:0705.3221 [hep-ph]].

[111] R. N. Mohapatra and J. W. F. Valle, Phys. Rev. D **34**, 1642 (1986).

[112] F. del Aguila and J. A. Aguilar-Saavedra, Nucl. Phys. B **813**, 22 (2009) [arXiv:0808.2468 [hep-ph]].

[113] J. A. Aguilar-Saavedra, P. M. Boavida and F. R. Joaquim, Phys. Rev. D **88**, 113008 (2013) [arXiv:1308.3226 [hep-ph]].

[114] S. Chatrchyan *et al.* [CMS Collaboration], Phys. Lett. B **718**, 348 (2012) [arXiv:1210.1797 [hep-ex]].

[115] CMS Collaboration [CMS Collaboration], CMS-PAS-EXO-17-006.

[116] CMS Collaboration [CMS Collaboration], CMS-PAS-EXO-16-002.

[117] CMS Collaboration [CMS Collaboration], CMS-PAS-EXO-14-001.

[118] G. Aad *et al.* [ATLAS Collaboration], Phys. Rev. D **92**, no. 3, 032001 (2015) [arXiv:1506.01839 [hep-ex]].

[119] [ATLAS Collaboration], ATLAS-CONF-2013-019.

[120] C. Biggio and F. Bonnet, Eur. Phys. J. C **72**, 1899 (2012) [arXiv:1107.3463 [hep-ph]].

[121] R. S. Chivukula and H. Georgi, Phys. Lett. B **188**, 99 (1987).

[122] A. J. Buras, P. Gambino, M. Gorbahn, S. Jager and L. Silvestrini, Phys. Lett. B **500**, 161 (2001) [hep-ph/0007085].

[123] G. D'Ambrosio, G. F. Giudice, G. Isidori and A. Strumia, Nucl. Phys. B **645**, 155 (2002) [hep-ph/0207036].

[124] V. Cirigliano, B. Grinstein, G. Isidori and M. B. Wise, Nucl. Phys. B **728**, 121 (2005) [hep-ph/0507001].

[125] S. Davidson and F. Palorini, Phys. Lett. B **642**, 72 (2006) [hep-ph/0607329].

[126] M. B. Gavela, T. Hambye, D. Hernandez and P. Hernandez, JHEP **0909**, 038 (2009) [arXiv:0906.1461 [hep-ph]].

[127] R. Alonso, G. Isidori, L. Merlo, L. A. Munoz and E. Nardi, JHEP **1106**, 037 (2011) [arXiv:1103.5461 [hep-ph]].

[128] P. Fileviez Perez, T. Han, G. y. Huang, T. Li and K. Wang, Phys. Rev. D **78**, 015018 (2008) [arXiv:0805.3536 [hep-ph]].

[129] J. Garayoa and T. Schwetz, JHEP **0803**, 009 (2008) [arXiv:0712.1453 [hep-ph]].

[130] O. J. P. Eboli, J. Gonzalez-Fraile and M. C. Gonzalez-Garcia, JHEP **1112**, 009 (2011) [arXiv:1108.0661 [hep-ph]].

[131] I. Esteban, M. C. Gonzalez-Garcia, M. Maltoni, I. Martinez-Soler and T. Schwetz, JHEP **1701**, 087 (2017) [arXiv:1611.01514 [hep-ph]].

[132] A. Abada, C. Biggio, F. Bonnet, M. B. Gavela and T. Hambye, JHEP **0712**, 061 (2007) [arXiv:0707.4058 [hep-ph]].

[133] J. Schechter and J. W. F. Valle, Phys. Rev. D **21**, 309 (1980).

[134] S. Antusch, C. Biggio, E. Fernandez-Martinez, M. B. Gavela and J. Lopez-Pavon, JHEP **0610**, 084 (2006) [hep-ph/0607020].

[135] R. Franceschini, T. Hambye and A. Strumia, Phys. Rev. D **78**, 033002 (2008) [arXiv:0805.1613 [hep-ph]].

[136] B. Bajc, M. Nemevsek and G. Senjanovic, Phys. Rev. D **76**, 055011 (2007) [hep-ph/0703080].

[137] F. del Aguila and J. A. Aguilar-Saavedra, Phys. Lett. B **672**, 158 (2009) [arXiv:0809.2096 [hep-ph]].

[138] G. Aad *et al.* [ATLAS Collaboration], JINST **3**, S08003 (2008).

[139] S. Chatrchyan *et al.* [CMS Collaboration], JINST **3**, S08004 (2008).

[140] T. Li and X. G. He, Phys. Rev. D **80**, 093003 (2009) [arXiv:0907.4193 [hep-ph]].

[141] feynrules.irmp.ucl.ac.be/wiki.

[142] M. Cacciari, G. P. Salam and G. Soyez, Eur. Phys. J. C **72**, 1896 (2012) [arXiv:1111.6097 [hep-ph]].

[143] E. Conte, B. Fuks and G. Serret, Comput. Phys. Commun. **184**, 222 (2013) [arXiv:1206.1599 [hep-ph]].